Inaugural dissertation

for

obtaining the doctoral degree

of the

Combined Faculty of Mathematics, Engineering and Natural Sciences

of the

Ruprecht - Karls - University

Heidelberg

Presented by

M.Sc. Carolina Araujo Sousa

born in: Natal, Brazil

Oral examination: 26th April 2022

Analysis of neuroactive peptides on mouse hypothalamic thermoregulation

Referees:

Prof. Dr. Ana Martin-Villalba

Dr. Cornelius Gross

Dr. Mikhail Savitski

Jun.-Prof. Dr. Daniela Mauceri

Inaugural-Dissertation

zur

Erlangung der Doktorwürde

der

Gesamtfakultät für Mathematik, Ingenieur- und Naturwissenschaften

der

Ruprecht-Karls-Universität

Heidelberg

vorgelegt von

Carolina Araujo Sousa, M.Sc.

aus Natal, Brasilien

Tag der mündlichen Prüfung: der 26 April 2022

Analyse der Wirkung neuroaktiver Peptide auf die Thermoregulation im Hypothalamus der Maus

Gutachter:

Prof. Dr. Ana Martin-Villalba

Dr. Cornelius Gross

Dr. Mikhail Savitksi

Jun.-Prof. Dr. Daniela Mauceri

ACKNOWLEDGEMENTS

First, I would like to thank and acknowledge my PhD supervisor, Prof. Dr. Jan Siemens, for the opportunity to join his lab. During all these years, I felt very privileged to work with a great team of colleagues, who helped me evolve as a scientist and from whom I learned a lot. Therefore, I am very grateful to Dr. Siemens for giving me this chance to work on this project, as well as, for his guidance and support, and for establishing the collaborations that made this work possible.

I would like to express my gratitude to Dr. Gretel Kamm, whose passion for science was and still is truly inspirational to me. During this time, Dr. Kamm co-supervised me and also contributed to this work, performing the calcium imaging experiments. In addition, I would like to thank her for always being happy to help whenever I had any issue during surgeries, experiments, or data analyses. I am also thankful for her constructive criticism, which helped to improve the quality of this work. Finally, I also want to thank her for her personal support.

Throughout these four years, I have been advised by a remarkable team of scientists who were part of my thesis advisory committee (TAC). Namely, I would like to thank Dr. Cornelius Gross, Prof. Dr. Ana Martin-Villalba, Dr. Paul Heppenstall, and Dr. Mikhail Savitski for their comments and suggestions on this project.

Moreover, I am grateful to Dr. Gross, Dr. Martin-Villalba, Dr. Savitski, and Jun. Prof. Dr. Daniela Mauceri for being part of my thesis defense committee.

A substantial part of this work was done in collaboration with the lab of Prof. Dr. Jeroen Krigsveld, at the German Cancer Research Center (DKFZ). I would like to thank him for the collaboration and for his comments and suggestions on the project. I also would like to acknowledge Dr. Daniele Colombo, who was a former postdoc at his lab, who performed all the liquid chromatography and tandem mass spectrometry (LC-MS/MS) analyses and taught me to process the samples for the analyses. I am very grateful for the time he spent with me on the sample and data analysis troubleshooting. His dedication and support were fundamental to this work, and I really appreciated all his effort. Currently, I am also collaborating with another member of the Krigjsveld lab, Dr. Dimitrios Papageorgiou, on further experiments motivated by this thesis, and I would like to take the chance to thank him for his keenness and thorough experimental planning.

I also had the privilege of being helped by Dr. Silvia Calderazzo, a biostatistician from DKFZ, who, together with Dr. Colombo, wrote the main code used in the proteomics data analysis. I really appreciated her enthusiasm, dedication, and patience in teaching me about the analysis.

I also would like to thank colleagues from another collaboration, who helped in the targeted mass spectrometry (MS) experiments. Namely, I would like to thank Prof. Dr. Med. Walter Haefeli, for the collaboration and support, as well as, to Dr. Max Sauter, a

postdoc at Haefeli lab, who performed the experiments. I am very grateful for the time and effort that Dr. Sauter dedicated to these challenging experiments.

I am also thankful to Dr. Maria Secci, a postdoc at the Central Institute of Mental Health, in Mannheim, who kindly taught me about microdialysis and was always available whenever I had doubts about this technique.

Additionally, I would like to thank everyone who gave me feedback on this doctoral thesis, especially Dr. Siemens and Dr. Kamm. I am also grateful for everybody who helped me in the data analysis and data visualization performed for this work. Namely, special thanks to Dr. Colombo, Dr. Calderazzo, Dr. Kamm, Dr. Bryan da Costa Souza, Dr. Juan Boffi, Dr. Muad Abd-El-Hay, and Kristina Žuža. I am also thankful to Dr. Katrin Schrenk-Siemens and Lisa Vierbaum for reviewing the German translation of the abstract.

Throughout my PhD period, I had the fortuitous experience of working together with great colleagues at the AG Siemens. And I would like to express my appreciation for all their help and constructive criticism, and for putting effort in the tough task of working as a team. I am also grateful for all shared moments of fun we had inside and outside of the lab. Huge thanks to everyone who was or still is part of the lab: Kristina Žuža, Sebastian Marty-Lombardo, Dr. Kamm, Dr. Schrenk-Siemens, Dr. Abd-El-Hay, Dr. Hagen Wende, Dr. Sara Nencini, Dr. Jörg Pohle, Ulrike Baur-Finck, Daniela Pimonov, Lisa Vierbaum, Lisa Weiler, Annika von Seggern, Kritika Mittal, Mildred Herrera, Manoj Yadav, Amandine Cevaroc, Daniel Erdelyi, Osmond Aruna, Burçe Kabaoglu, Kaya Baumert, Nadine Winkler, Dr. Wojciech Ambroziak, Miriam Lohnert, and Christina Steinmeyer-Stannek.

I am very grateful for the privilege of having conducted my doctoral work in excellent, well-funded institutions, such as the Heidelberg University and EMBL. And I would like to thank everyone from these organizations who, directly or indirectly, helped me and/or contributed to my project. I am very thankful for the staff of the Heidelberg University animal facility (IBF), for taking care of the mice, and for the cleaning staff working at the Pharmacology Institute, for keeping the rooms tidy. I am also thankful to my colleagues from the Pharmacology Institute who were happy to help when I needed. From EMBL, I especially would like to thank former and current members of the Graduate Office, for always being ready to guide me and answer bureaucratic questions. I also want to thank Patricia Cabezas, for her career advices, and the EMBL Communications Office, for giving me the chance to write about science for general audience. Last but not least, I would like to thank the financial support that made this project become true.

I also would like to demonstrate my appreciation for everyone who put effort in making science more accessible. Specifically, I would like to acknowledge and thank the R community and the developers of open-source software and algorithms used in this work. Additionally, I want to thank everyone who advocates for a fairer, and more diverse and inclusive academia. Special thanks to everyone from the Feminism (in science) book club and to Flavia-Bianca Cristian, for initiating this project with me.

I would like to reinforce my fond gratitude to two friends from AG Siemens, Kristina and Sebastian. Especially to Kristina, I would like to thank her for being an amazing friend since I joined the lab. Her emotional support during hard moments meant a lot to me and was essential for the completion of this work. I am thrilled to have walked through this pathway having her by my side, and I would like to thank her supportive and nurturing friendship. Also special thanks to Sebastian for his friendship and genuine eagerness to help me during my PhD. I will always be grateful to him for being there during cheerful or difficult times. Thanks for bringing so much joy, lightness, and music to my days.

Doing a PhD in another continent was definitely not an easy task. However, I was very fortunate to have encountered lovely people who became my safe harbor on this side of the ocean. Thus, I would like to demonstrate my gratitude to them for having shared so many great memories, but also for helping me navigate through challenging periods. Special thanks to Erica Margiotta, Ivan Labic, Rajwinder Singh, Mariana Alves, Gabriel Cavalheiro, Sara Götz, Natalie Horvat, Veronika Saharuka, Lisa Vierbam, Kritika Mittal, Bianca Fischer, Virginia Pierini, Chris Neufeldt, Jakub Macošek, and Juliana Araújo.

Despite being physically far, the distance reinforced the importance of long-term friends, who kept cheering for me and supporting me throughout this time. Thus, I would like to thank them for being and remaining present in my life. Remembering all the moments we spent together makes me realize how privileged I am for having so many meaningful shared memories. In special, I would like to thank Bryan da Costa Souza, Annie da Costa Souza, Daiane Golbert, Carolina Sousa, Amanda Freire, Bruna Louzá, Vanessa Augusta, Rafaela Souza, Juliana Brandão, Fernando Henrique, Erika Cordeiro, Tamyres Queiroga, Maria Eduarda Costa, Natalia Boccardi, Vitor Santos, and Nabila Ibrahim.

I also would like to thank the fundamental professional support of Thamara Tabera that helped me during my PhD journey.

I am also very lucky to be part of a family that genuinely supports and cheers for all my decisions. And I am extremely grateful for them to be there whenever I needed. Your love and care mean the world to me. In special, I would like to thank my grandparents Dolores and João Paulo, my aunts Branca, Ludgarda, and Toinha, my uncle Ludgero, and my cousin Clara Rocha.

Last but not least, I would like to express all my gratitude to my core family, my parents, Jefferson and Ludmila, and my brother, Arthur, for always for caring for me and for each other. No words are enough to thank their unconditional love and support. In special to my parents, Jefferson and Ludmila, I am thankful to them for giving their best while raising me and for providing me the best education they could. Esta tese é dedicada a vocês, de todo o meu coração.

SUMMARY

Keeping balance is essential for the survival of mammals. When facing challenges, these animals rely on a neural system that promptly coordinates physiological and behavioral adaptations that are triggered to maintain homeostasis. In such context, neuroactive peptides, including neuropeptides and some peptide hormones, have been proposed to play an important role in the modulation of neural activity. These molecules have been implicated in the control of several processes, such as sleep, reproduction, and feeding, and are also believed to influence thermoregulation. The mammalian core body temperature (Tcore) is maintained by the thermoregulatory circuitry, which is orchestrated by the preoptic area (POA) of the hypothalamus. Different lines of evidence have suggested a role for neuroactive peptides in thermal balance, especially acting at the POA. Despite this, the molecular mechanisms that modulate Tcore during thermal challenges remain unclear.

Here, to investigate which neuroactive peptides are released at the level of the POA during thermal challenges, an unbiased screening of samples collected *in vivo* from male mice was performed. For this, first, to enrich neuroactive peptide detection, an optimized protocol was established for the *in vivo* sampling and the sample preparation for liquid chromatography and tandem mass spectrometry (LC/MS-MS) analysis. Next, the optimized protocol was applied on samples collected from the POA of freely behaving adult male mice during three different types of thermal stimuli. These included the chemogenetic activation of a subpopulation of preoptic thermoregulatory neurons expressing the vesicular transporter VGLUT2 (POA^{VGLUT2}), which induced hypothermia, and the ambient warm and cold temperature stimulation. The results suggested that, in total, peptides deriving from 18 neuroactive peptide precursors were detected to be differentially released at the mouse POA during thermal challenges. Among these precursors and respective peptides, somatostatin and secretogranin 1 were differentially detected in samples collected during the stimulation of POA^{VGLUT2} neurons compared to the control group. Additionally, in comparison to control conditions, the results suggest a differential release of peptides from the precursors of orexins, nociceptin, and nucleobindin 1 in warm-exposed mice, as well as, thyrotropin-releasing hormone (TRH),

and diazepam binding inhibitor (DBI) in animals peripherally stimulated with cold. Moreover, the verification of the unbiased screening focused on two candidates, orexin and adiponectin. For both, *in vivo* samples collected either during warm or cold peripheral stimulation were evaluated with ELISA. In addition, further experiments investigated a potential role of orexins in thermoregulation, by focusing on the POA distribution of orexin receptor 2, the influence of orexin-A on preoptic neurons, and the injection of orexin receptor antagonists into the POA. Results of these experiments may have provided further evidence for the engagement of pro-orexin derived peptides in Tcore control. Additional studies are required to define these and the other peptides as modulators of preoptic thermoregulation. Nonetheless, the list of candidates of thermoregulatory peptides provided by this thesis could contribute to a better comprehension of the molecular control of POA during adaptation to thermal challenges. Given the vital importance of maintaining the Tcore in mammals, such candidates could potentially also be implicated in health and disease.

ZUSAMMENFASSUNG

Den Organismus in Balance/Homöostase zu halten, ist für Säugetiere überlebenswichtig. Wenn sie mit Herausforderungen konfrontiert werden, verlassen sich diese Tiere auf ein neuronales System, das physiologische und verhaltensbezogene Anpassungen, die zur Aufrechterhaltung der Homöostase aktiviert werden, umgehend koordiniert. In diesem Zusammenhang wurde vermutet, dass neuroaktive Peptide, darunter Neuropeptide und einige Peptidhormone, eine wichtige Rolle bei der Modulation der neuronalen Aktivität spielen. Diese Moleküle werden mit der Steuerung verschiedener Prozesse wie Schlaf, Fortpflanzung und Nahrungsaufnahme in Verbindung gebracht, und es wird angenommen, dass sie auch die Thermoregulation beeinflussen. Die Körperkerntemperatur (Tcore) von Säugetieren wird durch den thermoregulatorischen Kreislauf aufrechterhalten, der vom präoptischen Areal (POA) des Hypothalamus orchestriert wird. Verschiedene Hinweise deuten auf eine Rolle neuroaktiver Peptide im Wärmehaushalt hin, die insbesondere in der POA wirken. Dennoch sind die molekularen Mechanismen, die Tcore bei thermischen Herausforderungen modulieren, nach wie vor unklar.

Um zu untersuchen, welche neuroaktiven Peptide bei thermischen Herausforderungen auf der Ebene der POA freigesetzt werden, wurde ein unvoreingenommene Untersuchung von Proben durchgeführt, die *in vivo* von männlichen Mäusen gesammelt wurden. Zunächst wurde ein optimiertes Protokoll für die *in vivo* Probenentnahme und die Probenvorbereitung für die Flüssigchromatographie und Tandem-Massenspektrometrie (LC/MS-MS) erstellt, wodurch die Detektion neuroaktiver Peptide verbessert werden konnte. Anschließend wurde das optimierte Protokoll an Proben angewandt, die während dreier verschiedener Arten von thermischen Reizen aus der POA von frei agierenden männlichen Mäuse entnommen wurden. Dazu gehörte die chemogenetische Aktivierung einer Subpopulation von präoptischen thermoregulatorischen Neuronen, die den vesikulären Transporter VGLUT2 (POA^{VGLUT2}) exprimieren, was eine Hypothermie auslöste, sowie die Stimulation durch warme und kalte Umgebungstemperaturen. In den Untersuchungen konnten insgesamt Peptide aus 18 neuroaktiven Peptidvorläufern nachgewiesen werden, die bei

thermischen Herausforderungen in der POA der Maus unterschiedlich freigesetzt werden. In Proben, die während der Stimulation von POA^{VGLUT2}-Neuronen gesammelt wurden, wurden im Vergleich zur Kontrollgruppe Somatostatin und Sekretogranin 1 nachgewiesen. Die Ergebnisse zeigen im Vergleich zu den Kontrollbedingungen eine differentielle Freisetzung von Peptiden aus den Vorläufern von Orexinen, Nozizeptin und Nukleobindin 1 bei wärmeexponierten Mäusen, sowie von Adiponectin, Thyrotropin-Releasing-Hormon (TRH) und Diazepam-Bindungsinhibitor (DBI) bei peripher mit Kälte stimulierten Tieren. Im weiteren Verlauf lag der Fokus auf zwei Kandidaten des Screenings, Orexin und Adiponectin. Für beide wurden *in vivo* Proben, die entweder während einer warmen oder kalten peripheren Stimulation gesammelt wurden, mit ELISA ausgewertet. In weiteren Experimenten wurde außerdem eine potenzielle Rolle der Orexine bei der Thermoregulation untersucht, wobei der Schwerpunkt auf der Verteilung des Orexin-Rezeptors 2 in der POA, dem Einfluss von Orexin-A auf präoptische Neuronen und der Injektion von Orexin-Rezeptor-Antagonisten in der POA lag. Dies könnte weitere Beweise für die Beteiligung von Pro-Orexin-abgeleiteten Peptiden an der Tcore-Kontrolle liefern. Weitere Studien sind erforderlich, um diese und weitere Peptide als Modulatoren der präoptischen Thermoregulation zu definieren. Nichtsdestotrotz könnte die Liste der in dieser Arbeit vorgestellten Kandidaten für thermoregulatorische Peptide zu einem besseren Verständnis der molekularen Kontrolle der POA während der Anpassung an thermische Herausforderungen beitragen. In Anbetracht der lebenswichtigen Bedeutung der Aufrechterhaltung der Tcore bei Säugetieren könnten diese Kandidaten möglicherweise auch bei Gesundheit und Krankheit eine Rolle spielen.

RESUMO

Manter o equilíbrio é essencial para a sobrevivência de mamíferos. Ao enfrentar desafios, estes animais dependem de um sistema neural que prontamente coordena adaptações fisiológicas e comportamentais, que são acionadas para manter a homeostase. Neste contexto, peptídeos neuroativos, incluindo neuropeptídeos e alguns hormônios peptídicos, foram propostos a desempenhar um papel importante na modulação da atividade neural. Estas moléculas já foram implicadas no controle de vários processos, tais como sono, reprodução e alimentação, e acredita-se que também influenciam a termorregulação. A temperatura corporal nuclear (Tcore) de mamíferos é mantida pelo circuito termorregulador, que é orquestrado pela área pré-óptica (POA) do hipotálamo. Diferentes linhas de evidência tem sugerido um papel dos peptídeos neuroativos no equilíbrio térmico, especialmente atuando na POA. Apesar disso, os mecanismos moleculares que modulam a Tcore durante os desafios térmicos permanecem pouco claros.

Sendo assim, para investigar quais peptídeos neuroativos são liberados a nível da POA durante estimulação térmica, foi realizada uma análise não-enviesada de amostras coletadas *in vivo* de camundongos machos. Para tanto, primeiro, para enriquecer a detecção dos peptídeos neuroativos, foi-se estabelecido um protocolo otimizado para a coleta *in vivo* e o preparo de amostras para análise de cromatografia líquida e espectrometria de massa em tandem (LC/MS-MS). Em seguida, este protocolo foi aplicado na avaliação de amostras coletadas da POA de camundongos machos adultos em livre comportamento durante três tipos diferentes de estímulos térmicos. Estes incluíram a ativação quimiogenética de uma subpopulação de neurônios pré-ópticos termorreguladores que expressam o transportador vesicular VGLUT2 (POA^{VGLUT2}), o que induziu hipotermia, e a estimulação periférica por temperaturas ambientes quente e fria. Os resultados sugerem que, no total, peptídeos derivados de 18 precursores de peptídeos neuroativos foram detectados diferencialmente liberados na POA de camundongos durante desafios térmicos. Entre estes precursores e respectivos peptídeos, somatostatina e secretogranina 1 foram diferencialmente detectados, em comparação com o grupo controle, em amostras coletadas durante a estimulação dos neurônios

POA^{VGLUT2}. Também em comparação às condições controle, os resultados sugerem uma liberação diferencial de peptídeos provenientes dos precursores de orexinas, nociceptina e nucleobindina 1 em camundongos expostos ao calor, bem como adiponectina, hormônio liberador de tireotrofina (TRH) e inibidor de ligação do diazepam (DBI) em animais estimulados perifericamente com o frio. Além disso, a verificação da análise não-enviesada concentrou-se em dois candidatos, a orexina e a adiponectina. Para ambos, amostras coletadas *in vivo* durante a estimulação periférica quente ou fria foram avaliadas com ELISA. Ademais, outros experimentos investigaram um papel potencial das orexinas na termorregulação, focando na distribuição do receptor 2 de orexina na POA, na influência da orexin-A em neurônios pré-ópticos, e na injeção de antagonistas de receptores de orexina na POA, e podem ter fornecido mais evidências para o engajamento de peptídeos derivados de pró-orexina no controle de Tcore. Mais estudos são necessários para definir estes e os outros peptídeos como moduladores da termorregulação pré-óptica. No entanto, a lista de candidatos a peptídeos termorreguladores fornecida por esta tese pode vir a contribuir para uma melhor compreensão do controle molecular da POA durante a adaptação a desafios térmicos. E dada a importância vital de manter a Tcore em mamíferos, tais candidatos também podem estar potencialmente implicados na saúde e na doença.

TABLE OF CONTENTS

LIST OF FIGURES

LIST OF TABLES

LIST OF ABBREVIATIONS

aa	amino acid
AAV	adeno-associated virus
ACN	acetonitrile
Adcyap1	gene of Pituitary adenylate cyclase-activating polypeptide
ADIPO	adiponectin protein
Adipoq	adiponectin gene
Adipor1	adiponectin receptor 1
Adipor2	adiponectin receptor 2
Agt	angiotensinogen gene
AGC	automatic gain control
ANOVA	analysis of variance
AP	antero-posterior
Arg	arginine
AT-II	angiotensin II
Avp	vasopressin
BAT	brown adipose tissue
BBB	blood brain barrier
BCA	bicinchoninic acid
BDNF	brain-derived neurotrophic factor
BNST	bed nucleus of stria terminalis
BSA	bovine serum albumin
CAA	chloroacetamide
CARTPT	cocaine and amphetamine related transcript
CBLN2	cerebellin-2
CMGA	chromogranin A
CNO	clozapine-N-oxide
CNS	central nervous system
Crh	corticotropin-releasing hormone
CSF	cerebrospinal fluid
C-term	carboxy-terminus
CTL	control
DBI	diazepam binding inhibitor
ddH2O	double distilled water
DE	differential expression
DH	dorsal horn
DIO	double floxed inverted
DMH	dorsomedial hypothalamus
dNTP	deoxynucleoside triphosphate
DREADDs	Designer Receptors Exclusively Activated by Designer Drugs
DRG	dorsal root ganglia
DV	dorso-ventral
ECL	enhanced chemiluminescence
EDTA	Ethylenediaminetetraacetic acid
ELISA	enzyme linked immunosorbent assay
EYFP	enhanced yellow fluorescent protein

FA	formic acid
FDR	false discovery rate
FEP	Fluorinated Ethylene Propylene
FWHM	full width at half maximum
GABA	gamma-aminobutyric
Gal	galanin
GCaMP6	calcium sensor composed of green fluorescent protein (GFP) fused to calmodulin, version 6
GFP	green fluorescent protein
GH	growth hormone
Ghrh	growth hormone releasing hormone
GPCR	G-protein coupled receptor
Hcrt:	hypocretin/orexin gene
hM3D	human Muscarinic acetylcholine receptor M3
hSyn	human synapsin
iCre	codon-improved cre recombinase
HRP	horseradish peroxidase
iBAQ	intensity-based absolute quantification
i.c.v.	intracerebroventricular
IGF2	insulin-like growth factor II
i.p.	intraperitoneal
ISF	interstitial fluid
KNG1	kininogen-1
LC	liquid chromatography
LC-MS	targeted liquid chromatography-mass spectrometry
LC-MS/MS	liquid chromatography tandem mass spectrometry
LDCV	large dense core vesicle
Lepr	leptin receptor
LFQ	label-free quantification
LHA	lateral hypothalamus
LPB	lateral parabrachial nucleus
LPBd	dorsal subdivision of LPB
LPBel	external lateral LPB
LPO	lateral preoptic area
Lys	lysine
ML	medial-lateral
MOPS	3-(N-morpholino)propanesulfonic acid
MnPO	median preoptic nucleus
MPA	medial preoptic area
mRNA	messenger RNA
MS/MS	tandem mass spectrometry
MS2	second MS analysis in MS/MS
MWCO	molecular weight cut-off
m/z	mass to charge ratio
NCE	normalized collision energy
NLP	nesfatin-1-like peptide
Nms	neuromedin S

NPY	neuropeptide Y
N-term	amino terminus
Nts	neurotensin
NUCB1	nucleobindin 1
O.D.	optical density
OFM	open-flow microperfusion
Opn5	opsin 5
OREX	orexin
ORL1	opioid receptor-like 1
OVLT	organum vasculosum of the lamina terminalis
OX1R	orexin receptor 1
OX2R	orexin receptor 2
PACAP	pituitary adenylate cyclase-activating polypeptide
PBS	phosphate buffer saline
PBST	PBS containing 0.1% Triton X-100
PCR	Polymerase chain reaction
Pdyn	prodynorphin
Penk	proenkephalin
PENK-A	proenkephalin A
PFA	paraformaldehyde
Pmch	pro-Melanin concentrating hormone
PNOC	pronociceptin
POA	preoptic area of the hypothalamus
POA^{VGLUT2}	Preoptic VGLUT2
Pomc	proopiomelanocortin gene
PRM	parallel reaction monitoring
PVH	paraventricular nucleus of the hypothalamus
QRFP	pyroglutamylated RFamide peptide
rBDNF	recombinant human BDNF
ROIs	region of interest
RIA	radioimmunoassay
RNA seq	RNA sequencing
RP	raphe pallidus
RT	room temperature
scRNA-Seq	single cell RNA sequencing
SCG1	Secretogranin-1
SCG2	Secretogranin-2
SCG3	Secretogranin-3
SDS	sodium dodecyl sulfate
SP	signal peptide
SP3	single-pot solid-phase-enhanced sample preparation
SPF	specific-pathogen-free
SMS	somatostatin protein
SRM	selected reaction monitoring
Sst	somatostatin gene
TBST	tris-buffered saline containing Tween
TCEP	tris (2-carboxyethyl)phosphine

Tcore	core body temperature
TRH	thyrotropin-releasing hormone
TRP	transient receptor potential
Tshell	shell body temperature
Ucn3	urocortin 3
VGF	neurosecretory protein VGF
VGLUT2	vesicular glutamate transporter 2
VLPO	ventrolateral preoptic nucleus
VMPO	ventromedial preoptic nucleus
WAT	white adipose tissue
WT	wild type

CHAPTER 1: INTRODUCTION

1 INTRODUCTION

From one minute to another, from one season to the next, the environment is constantly changing. In such dynamic scenario, being able to adapt to changes is a must in order to survive. Mammals are great examples of versatility. To keep homeostasis, these animals require a flexible neural system that promptly coordinates physiological and behavioral adjustments[1]. Among different levels of regulation, neuroactive peptides, including neuropeptides and some peptide hormones, are important players in tuning neural activity[2].

Adapting to variations in external and internal temperatures is essential for the survival of mammals. For this, the mammalian body temperature is maintained by the thermoregulatory circuitry, which has its center at the preoptic area (POA) of the hypothalamus[1,3]. The POA is located in a very strategic position to receive modulatory inputs. However, it is still elusive how this region is molecularly regulated during thermal challenges.

In this context, with this thesis, I aimed to investigate molecules that could be involved in the integration of thermal information and in the control of body temperature. My hypothesis was that neuroactive peptides are released at the POA during thermal stimuli and these molecules modulate the activity of preoptic neurons during thermoregulation. To investigate this, I performed an unbiased screening of neuroactive peptides arriving at the POA during three different types of thermal challenges. Thus, in this thesis, I will first introduce the relevant topics that will hopefully help comprehend the following chapters. Next, I will detail the materials and methods used in all the experiments. From the third until the fifth chapters, I will describe and discuss the results of my experiments. Finally, in the sixth chapter, I will contextualize all the findings in a broader perspective.

1.1 Energy homeostasis in mammals

Homeothermy (derived from ancient Greek *homoios-*, meaning 'similar', and –thermy, meaning 'heat') is defined as the maintenance of the internal body temperature within a narrow range and relatively independent from the ambient temperature[4]. This is how mammals and birds keep their body temperature. The opposite of homeothermy is poikilothermy (derived from ancient Greek *poikilo-*, meaning 'varied', and –thermy), characterized by variations in internal body temperature according to the external temperature. Fishes, amphibians and reptiles are examples of poikilothermic animals[4]. Because this thesis was devoted to investigate thermoregulation in mice, I will focus on mammals from now on.

When facing changes in external temperatures, mammals manage to keep their body temperature fairly stable by eliciting physiological and behavioral adjustments[4]. While it is unknown why mammals are homeotherms[1], this capacity enables this large group of animals to survive daily and seasonal temperature variations, with some species successfully inhabiting environments as extreme as deserts and the Polar Regions[5,6].

On top of being homeotherms, mammals are considered endotherms, i.e. animals capable of producing their own heat. Such heat generation requires continuous energy supply, what comes from nutrients obtained through the diet[1,4]. Thus, as homeothermic and endothermic animals, mammals are in a constant energy balance between heat production and consumption, and the regulation of such homeostasis is extremely important for their survival.

1.2 Thermoregulation and the core body temperature

The body temperature is composed of the shell body temperature (Tshell), represented by the temperature at the surface of the body, for instance, the skin temperature, as well as by the core body temperature (Tcore), which encompasses the temperature from the viscera and the brain. While Tshell is more subject to change due to external temperatures, the Tcore is tightly regulated[4]. Keeping the Tcore relatively constant is essential for the

optimal functioning of the entire organism, as the efficiency of biological processes depends on temperature[4]. For example, a balanced Tcore benefits biochemical reactions and promotes faster cell signaling. Being crucial to mammals, the body temperature, then, is considered one of the four vital signs, among pulse rate, respiration rate, and blood pressure. The impressive ability of maintaining the Tcore is made possible due to the thermoregulatory system, which receives thermal information and triggers thermal homeostasis via autonomic and behavioral adaptations[1,3].

1.3 Thermoregulatory circuitry

Thermal information arrives in the thermoregulatory system from the periphery, but temperature is also detected within the brain itself. Peripheral information comes from primary thermosensory neurons that innervate the skin and viscera. In addition, the splachnic and vagus nerve carry thermosensory information from the abdomen. Their cell bodies are located at the trigeminal ganglia and dorsal root ganglia (DRG), which bring thermal information from the head and the rest of the body, respectively. The thermosensitivity of these primary neurons is promoted by the expression of cold or warm sensors, with the majority described to date coming from the transient receptor potential (TRP) channel family. These channels contribute to the conversion of thermal stimuli into electrical signals by allowing the entrance of sodium and calcium into the neurons, a process called sensory transduction[1,3,4].

The primary thermosensory neurons are pseudounipolar, meaning that their axons split and part of it innervates the skin and viscera, where it collects thermal information, and the other part projects to the secondary neurons in the dorsal horn (DH) of the spinal cord, to where it transmits the gathered information to the rest of the system, majorly via unmyelinated C-fibers[1,3,7]. In the spinal cord, the primary neurons synapse with secondary projecting neurons, whose axons cross from one side to another of the spinal cord. From there, these spinal projections carry contralateral thermal information to the brain, i.e. the thermal information from one side of the body is processed by the other side in the rest of

the thermoregulatory system. When the projections of secondary spinal neurons reach the brain, part of them reaches the somatosensory cortex via thalamus, a pathway implicated in thermal perception, while others branch off to the lateral parabrachial nucleus (LPB) to reach the preoptic area of the hypothalamus (POA), the network that mediates thermoregulation[1,4].

The POA is considered the thermoregulatory center. After receiving and integrating thermal information, this region regulates Tcore by coordinating the actions of downstream regions that promote autonomic and behavioral responses. These regions include the dorsomedial hypothalamus (DMH), raphe pallidus, and the ventral horn of the spinal cord[1,3]. Then, depending on the demand, if heat needs to be dissipated or generated, the thermoregulatory system will exert its function by autonomic responses, acting on brown adipose tissue (BAT) thermogenesis, shivering, evaporative cooling, and control of blood flow. In addition, it also drives changes in behavior accordingly[1].

For instance, using mice as an example, when exposed to warmth, animals need to remove the excessive heat gained from the exposure and decrease their own heat generation. This occurs by vasodilation and evaporating water through saliva spreading on the body surface, as well as by inhibiting shivering and BAT thermogenesis. Additionally, to increase the surface area for heat dissipation, they also extend their bodies. In contrast, an exposure to cold evokes vasoconstriction, shivering and activation of BAT thermogenesis, in addition to nest building[1,4]. All these mechanisms have the final goal of reaching thermal balance and keeping Tcore around the balance point, around 37°C in mice.

1.4 The preoptic area of the hypothalamus and thermoregulation

The hypothalamus has long been implicated in the control of body temperature in mammals, with studies from as early as the end of the 19th century supporting this hypothesis[8]. Local thermal stimulation and lesion studies performed in cats, monkeys, goats, and rats have since supported this notion, and narrowed the region to the POA

(figure 1.1)[9–15]. For instance, heating the POA region is sufficient to engage peripheral thermoregulatory responses, such as panting and sweating in cats[11]. In addition, lesions in the medial preoptic region of rats resulted in hyperthermia, with animals showing an increase in brain temperature[14].

Being the center of the thermoregulatory system, the POA is believed to work similarly to a thermostat: constantly receiving thermal information and triggering the needed adjustments to maintain Tcore around the balance point[4]. For this, this area is proposed to contain three categories of neurons: thermoresponsive, which respond to peripheral temperature; thermosensitive, defined as neurons that change their activity – action potential firing rate – upon thermal stimulation[16,17]; and thermoregulatory, whose stimulation regulate body temperature, by eliciting adaptations. It is currently unknown if all these neuronal categories overlap[18,19]. On top of its role in thermoregulation, the POA has also been involved with other functions. These include the control of water consumption[20,21], as well as the regulation of some behaviours, such as hunting[22], parenting[23], and reproduction[23].

The POA location in the brain is very strategic for the regulation of body temperature, being reachable to several modulatory inputs. The area is part of an intricate neural circuitry, receiving inputs from the periphery, brought by the LPB[24–26]. It also receives central projections from neuroendocrine regions, such as the paraventricular nucleus of the hypothalamus (PVH), and from other regions related to homeostasis and emotional processing, such as the lateral hypothalamus (LHA) and the bed nucleus of stria terminalis (BNST), respectively[23]. On top of this, the POA position allows ready access to molecules coming from the cerebrospinal fluid (CSF) and the blood, as it surrounds the third ventricle and a structure that lacks the endothelial protection of the blood brain barrier (BBB) and have fenestrated capillaries instead, the organum vasculosum of the lamina terminalis (OVLT)[27]. All of these potentially make this region more accessible to modulation by neural and molecular inputs. The neural inputs would come from axonal

afferents[24–26], and the molecular, from diffusion in the interstitial fluid (ISF) and the CSF, and from the bloodstream[27].

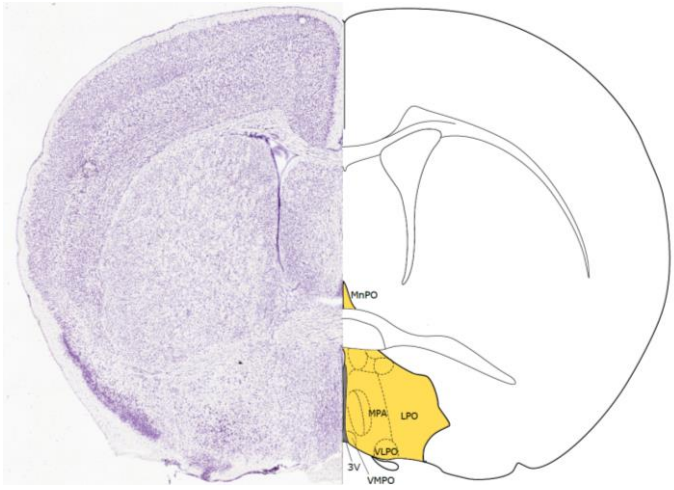

Figure 1.1: The preoptic area of the hypothalamus in a coronal brain section

The figure was adapted from the mouse brain reference atlas of the Allen Institute[28] (the left side, Nissl staining) and from Franklin and Paxinos, 2008 (the right side). 3V: third ventricle, LPO: lateral preoptic area, MnPO: median preoptic nucleus, MPA: medial preoptic area, VLPO: ventrolateral preoptic nucleus, and VMPO: ventromedial preoptic nucleus.

The recent years have seen many studies dissecting the preoptic cellular components. Based on such studies, several molecular markers for thermoregulatory neurons and/or neurons responsive to peripheral temperature have been found[20,29–34]. These include the vesicular glutamate transporter 2 (VGLUT2)[20,29], pituitary adenylate cyclase-activating polypeptide (PACAP) and brain-derived neurotrophic factor (BDNF)[35], leptin receptor (Lepr), pyroglutamylated RFamide peptide (QRFP)[30], and Opsin 5 (Opn5)[33]. Together, these cell subpopulations, which are hypothesized to at least partially overlap[18,19,36], contribute to the preoptic circuitry regulating body temperature.

1.4.1 Glutamatergic VGLUT2 neurons of the POA

Preoptic VGLUT2 (POA^{VGLUT2}) neurons have been shown by different reports to play a role in thermoregulation[20,29,37]. VGLUT2 acts as vesicular transporter of the

neurotransmitter glutamate, therefore marking excitatory neurons. When these POA glutamatergic neurons were stimulated by chemogenetics[29,37], there was a decrease in T_{core}. In agreement, using optogenetic stimulation on POA^{VGLUT} neurons, it was observed a decrease in heart rate along with a drop in body temperature[20]. VGLUT2 was also found to highly colocalize with other thermoregulatory neurons at the POA, such as the Lepr+[38], Opn5+[39], and QRFP+[30], where '+' means neurons in which these genes are expressed. Lepr was shown to colocalize with VGLUT2 by immunostaining done on POA slices of mice expressing enhanced yellow fluorescent protein (Vglut2-EYFP)[38], whilst Opn5[39], and QRFP[30], were both demonstrated to be colocalized at the messenger RNA (mRNA) level. The ablation of VGLUT2 neurons in a subregion of POA, the MnPO (shown in figure 1.1), led to an increase in Tcore during warm exposure to 37°C. However, no effect was seen when mice were exposed to a cold temperature, at 4°C, suggesting that these neurons are rather required when the body needs to defend the Tcore during a warm challenge. This is in agreement with the hypothermic effect upon glutamatergic activation mentioned above. Additionally, POA^{VGLUT2} neurons project to brain regions involved with thermal homeostasis, such as the raphe pallidus (RP), the DMH, and the PVH[21]. Taken together, all these studies indicate glutamatergic preoptic neurons as being a foremost POA subpopulation engaged in thermoregulation.

1.5 Warm and cold sensation

Some specifications in the thermoregulatory system enable to differentiate between warm and cold, starting from molecular sensors expressed at the primary thermosensory neurons. While TRPM8 is established as the main cold-sensitive receptor, TRPV1 and TRPM2 are suggested to detect warm information[1,4,40,41]. Differences are also seen at the level of DH spinal neurons, with a calcium imaging study showing differential engagement of these neurons to either warm or cold, with some of them responding to both[42]. Segregation of thermal information is also seen at the LPB, with warm stimulus increasing activity of neurons present at the dorsal subdivision of LPB (LPBd)[25] and cold stimulus majorly activating external lateral LPB (LPBel) neurons[26]. Finally, warm or cold

ambient temperature stimulation also activate POA neurons dissimilarly[43,44]. Together, these observations point to the existence of divergent transmission of warm and cold thermosensory information.

1.6 Neuroactive peptides

More than 100 peptides have been classified as neuropeptides, i.e. peptides produced in the brain, released in a regulated manner, and involved in cell-cell communication. Given the incredible complexity of nervous systems, it comes with no surprise that those are not the only regulatory peptides to act in the brain. On top of those, some peptide hormones, which are produced by peripheral organs and released in the bloodstream to signal between different organs, also have the central nervous system (CNS) as their target[45]. For simplicity, throughout the thesis, I will refer to neuropeptides and peptide hormones that act in the brain as neuroactive peptides. Together, these molecules play an important role in the regulation of different physiological and behavioural processes, including sleep, feeding, and reproduction[2,46].

Typically, a neuroactive peptide is produced as a precursor, an amino acid sequence that contains one or more bioactive peptides and a signal peptide (SP). The former are peptides with cell communication functions, the latter is an N-terminal sequence that directs the precursor to the secretory pathway[45]. Inside a secretory large dense core vesicle (LDCV), the precursor is cleaved into smaller peptides by enzymatic action of peptidases in specific cleavage sites (Table 1.1), producing the mature forms of neuroactive peptides. In addition, other posttranslational modifications may occur, such as C-amidation[45].

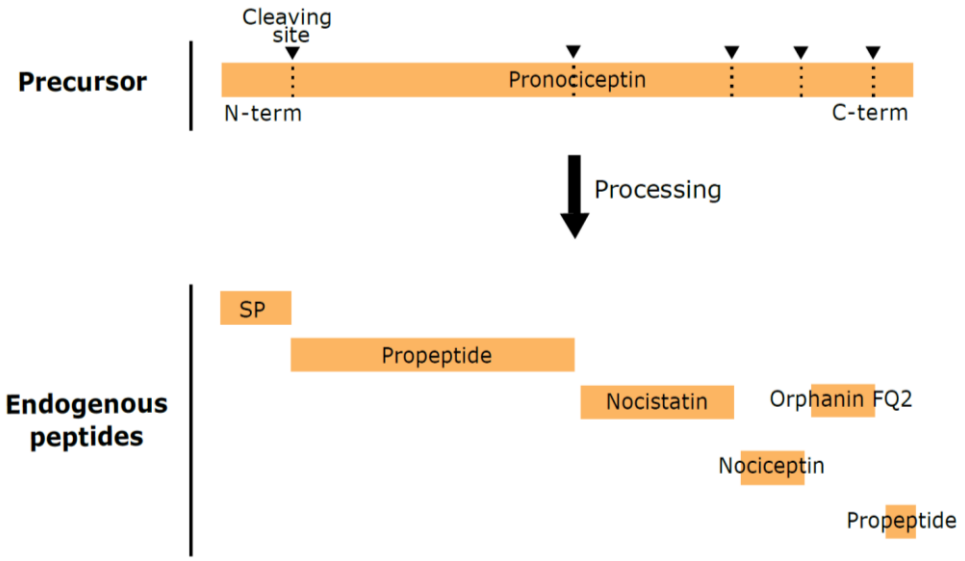

Figure 1.2: Neuroactive peptide processing

The scheme represents how a precursor of neuroactive peptide is processed into smaller endogenous peptides.

Table 1.1: Cleavage pattern of the main peptidases involved in neuropeptide and peptide hormone cleavage

Peptidase	**Cleavage pattern(s)**
Prohormone convertase 1	-Arg-Arg- -Lys-Arg-
Prohormone convertase 2	-Arg-Arg- -Lys-Arg-
Carboxypeptidase E	-Arg (C-term) -Lys (C-term)
Carboxypeptidase D	-Arg (C-term) -Lys (C-term)
Furin	Arg-Xaa-Arg-Arg- Arg-Xaa-Lys-Arg- Arg-Xaa-Xaa-Arg-

The release of neuroactive peptides from LDCVs into the extracellular space is favoured upon an increase in cytoplasmic calcium levels. On top of the release at synapses, LDCVs can also be released extrasynaptically[2]. Additionally, they are able to diffuse to long distances through the CSF, in a process called volume transmission[2,45,47,48]. Neuroactive

peptides usually act on G-protein coupled receptor(s) (GPCRs), which are typically specific to each peptide. The interaction between a neuroactive peptide and its receptor(s) promotes a conformational change in the receptor, what further activates the G protein signalling cascade. Through this mechanism, they are able, for instance, within seconds or minutes, to directly regulate neuronal activity, either increasing or decreasing it, depending on the G protein coupled to the receptor. In addition, neuroactive peptides can influence gene expression within hours to days[2]. Hence, neuropeptides represent an additional layer of modulation of neural transmission and plasticity.

1.7 Neuroactive peptides and preoptic thermoregulation

Despite the cellular and anatomical efforts in characterizing the thermoregulatory system, especially the POA, the molecular mechanisms that modulate body temperature remain elusive. As mentioned above, the POA location is accessible to several modulatory inputs, including projections from different brain areas, and molecules coming from the CSF and the blood. In this context, it is reasonable to postulate that neuroactive peptides could act in the POA to modulate Tcore.

Different lines of evidence support the hypothesis of a peptidergic modulation of thermoregulation. Injection studies of neuroactive peptides and their antagonists into the POA or the ventricles have suggested a few thermoregulatory candidates. These studies have demonstrated that some peptides can lead to hypothermia, such as neuropeptide Y (NPY), cocaine and amphetamine related transcript (CARTPT), and angiotensin II (AT-II), or hyperthermia, such as orexin-A, somatostatin-28 and, thyrotropin-releasing hormone (TRH) (Table 1.2)[49–53]. Although important, these injection studies have limitations. First of all, they measured the effect of a molecule being introduced in an unnatural manner: it is not known whether and under which situations these peptides are actually released and what their native function may be in the context of thermal homeostasis. In addition, the effect of the peptide on Tcore may be dose-dependent, as shown by a study with injection

of neurotensin into the POA in rats. While a higher dose (5 μg) induced hypothermia, lower doses (5 ng and 50 ng) increased body temperature[52]. Additionally, some infusion studies only measured the impact of the peptide on temperature, without considering other parameters, such as food intake and locomotor activity[49,52], which influence body temperature. Therefore, the temperature changes could be a by-product of the peptides' action on another physiological process, such as feeding or locomotion. Finally, this type of study requires *a priori* knowledge regarding the peptide identity, thus biasing the investigations to certain peptides. Taking all these limitations into consideration, intracerebroventricular (i.c.v.) and POA injection studies still provide a list of possible peptides that may play a role in the control of Tcore.

Based on a different approach, differential expression (DE) analyses found that thermal challenges can alter the transcription rate of certain peptidergic genes in the POA (Table 1.3). For instance, the RNA sequencing (RNA seq) of POA neurons activated by four-hour 37°C stimulation identified higher expression of genes encoding precursors of PACAP, BDNF, urocortin 3 (Ucn3), TRH, and corticotropin-releasing hormone (Crh)[35]. Using a similar strategy, but applying 38°C of stimulation, another report also detected higher levels of the genes of PACAP, BDNF and CRH. In addition, it also found galanin (Gal) and neurotensin (Nts) to be upregulated upon warm challenge. However, it is important to mention none of the DE analyses investigated the neuroactive peptides besides the mRNA level. Therefore, it is still elusive if these peptides are naturally released at the POA during thermal challenges.

Altogether, those studies suggest that different peptides may be involved in thermoregulation in the hypothalamus. However, based on the current literature, it is still elusive if those or other peptides are released at the POA in order to adapt to thermal challenges.

Table 1.2: Putative thermoregulatory peptides as suggested by brain injection studies

Gene	Peptide	Evidence supporting influence on Tcore	Reference(s)
Peptides that increased Tcore			
Hcrt	Orexin-A	• I.c.v. injection in rats	[50,54]
Hcrt	Orexin-B	• I.c.v. injection in rats	[54]
Pomc	Beta-endorphin	• I.c.v. injection in mice • POA injection in rats	[55,56]
Sst	Somatostatin	• I.c.v. injection in rats • Intracisternal injection in mice	[49,57]
Trh	Thyrotropin releasing hormone	• POA injection in rats • I.c.v. injection in mice • Intraperitoneal injection in mice • Increased mRNA expression upon peripheral warm stimulation in mice	[35,58–60]
Peptides that decreased Tcore			
Cartpt	Cocaine and amphetamine related transcript	• I.c.v. injection in rats	[61]
Npy	Neuropeptide Y	• I.c.v. injections in rats • I.c.v. injections in mice	[62,63]
Pdyn	Dynorphin-A	• I.c.v. injections in rats	[64]
Agt	Angiotensin II	• I.c.v. injections in rats	[65]
Pnoc	Nociceptin	• I.c.v. injections in rats	[66]
Peptides with unclear thermoregulatory effect			
Nts	Neurotensin	• Injection of 10 μg to 30 μg in the cisterna magna leads to hypothermia in mice • Injection of 5 μg in the POA leads to hypothermia in rats • Injection of 5 ng and 50 ng in the POA leads to hyperthermia in rats	[52,67]

Avp	Vasopressin	• I.c.v. injection leads to hypothermia in rats • POA injection leads to hyperthermia in rats • MnPO injection leads to hypothermia during dark phase in rats	[53,68]
Penk	Met-enkephalin	• 100 μg i.c.v. injection led to hyperthermia • 400 μg i.c.v. injection led to hypothermia • No effect observed in mice	[57,69]
Adipoq	Adiponectin	• POA injection in mice leads to hyperthermia • Cold exposure in one knockout model is accompanied by hypothermia • Cold exposure in another knockout model is accompanied by hyperthermia	[70–72]

Table 1.3: Putative thermoregulatory peptides as suggested by DE analyses

Differential mRNA expression of peptidergic genes upon peripheral thermal stimulation			
Adcyap1	Pituitary adenylate cyclase-activating polypeptide	• Increased upon warm stimulation	[35,73]
Bdnf	Brain derived neurotrophic factor	• Increased upon warm stimulation	[35,73]
Crh	Corticoliberin	• Increased upon warm stimulation	[73]
Gal	Galanin	• Increased upon warm stimulation	[73]
Ghrh	Somatoliberin	• Increased upon warm stimulation	[35]
Nms	Neuromedin S	• Increased upon warm stimulation	[73]

Nts	Neurotensin	• Increased upon warm stimulation	[73]
Pmch	Melanin concentrating hormone	• Increased upon warm stimulation	[73]
Trh	Thyrotropin releasing hormone	• Increased upon warm stimulation	[35]
Ucn3	Urocortin-3	• Increased upon warm stimulation	[35]

1.7.1 Orexins and thermoregulation

The gene Hcrt encodes a protein of 130 amino acids that is further processed into the mature peptides Orexin-A (33 amino acids) and Orexin-B (28 aas). Orexins are exclusively synthesized in neurons whose cell bodies are localized at the LHA and the perifornical area. Such neurons innervate different regions throughout the brain, including other parts of the hypothalamus, the cerebral cortex, thalamus, and brain stem[74–76].

In addition to a well described role in the control of sleep and wakefulness[46,77,78] and food intake[79,80], orexins have also been suggested to participate in thermoregulation. In agreement with this hypothesis, injection of orexin A into the brain ventricles leads to hyperthermia in rats[50,54]. Orexin-B may also have an effect, but this is still unclear. While one study observed that this peptide led to an increase in Tcore[54], another found no change in body temperature[81]. Compatible with a role of orexins in the regulation of Tcore, several areas related to thermoregulation are innervated by orexin neurons and express at least one of the orexin receptors, orexin receptor 1 (OX1R) or orexin receptor 2 (OX2R). Among these areas, the POA, dorsal raphe, and the periaqueductal gray[76,82,83]. Thus, these studies suggest orexins as possible thermoregulatory peptides.

Despite of these findings, orexin knockout mice and orexin-neuron ablated mice have normal Tcore at room temperature (RT), indicating that neither the peptides alone nor the cells that produce them are essential for Tcore maintenance. However, when challenged

with a cold stimulus of 5°C, orexin neuron-ablated mice fail to maintain their Tcore in comparison to wild type (WT) mice[84]. This suggests that these neurons are crucial for Tcore upon cold stimulation. Conversely, orexin knockout mice are as capable as WT mice of keeping their Tcore upon cold challenge[84], suggesting that orexin peptides are not critical for this. However, in both animal models, mice have global orexin deficiency since birth, what may disturb other homeostatic systems that influence thermoregulation, as orexins play an important role in sleep[46,78,79] and food intake[79,80]. Also, the absence of orexins' inputs to different regions makes it difficult to distinguish where the effect of orexins on Tcore, as suggested by the injection studies, could come from. Thus, it remains elusive if orexinergic signaling at the POA is relevant for keeping Tcore during cooling of adult healthy animals.

1.7.2 Adiponectin and thermoregulation

Adiponectin (Adipoq) is a hormone secreted by the adipose tissue. Based on its size (mature form: 230 amino acids), this molecule is considered a protein. Nevertheless, it is included in a reference database[85] as a neuroactive peptide, thus I will refer to it here as one of these molecules. This hormone acts in different organs, including the brain, via its receptors, adiponectin receptor 1 (Adipor1) and adiponectin receptor 2 (Adipor2)[86,87]. According to the data coming from a single cell sequencing (scRNA-Seq) of the preoptic area[88], both receptors of adiponectin are expressed in the POA, especially in neurons and mature oligodendrocytes. Adiponectin is considered to be involved with insulin metabolism and inflammation, and the recent literature also suggests a role in thermogenesis[87].

Two studies have implicated adiponectin in the adaptation to cold exposure. Evaluating Adipoq knockout male mice, a study observed that despite having a normal Tcore at room temperature, the animals were unable to keep the body temperature under cold challenge comparing to wild type animals. Six hours of exposure to 4°C decreased 6°C of Tcore in the transgenic mice[72]. In agreement with a possible role of adiponectin in cold adaptation,

another work reported that 6°C stimulus increased adiponectin levels in the subcutaneous white adipose tissue (WAT) of male mice after six hours at the mRNA level, and after six days at the protein level. However, the plasma levels of adiponectin were found decreased upon cold exposure for six days. Nevertheless, the same study also evaluated the role of adiponectin on the browning of the WAT, a process that transforms white adipocytes, which are responsible for energy storage, into brown-like adipocytes, which have the capacity to produce heat. Interestingly, the authors observed WAT browning to be increased in WT male mice exposed to 6°C for six days in comparison to Adipoq knockout animals[89]. Thus, together, these two studies suggest that adiponectin could be a thermogenic hormone that helps in the adaptation to cold.

On the other side, the hypothesis that adiponectin increased thermogenesis has been challenged with another study that also exposed Adipoq knockout male mice to 4°C for four hours. In this case, the lack of adiponectin prevented the hypothermia induced by cold exposure that was observed in WT animals[71]. Noteworthy, this study used an adiponectin knockout model with insulin resistance, differently from the other report described above[72], thus, the divergent results could come from this discrepancy. Nevertheless, more studies are needed to clarify if adiponectin plays a role in thermoregulation.

1.8 Methodology used

1.8.1 Techniques to study neuropeptide release *in vivo*

Neuroactive peptides play an important role in the regulation of different physiological and behavioural processes, being relevant in healthy and diseased contexts. Because of that, there is much interest in studying them. However, they are challenging to investigate, due to low extracellular levels (pico- to femtomolar levels), rapid degradation, adsorption of these molecules to surfaces (i.e. tubings and probe), and complexity in regard to their synthesis, release, and action [90–92]. In spite of this, several technical advances

have been made to probe these molecules through three main aspects: structure, location, and function. Structural analyses have enabled the discoveries of new peptidergic sequences and secondary structures. Further investigations have provided valuable information concerning the tissue distribution of neuroactive peptides and the components of their signalling pathways. Finally, *in vivo* and *in vitro* functional studies have implicated many neuroactive peptides in different behavioural and physiological processes[90].

Since this thesis was focused in exploring peptides released during thermal challenges and possibly involved with thermoregulation, I considered different techniques that could be used to detect these molecules in freely behaving mice. Among them, *in vivo* sampling techniques, *in vivo* voltammetry, or genetically encoded GPCR fluorescent sensors.

In vivo sampling techniques have the great advantage of allowing the simultaneous collection of multiple substances of interest present in the ISF[93,94]. Nevertheless, since samples take minutes to hours to be collected, this technique has low temporal resolution. On the other hand, *in vivo* voltammetry, which estimates the concentration of a specific molecule based on its redox characteristics[95], has higher temporal resolution, ranging from milliseconds to seconds. However, with this method, only one compound can be evaluated at each time[93]. Finally, GPCR sensors signal the detection of a molecule of interest upon ligand binding to the cells that express the sensor[96–98]. These sensors have just recently been used to track neurotransmitter dynamics *in vivo*[96–98]. Preliminary results have suggested that this strategy could also be applied to peptide receptors[97]. Although promising, this approach is still in its first steps, and more studies are needed to popularize this technique for neuroactive peptides' detection. Taking in consideration all these available techniques, as my aim was to perform an unbiased screening of several peptides, I opted for *in vivo* sampling. Therefore, I explain this method in more detail below.

In vivo sampling techniques: microdialysis and open flow microperfusion

In vivo sampling techniques, such as microdialysis and open-flow microperfusion (OFM), are used to collected molecules of interest from the ISF of alive animals[93,94]. In such methods, a probe with an inlet and outlet is implanted at the region of interest, which is constantly perfused with a liquid of similar composition to the extracellular medium.

In microdialysis, the tip of the probe has a membrane with a defined molecular weight cut-off (MWCO), and molecules smaller than the MWCO pass through this membrane by diffusion[93] (figure 1.3). For instance, the device I used in my experiments had a 1000 kDa MWCO, thus molecules smaller than this size are expected to be able to cross the membrane.

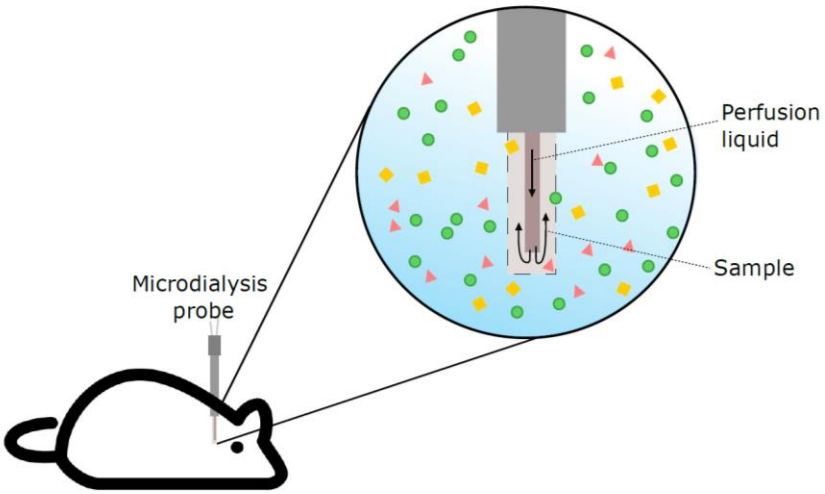

Figure 1.3: Brain microdialysis in mouse

The scheme represents a microdialysis sampling from the brain. Through a microdialysis probe implanted in the tissue, by diffusion, molecules present in the interstitial fluid and smaller than the MWCO of the probe membrane can be sampled. The arrows indicate the direction of the perfusion fluid and the sample.

In contrast, OFM probes have no membrane (figure 1.4). Instead, their tips have macroscopic openings that allow an unrestricted access to the whole ISF. Thus, with this probe it is possible to sample a wider range of molecules present in ISF[94,99]. The membrane-

free structure of OFM offers the possibility of collecting nearly all diffusible molecules present in the extracellular space around the probe, in opposition to the 1000 kDa probe. However, I hypothesize that this same feature could bring more complexity to OFM samples, turning them more difficult to analyse. For instance, highly abundant proteins could hinder the detection of low-abundance neuroactive peptides[100]. Therefore, the application of one of these techniques depends on the research question and the specific technical aspects have to be taken in consideration when choosing one over the other.

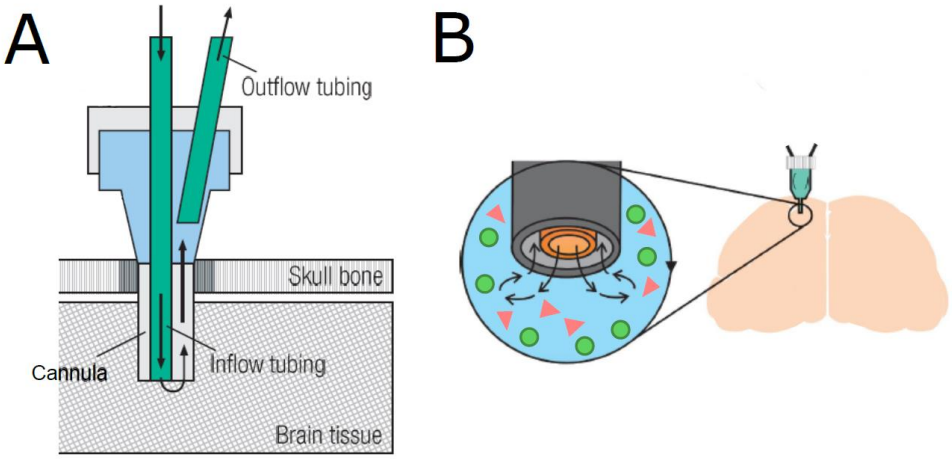

Figure 1.4: Brain microperfusion

A: The scheme represents an open flor microperfusion (OFM) probe implanted in the brain. The arrows on the left diagram indicate the direction of the perfusion fluid and the sampling. B: Microperfusion sampling from the brain occurs through a membrane-free probe, at the tip of it, as represented here in detail. Figures adapted from the OFM manufacturer's webpage[101].

In both techniques, the sample (perfusion fluid and ISF molecules) is collected through a tubing attached to the outlet. In the case of 1000 kDa microdialysis probes and OFM probes, since these devices have large openings, they are prone to perfusate leakage into the tissue. Therefore, a push-pull system, composed of a syringe pump (push force) and a peristaltic pump (pull force), has to be used for both of them in order to prevent this and to achieve more consistent and stable sample volumes[102].

Microdialysis with 1000 kDa probe has been used to collect several peptides, such as CRH and ghrelin. They have been sampled from the BNST of rats and from the LHA of mice, respectively[103,104]. Using OFM device, leptin injected peritoneally has been collected at the hypothalamus of mice[105], and tumor necrosis factor alpha, interleukins 6 and 10 have been collected from the frontal cortex of rats[99]. Therefore, both techniques have been shown to be suitable for neuroactive peptide sampling.

Detection of neuroactive peptides in samples collected *in vivo*

As mentioned above, several reports have described the presence of neuroactive peptides in samples collected by *in vivo* sampling, either using microdialysis or OFM. Nevertheless, in addition to the low brain concentrations of these signaling peptides, the samples collected with these two probes are more diluted than the ISF, making the detection of peptides in these samples very challenging. Because of these reasons, highly sensitive and targeted methods, such as radioimmunoassay (RIA) and targeted liquid chromatography-mass spectrometry (LC-MS), have mostly been preferred to analyze these types of samples[106]. Using one of these two analytical methods, researchers have been able to detect, among other examples, NPY[107], NTS[108], orexin-A[109], CRH[103], leptin[105], and ghrelin[104].

In contrast, unbiased methods have not been largely explored to analyze samples collected with microdialysis or OFM. The unbiased profiling of neuroactive peptides requires a high-throughput approach, which is able to analyse hundreds of proteins and peptides present in the same sample. Additionally, due to the lowly concentrated nature of the peptides of interest, the analytical method of choice needs to have high sensitivity. Considering these two main points, proteomics approaches are well suited for the analysis of those samples[90]. Because of that, one of these techniques, namely liquid chromatography tandem mass spectrometry (LC-MS/MS), was my method of choice to analyse the samples.

In LC-MS/MS applied to proteomics, peptides present in samples are separated on the basis of their hydrophilicity by liquid chromatography (LC). In sequence, peptides eluted from the LC are then identified in the tandem mass spectrometry (MS/MS). More specifically, firstly, the peptides are ionized. Then, they are separated in the first stage of MS based on their mass to charge ratio (m/z), due to an electric or magnetic field present in the mass spectrometer. In the second MS stage, isolated peptide ions are fragmented by collisions with an inert gas and their mass spectra are generated[100,110]. Following these steps, peptides are separated and identified with LC-MS/MS.

To my knowledge, only one study has applied this technique to unbiasedly analyse brain microdialysates collected *in vivo* from rodents. In this work, the authors have managed to detect peptides from 85 proteins, including the neuroactive peptides proenkephalin A (PENK-A), neuropeptide Y, somatostatin and cholecystokinin, from the rat striatum[111]. Thus, based on this report, it should be possible to perform an unbiased profiling of peptides collected with *in vivo* sampling.

1.8.2 Techniques to stimulate or record from a specific cell population

Chemogenetics

Chemogenetics is a molecular tool in which a protein (e.g. a receptor or an enzyme) is engineered to interact with a biologically inert ligand. When this protein is expressed by a cell, the binding of the exogenous ligand elicits a response, depending on the type of designed protein. In this thesis, I used one class of these proteins, namely Designer Receptors Exclusively Activated by Designer Drugs (DREADDs). In this case, a GPCR is engineered to bind to an inert compound. The type of G protein dictates the kind of cell modulation. For instance, if the engineered GPCR is coupled to a Gq protein is expressed in a neuron, the Gq signalling cascade of this neuron is expected to be activated upon binding to the inert ligand, thus activating this cell[112]. DREADDs gain another level of control when the protein expression is driven by a recombinase, like cre, in a given cell

population, e.g. neurons that express VGLUT2. This gives specific access to stimulate or inhibit a target population[112].

Genetically encoded calcium indicators

Inside cells, calcium (Ca^{2+}) acts as second messenger in several signaling pathways. In neurons, among other functions, such as the regulation of gene transcription, Ca^{2+} is essential for classical neurotransmission. Upon neuronal excitation, an influx of Ca^{2+} leads to the release of synaptic vesicles containing neurotransmitters. Because of this, Ca^{2+} intracellular fluctuations can be used to infer neural activity[113]. Such calcium dynamics can be investigated using calcium-sensing molecules. Among these, genetically encoded calcium indicators are very useful and have the possibility of being expressed in a target population, for instance, driven by cre recombination. These indicators have a calcium-binding domain attached to one or two fluorescent proteins, whose fluorescence changes upon calcium binding. One example of these indicators is GCaMP, a family of calcium sensors, composed by green fluorescent protein (GFP) fused to calmodulin. Upon binding to Ca^{2+}, a conformational change occurs in GCaMP, increasing the intensity of fluorescence coming from GFP[114,115].

1.9 Aim of this study

In mammals, keeping the core body temperature (Tcore) around a balance point is essential for their survival. The Tcore maintenance is promoted by the thermoregulatory system and coordinated by the POA. Despite several efforts to elucidate how Tcore is regulated, specifically at the POA, the molecular processes that modulate this region still remain elusive. In this thesis, I hypothesized that neuroactive peptides contribute to the regulation of Tcore, by being released and acting at the POA. To investigate this, I performed an unbiased screening of neuroactive peptides that arrive at the preoptic

region and correlated this with three different thermal stimuli. Specifically, I wanted to address the following questions:

- Which neuroactive peptides are released at the POA?
- During the stimulation of VGLUT2 thermoregulatory neurons, are neuroactive peptides differentially secreted at the POA?
- Does the POA receive differential peptidergic inputs during warm or cold thermal challenges?
- Is there any difference between neuroactive peptides released at the POA during central thermoregulatory neuron activation or peripheral thermal stimulation?
- Are neuroactive peptides released at the POA capable of modulating POA neurons?

CHAPTER 2: MATERIALS AND METHODS

2 MATERIAL AND METHODS

2.1 Materials

2.1.1 Primers

Table 2.1: Primers used

Primer	Animal line	Sequence
iCre - forward	Vglut2cre	5′ AGA TGC CAG GAC ATC AGG AAC CTG 3′
iCre - reverse	Vglut2cre	5′ ATC AGC CAC ACC AGA CAC AGA GAT 3′
LRC –forward	LepRcre-HTB	5′ TCC AAG AAG CCT CAA GGT TCC A 3′
LRC - reverse	LepRcre-HTB	5′ ACG CAC ACC GGC CTT ATT CC 3′

2.1.2 Antibodies

Table 2.2: Antibodies used

Name	Source	Identifier
Rabbit Anti-OX2R	Millipore	AB3094
Rabbit polyclonal anti-mCherry	Abcam	ab167453
Rabbit monoclonal anti-BDNF	Abcam	ab108319
Peroxidase Goat Anti-Rabbit IgG (H+L)	Jackson ImmunoResearch	RRID: AB_2307391
Rabbit polyclonal anti-Orexin-A/B	Santa Cruz Biotechnology	sc-28935
Chicken polyclonal anti-GFP	Novus Biologicals	NB100 1614
Cy™3 Donkey Anti-Chicken IgY (IgG) (H+L)	Jackson Immuno research	RRID: AB_2340363
Goat Anti-Rabbit IgG (H+L), Alexa-647	Life Technologies	A21244

2.1.3 ELISA kits

Table 2.3: ELISA kits used

Name	Source	Identifier
Mouse Adiponectin/Acrp30 Quantikine ELISA Kit	R&D systems	MRP300
Mouse OXA(Orexin A) ELISA Kit; 96-Strip-Wells	MyBioSource	MBS2505504 96T

2.1.4 Adeno-associated viruses (AAVs)

Table 2.4: AAVs used.

Name	Sorotype	Source	Catalog number
pAAV-hSyn-DIO-hM3D(Gq)-mcherry	AAV8	Addgene	44361-AAV8
pAAV1.CAG.Flex.GCaMP6s.WPRE.SV40	AAV1	Addgene	100842-AAV1
ssAAV-1/2-hSyn1-chl-iCre-WPRE-SV40p(A)	AAV-1/2	Viral Vector Facility (VVF), University of Zurich	v223

2.1.5 Chemicals, drugs, peptides and recombinant proteins

Table 2.5: Chemicals, drugs, and recombinant proteins used.

Name	Source	Catalog number
Paladur Powder	Kulzer	032143
Paladur liquid	Kulzer	032136
Silver nitrate ≥99,9 %, for staining of proteins, Proteicolor®	Carl Roth	6207.1
NaCl 0,9%	B.Braun	1002575
Ringer Infusionslösung 500 ml Ecoflac	B.Braun	3310950
SB 334867	Hello Bio	HB2913-10mg
Seltorexant	MedchemExpress	HY-109012
CNO	Enzo	BML-NS105-0025
Sedin® Medetomidine hydrochloride 1 mg / mL solution for injection	Vetpharma	N/A
Dormicum® - Midazolam 15 mg/3 mL solution for injection	Roche	N/A
Fentanyl®-Piramal 0.1 mg solution for injection	Piramal Critical care	N/A
Flumazenil Kabi 0.1 mg/mL	Fresenius Kabi	N/A
Naloxon Inresa 0.4 mg/mL solution for injection	Inresa Arzneimittel GmbH	N/A
Atipazole - Atipamezole hydrochloride 5 mg/mL	Prodivet	N/A
Carprosol – Carprofen 50 mg/mL	CP-Pharma	N/A
Rompun® 2% - Xylazin solution for injection	Bayer	N/A
Ketamine 10% - Ketamine solution for injection	Medistar	N/A
Bepanthen®	Bayer	N/A

Hair Removal Cream for Sensitive Skin	Veet	N/A
Orexin-A (human, rat, mouse)	Tocris	1455
Recombinant Human BDNF	PeproTech	450-02

2.1.6 Consumables

Table 2.6: Consumables used.

Name	Source	Catalog number
Dako Pen, Delimiting pen	Agilent - Dako	S200230-2
Sugi Saugstreifen 62x4 mm	Kettenbach	31301
Tissue-Tek O.C.T. Compound	Sakura Finetek	4583
Solid Drink®	Triple A Trading	SDBU-150
NuPAGE™ 4-12% Bis-Tris Protein Gels, 1.0 mm, 15-well	ThermoFisher Scientific	NP0323BOX
Amersham™ ECL™ Prime Western Blotting Detection Reagent	Amersham-GE Healthcare	RPN2232
Pierce™ BCA Protein Assay Kit	Thermo Fischer Scientific	23225
Immu-Mount	Thermo Fischer Scientific	9990402
Oasis PRiME HLB 96-well μElution Plate, 3 mg Sorbent per Well, 1/pk	Waters™	186008052
AtmosLM™ Dummy Probes, PED-X	Amuza Inc.	PED-4
AtmosLM™ Guide Cannulae, PEG-X	Amuza Inc.	PEG-4
AtmosLM™ Peptide Microdialysis probe with sterilization	Amuza Inc.	PEP-6-02
Cap Nut	Amuza Inc.	AC-5
Cerebral OFM Probe	Joanneum Research	cOFM-P-6-2
Mouse screw packet 100 screws	Plastics1	00-96x1/16
FEP Tubing 1m x 10/pkg	Harvard Apparatus	8409501
Tygon ST 0.13 mm ID tubing	ISMATEC	SC0189
Tygon ST 0.25 mm ID tubing	ISMATEC	SC0050
Tubing adapter pack of 10	Harvard Apparatus	3409500
BLAUBRAND® disposable micropipettes, intraMark	BRAND®	7087 07
TA-F10 Mouse Temperature Transmitter	Data Sciences International	TA11TA-F10

2.1.7 Surgical tools and other devices

Table 2.7: Surgical tools and other devices used.

Name	Source	Catalog number
Dissecting Scissors, straight, 10cm straight	World Precision Instruments Germany	14393-G
Dressing forceps, 12.5 cm, serrated, straight	World Precision Instruments Germany	501217
#76 Drill .310" LOC 130 PT	Kyocera Precision Tools	105-0200.310
Student Bone Scissors	Fine science tools	91604-09
Syringe 2.5 mL for CMA pump	Harvard Apparatus / Hugo Sachs	8309021
AtmosLM™ Stereotaxic Adaptor, PESG-X	Eicom - Amuza Neuroscience	PESG-X
22 gauge dual channel swivel for microdialysis with mice	Harvard Apparatus	72-0000
3.5 inch adjustable spring counter-balance lever arm	Harvard Apparatus	61-0024
Head block tether for mice	Harvard Apparatus	61-0037
ThermoLux® Wärmeunterlagen	Thermolux	461265
Pedalhink EKO Luna 3 litres stainless steel	EKO	N/A
Masterflex L/S® Precision Pump Tubing, Platinum-Cured Silicone, L/S 16	Masterflex®	96410-16
Non-Slip Carpet Stopper	TROP	N/A

2.1.8 Equipments

Table 2.8: Equipments used.

Name	Source	Catalog number
CMA 4004 syringe pump, 4-SYR	Harvard Apparatus	400400
Peristaltic pump Reglo ICC ISM 4208	ISMATEC	ISM 4208
Data exchange matrix	Data Sciences International	N/A
DSI PhysioTel® Receivers – RSC-1 for Specialty Applications	Data Sciences International	RSC-1
DSI PhysioTelTM Receivers – RPC-1 for Mice and Small Animals	Data Sciences International	RPC-1
Stereotaxic Alignment System	David Kopf Instruments	1900
Cooling incubator	Binder	KB 720
Haake heating circulator bath	Haake	DC1-B3
ARCTIC A10 Refrigerated circulator	ThermoFisher Scientific	155-5108
Leica SM 2010R microtome	Leica Biosystems	2010R

Leica Cryostat CM3050S	Leica Biosystems	CM3050S
XCell II™ Blot Module	Thermo Fischer Scientific	EI9051
Xcell SureLock TM mini cell system	Thermo Fischer Scientific	EI0001
ImageQuant™ LAS 4000	GE Healthcare	LAS 4000
CMA 110 liquid switch	Harvard Apparatus	8308200
C2+ confocal microscope	Nikon	N/A
Ni-E wide field microscope	Nikon	N/A
Plate reader Infinite M200 pro	Tecan	M200
Osada Success 40	Osada Electric Co., Ltd.	OS-40
Steri 350 Sterilizer	Inotech	Steri 350
Digital temperature controller	Conotec	Fox-1004
200S Readout System	Acu-rite®	200S 3X G

2.1.9 Software and algorithms

Table 2.9: Software and algorithms used.

Name	**Source**
R for Windows versions R-3.3.3 and R-4.0.3	R Consortium
RStudio	https://www.rstudio.com/
Metafluor Software	Molecular Devices
MetaMorph 7.1 Software	Molecular Devices
ImageJ/Fiji	ImageJ Consortium
GraphPad Prism for Windows V5.00	GraphPad software
Dataquest ART	Data Sciences International
Inkscape	Software Freedom Conservancy
MaxQuant version 1.6.2.6	https://www.maxquant.org/
NIS-Elements AR	Nikon
i-control version 1.12	Tecan
CNMF - CaImAn	https://github.com/flatironinstitute/CaImAn
Jupyter notebook	https://jupyter.org/

2.2 Methods

2.2.1 Mouse lines

Table 2.10: Mouse lines used.

Name	**Official nomenclature**	**Source**
Wildtype (WT)	C57BL/6NRj	IBF – Heidelberg University or Janvier labs

Vglut2cre	C57BL/6-Tg(Slc17a6-icre)10ki/Kctt	Borgius et al, 2010
LepRcre-HTB	$LepR^{Cre}$; $R26^{ds\text{-}HTB}$	LepR-cre mice (https://www.jax.org/strain/032457) crossed to the $R26^{ds\text{-}HTB}$ reporter line (Stam et al, 2012)

2.2.2 Animal housing

All experimental animals were housed under specific-pathogen-free (SPF) conditions at the interfacultary biomedical animal (IBF) housing of Heidelberg University. Before all the experiments, mice were transferred from the SPF barrier into the experimental rooms. In all these areas, the animals were kept at 12-12 hour day-night cycle (08:00-20:00), 22 ± 1°C, 50-60% humidity, unless otherwise specified. Mice had *ad libitum* access to water and food (Altromin Rod 16 or Rod 18 food pellets). All the experiments presented in this thesis were approved on the ethical protocols G169/18, T05/19, and T09/21.

2.2.3 Genotyping

Biopsy digestion of Vglut2cre and LepRcre-HTB mice tissue

For the genotyping of Vglut2cre and LepRcre-HTB mice used in experiments, tail or ear tissue biopsies were obtained by the staff of the animal facility. Biopsies were treated overnight at 56°C with proteinase K (0.3 mg) diluted in biopsy buffer (100 mM Tris, 5 mM EDTA and 0.2% SDS). At the next day, the proteinase K was inactivated by incubating the samples at 96°C for 10 minutes. Later, 350 µl double distilled water (ddH_2O) were added to each sample vial. The samples were maintained at 4°C until the genotyping.

Polymerase chain reaction (PCR)

Digested biopsies from Vglut2cre and LepRcre-HTB mice were diluted in a PCR master mix, containing PCR buffer (45 mM Tris pH 8.8, 3.5 mM $MgCl_2$, 11 mM $(NH_4)2SO_4$, 13% sucrose, 0.005% Cresol red, 1:1000 β-Mercapto ethanol), 250 µM dNTPs, 0.4 µM of forward and reverse primers, 0.25 µL Taq polymerase and ddH_2O. 1µL of DNA was added to 19

μL of the master mix, and the reaction was run following the protocol in tables 2.11 or 2.12. After the PCR, the samples were run in a 1.5% agarose gel containing ethidium bromide (1:10) for 45 minutes at 130V.

Table 2.11: PCR program for Vglut2cre genotyping

Step	Temperature (°C)	Time	Note
1	94	3 min	-
2	94	30 sec	Steps 2-4 repeated for 35 cycles
3	64	45 sec	
4	72	45 sec	
5	72	2 min	-
6	10	∞	Hold

Table 2.12: PCR program for LepRcre-HTB genotyping

Step	Temperature (°C)	Time	Note
1	94	2 min	-
2	94	30 sec	Steps 2-4 repeated for 34 cycles
3	60	30 sec	
4	72	1 min	
5	72	10 min	-
6	12	∞	Hold

2.2.4 *In vitro* sampling

This experiment is described in chapter 3. *In vitro* sampling was performed with two sampling probes, the open flow microperfusion (OFM) probe (6 mm long cerebral OFM, 2 mm exchangeable area, Joanneum Research, Austria) and an 1000 kDa microdialysis probe (AtmosLM™ Peptide Microdialysis probe with sterilization, Amuza, USA). The probes were connected via Fluorinated Ethylene Propylene (FEP) tubings (Harvard Apparatus, USA) to the sampling system, consisted of a syringe pump (CMA 4004 syringe pump, Harvard Apparatus, USA) and a peristaltic pump (Reglo ICC, ISMATEC, Germany). For the sampling, probes were placed in a tube with 55 μM BDNF solution, in which recombinant human BDNF (rBDNF) (PreproTech, USA) dissolved in 0.1% bovine serum albumin (BSA) was diluted in Ringer solution (B. Braun, Germany) (figure 2.1).

Samples were collected at 1 μL/min for 20 minutes and evaluated by western blot (explained below).

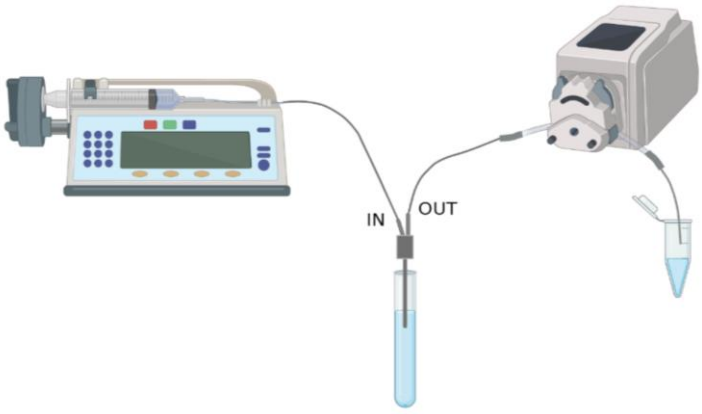

Figure 2.1: *In vitro* sampling setup

In the *in vitro* sampling setup, the pushing force was applied by a syringe pump, which was loaded with a syringe filled with Ringer solution. The syringe was connected to the inlet tubing (IN), whose other extremity is connected to the probe. The outlet of the probe was then attached to another tubing (OUT), which was connected to a peristaltic pump that applied the pulling force. Finally, the sample was collected inside a tube. In the *in vitro* arrangement, the sampling happened with the probe inserted into a BDNF solution. Figure created with BioRender.com[116].

2.2.5 Western blot

As described in chapter 3, western blot was performed to analyse samples collected *in vitro*. For this, first 10 μL *in vitro* samples were mixed with 2 μL Laemmli buffer (2% SDS, 5% β-mercaptoethanol, 10% glycerol, 62.5 mM Tris-HCl (pH 6.8) and 0.002% bromophenol blue) and denatured at 70°C for 10 minutes. In sequence, samples were loaded into the wells of a 4-12% Bis-Tris polyacrylamide gel (4-12% NuPAGE® Bis-Tris Mini Gels, Thermo Fisher Scientific, USA) to separate the protein content of the samples (BDNF and BSA) using electrophoresis. For that, electrophoresis was run at 200 V for 35 minutes in MOPS buffer (50 mM MOPS, 50 mM Tris Base, 0.1% SDS, 1 mM EDTA, pH 7.7) using Xcell SureLock TM mini-cell electrophoresis system (Thermo Fisher Scientific, USA). After separation, the content of the gel was transferred onto a polyvinylidene fluoride (PVDF) membrane in XCell II™ Blot Module (Thermo Fisher Scientific, USA) using transfer buffer

(25 mM Bicine, 25 mM Bis-Tris (free base) and 1 mM EDTA, pH 7.2) for 35 minutes at 30 V. In sequence, the membrane was blocked with 5% milk (Roth, Germany) in tris-buffered saline containing Tween (TBST) for 1 hour at RT. After blocking, the membrane was incubated with a rabbit monoclonal anti-BDNF antibody (1:2000, Abcam, United Kingdom) diluted in 3% bovine serum albumin (BSA) and 0.02% sodium azide in TBST overnight at 4°C. On the following day, the membrane was washed five times for five minutes each, and incubated with a goat anti-rabbit IgG antibody conjugated to peroxidase (1:20000, Jackson Immuno Research, United Kingdom) for 2 hours at RT. Finally, the BDNF bands were developed with enhanced chemiluminescence (ECL) Prime Western Blotting Detection Reagent (Amersham, USA) and detected using ImageQuant LAS 4000 system (GE Healthcare, USA).

2.2.6 Cannula implantation for *in vivo* sampling optimization

As described in chapter 3, two *in vivo* sampling techniques were compared in regard to their efficiency in collecting neuroactive peptides. For these tests, 2 month old C57 BL/6 male mice were used. Cannula implantation were performed aseptically, with sterilized surgical tools (Steri 350 Sterilizer, Inotech, Switzerland), and as previously described[29]. Before the surgery, mice received an intraperitoneal (i.p.) injection of an anesthetic mix, composed of medetomidin (0.5 mg/kg), midazolam (5 mg/kg) and fentanyl (0.05 mg/kg). A depilatory cream (Hair Removal Cream for Sensitive Skin, Veet, Canada) was used to remove the animal head fur. The mouse eyes were protected with application of an eye ointment (Bepanthen, Bayer, Germany). Cannula implantation occurred in a stereotaxic equipment (Model 1900 Stereotaxic Alignment System; David Kopf Instruments, USA) while the animal body was on a homemade heating pad connected to a digital temperature controller (Conotec, South Korean). After a small incision on the head skin and exposure of the skull, one small hole was made on the right side of the skull using a dental drill (Osada Electric Co., Ltd., Japan). One cohort of mice was implanted with an OFM cannula (cOFM-P-6-2, Joanneum Research, Austria) and another cohort was implanted with an 1000 kDa microdialysis probe (AtmosLM™ Peptide Microdialysis

probe with sterilization, Amuza, USA). For experiments in chapters 4 and 5, I only used OFM probes (cOFM-P-6-2, Joanneum Research, Austria). Both cannulae were implanted with their respective dummies, i.e. devices that resembled the probes and served as substitutes for them until the moment of the experiment. They were used to avoid the cannulae from becoming clogged with tissue debris. The implantation of any of the probes followed the coordinates antero-posterior (AP): +0.14 mm, medial-lateral (ML): +0.5 mm, dorso-ventral (DV): -5.2 mm[117]. To secure the implant on the skull, two additional holes were drilled to open space for two small screws (00-96 X 1/16, Bilaney Consultants, Germany). The cannula and the screws were fixed with a mixture of dental cement (mixture of Paladur Powder and Paladur Liquid, Kulzer, Germany). At the end, an i.p. mix of atipamezol (2.5 mg/kg), flumazin (0.5 mg/kg) and naloxon (1.2 mg/kg) was given to mice to reverse the effects of the anesthetic mix. After the surgery, a subcutaneous (s.c.) injection of carprofen (5 mg/kg) was also administered to the mice. Mice were placed on a heating pad (ThermoLux®, Germany) at 37°C to help in the recovery. On the following day, a second shot of carprofen s.c. (5 mg/kg) was given. Mice were kept on the heating pad at 37°C until full recovery, usually up to two days after the surgery, and were allowed to recover for two weeks before experiments, as this period allows better healing of the implanted region[118].

2.2.7 AAV injection and cannula implantation for *in vivo* sampling using Vglut2cre mice

Adeno-associated virus (AAV) injection and cannula implantation were performed for *in vivo* sampling using 2 month old Vglut2cre male mice, explained in chapter 4. Stereotactic surgeries were performed as described in the previous section. For the viral injection, 250 nL of an AAV coding for a cre-dependent engineered muscarinic receptor coupled to protein Gq (AAV-hSyn-DIO-hM3D(Gq)-mcherry, Addgene, USA) (DREADDs-Gq-mCherry) were delivered bilaterally in the coordinates: AP: +0.14 mm, ML: - and +0.3 mm, DV: -5 mm[117]. After the injections, an OFM cannula and dummy (cOFM-P-6-2, Joanneum Research, Austria) were implanted on the right hemisphere, at the coordinates AP: +0.14

mm, ML: +0.5 mm, DV: -5.2 mm[117]. Mice were kept on the heating pad at 37°C until full recovery, usually up to two days after the surgery, and were allowed to recover for two weeks before experiments, as this period allows better healing of the implanted region[118].

2.2.8 Cannula implantation for *in vivo* sampling done in parallel to thermal challenges and for orexin receptor antagonists' injections

The procedure to implant cannula for *in vivo* sampling done in parallel to thermal challenges (described in section 5.2.1 and 5.2.3) and for the injection of orexin receptor antagonists (section 5.2.2.4) was performed similarly. For the *in vivo* sampling implantation (section 5.2.1 and 5.2.3), 2 month old C57 BL/6 male mice were used. For the implantation for orexin receptor antagonists' injections (section 5.2.2.4), 2-3 month old C57 BL/6 male and female mice were used. Cannula implantation as described in the previous sections. OFM cannula and dummy (cOFM-P-6-2, Joanneum Research, Austria) were implanted at following coordinates AP: +0.14 mm, ML: +0.5 mm, DV: -5.2 mm[117]. Mice were kept on the heating pad at 37°C until full recovery, usually up to two days after the surgery, and were allowed to recover for two weeks before experiments.

2.2.9 AAV injection for *ex vivo* calcium imaging

In experiments described in section 5.2.2.2, AAV injection was performed for *ex vivo* calcium imaging preparation. The surgery was conducted aseptically, as described in the previous section After a small incision on the head skin and exposure of the skull, one small hole was made on the animals' skull using a dental drill (Osada Electric Co., Ltd., Japan) at the coordinates: AP: +0.14 mm, ML: +0.5 mm, DV: -5 mm[117]. A unilateral injection of 250 nL of a mix of AAV encoding for iCre (AAV-1/2-hSyn1-chl-iCre-WPRE-SV40p(A), Viral Vector Facility of University of Zürich, Switzerland) together with an AAV coding for a cre-dependent calcium indicator GCaMP6s (AAV.CAG.Flex.GCaMP6s.WPRE.SV40, Addgene, USA) was delivered into the POA. With the combination of these two viruses, cre recombinase was expected to be expressed only in neurons and GCamP6s was

expected to be expressed only in cre positive cells, thus restricting the expression of the calcium indicator to neurons. At the end, the head skin was sutured with absorbable surgical threads (Marlin, Catgut, Germany). After this, an i.p. mix of atipamezol (2.5 mg/kg), flumazin (0.5 mg/kg) and naloxon (1.2 mg/kg) was administered to mice to reverse the effects of the anesthetic mix. After the surgery, a subcutaneous (s.c.) injection of carprofen (5 mg/kg) was also given and mice were put on a heating pad (ThermoLux®, Germany) at 37°C to help in the recovery. On the following day, a second shot of carprofen s.c. (5 mg/kg) was given and mice were kept on the heating pad at 37°C until full recovery, usually up to two days after the surgery. Mice were allowed two weeks for satisfactory AAV expression.

2.2.10 Telemetry transmitter implantation

Telemetry transmitters were implanted for experiments described in chapter 4 (POA^{VGLUT2} neuron chemogenetic stimulation) and section 5.2.2.4 (injections of orexin receptor antagonists). The surgical procedures were conducted aseptically. Mice were anesthetized with an i.p. injection of an anesthetic mix (medetomidin (0.5 mg/kg), midazolam (5 mg/kg) and fentanyl (0.05 mg/kg)). The belly's fur was removed with depilatory cream ((Hair Removal Cream for Sensitive Skin, Veet, Canada) and the eyes protect from drying with an eye ointment (Bepanthen, Bayer, Germany). After an incision on the abdomen region, a sterile telemetric temperature transmitter (TA11TA-F10, Data Sciences International, USA) was implanted in the abdominal cavity. In sequence, muscles and skin were separately sutured with absorbable surgical threads (Marlin, Catgut, Germany). At the end, an i.p. mix of atipamezol (2.5 mg/kg), flumazin (0.5 mg/kg) and naloxon (1.2 mg/kg) was administered to mice, to reverse the effects of the anesthetic mix. After the surgery, a s.c. injection of carprofen (5 mg/kg) was given to mice. After this, mice were put on a heating pad (ThermoLux®, Germany) at 37°C to help in the recovery. A second shot of carprofen (5 mg/kg) was given on the following day and mice were maintained on the heating pad at 37°C until full recovery. Mice were allowed to recover for at least one week after the telemetry transmitter implantation before experiments.

2.2.11 Temperature monitoring

Tcore was monitored for experiments explained in chapter 4 (POA^{VGLUT2} neuron chemogenetic stimulation) and section 5.2.2.4 (injections of orexin receptor antagonists). For this, telemetry transmitters (TA11TA-F10, Data Sciences International, USA) implanted intraperitoneally coded the core body temperature in radio signals. These were sampled by a telemetry system, composed of receiver plates (PhysioTel® Receivers – RSC-1 or RPC-1, Data Sciences International, USA) connected to a data processor (Data exchange matrix, Data Sciences International, USA). Data was acquired and converted using Dataquest ART (Data Sciences International, USA). The same system was also used to measure the temperature of the homemade chamber used in warm and cold stimulation experiments. For this, a telemetry transmitter was hanged on the thermal cage, close to its floor, to measure the air temperature before the chamber was used for experiments.

2.2.12 *In vivo* sampling and stimulation

In the experiments of chapter 3, *in vivo* sampling was performed with the 1000 kDa and OFM probes for the comparison of these two devices. In the experiments described in chapters 4, 5, and 6, only OFM was used. Except for the differences in the probes, all the other procedures were performed in the same manner, as described below. For these experiments, only C57BL/6N and Vglut2cre male mice were used (specified below).

In vivo sampling

On the day prior to the *in vivo* sampling, mice were put in individual experimental cages (specified below) for habituation. On the day of the experiment, the dummy was substituted by the real probe in the implanted cannula. The probe was previously connected to an inlet and an outlet FEP tubings (0.12 mm ID, Harvard Apparatus, USA) for perfusion and sampling. In the inlet side, the FEP tubing was attached to a syringe (Syringe 2.5 mL for CMA pump, Harvard Apparatus, USA), placed on a syringe pump (CMA 400400, CMA, USA). The outlet tubing was attached to Tygon ST tubing (0.25 mm ID, ISMATEC, Germany), which was placed on a peristaltic pump (Reglo ICC ISM 4208,

ISMATEC, Germany) (figure 2.2). Once connected all tubings were connected and the probe was inserted into the cannula in the animal's head, mice went through an equilibration period, in which the probe was perfused with the vehicle (Ringer solution, B. Braun, Germany) for 20 minutes at 1 μl/min flow rate, and then for 1 hour at 0.5 μl/min, as suggested by manufacturers. This period allowed the mice to habituate to the tubings attached to their heads and avoided the probes from getting clogged after the probe placement. After the equilibration, the flow rate was maintained at 0.5 μl/min for the whole *in vivo* sampling and the samples were collected under baseline and stimulus conditions, as specified below. During the experiment, the collecting vials were kept on ice. Samples were snap frozen in liquid nitrogen right after collection and stored at -80°C until analysis. During the whole experiment, mice had *ad libitum* access to food and water. The data analysis included only samples that came from experimental and control mice with correct cannula implantation and/or AAV injection (explained in sections 2.2.13 and 2.2.18).

The *in vivo* sampling was performed simultaneously to either ambient temperature stimulation (warm or cold) or POA^{VGLUT2} neurons' activation, as explained below. Control groups were included in all experiments to evaluate if levels of neuroactive peptides were changing due to reasons different from the stimuli, such as a circadian variation, as some studies suggest[109,119], or due to analyte depletion in the collected region after the long sampling time, as previously proposed[93].

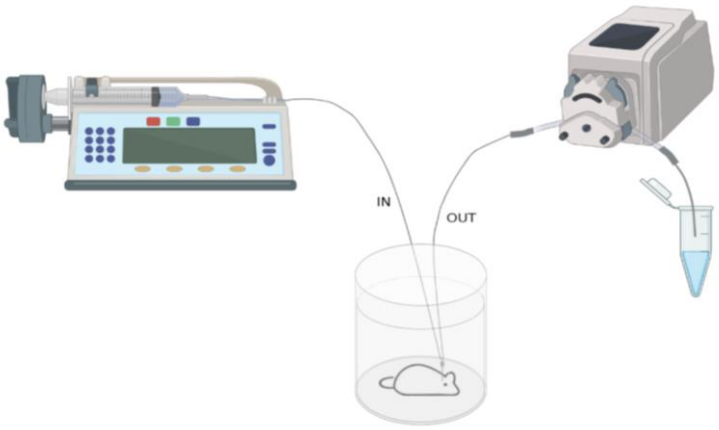

Figure 2.2: *In vivo* sampling setup

The scheme represents how the *in vivo* sampling occurred. The probe inserted into the animal's brain was constantly perfused with Ringer solution, delivered by a syringe pump through the inlet tubing (IN). The samples were collected through the outlet tubing (OUT), pulled by a peristaltic pump. Figure created with BioRender.com[116].

POA^{VGLUT2} neuron activation

For the experiments described in chapter 4, in parallel to the *in vivo* sampling, it was also performed the stimulation of POA^{VGLUT2} neurons using chemogenetics (more details in section 1.8.2). For this experiment, Vglut2-cre mice were previously injected with DREADDs-Gq-mCherry (explained in section 2.2.7). On the day before the experiment, mice were put in the experimental cage (72-0016, Harvard Apparatus, USA) for habituation and Tcore monitoring via telemetry receivers placed under the cages (PhysioTel® Receivers – RSC-1 or RPC-1, Data Sciences International, USA). On the day of the experiment, baseline samples were collected from the POA region under the perfusion of vehicle (Ringer solution) for two hours, and then stimulus samples were collected while a 10 μM clozapine-N-oxide (CNO) solution (diluted in Ringer) was perfused during additional two hours. Both solutions were delivered directly into the POA via the implanted OFM probe (cOFM-P-6-2, Joanneum Research, Austria), at the flow rate of 0.5 μl/min, in parallel to the sampling. A liquid switch (CMA 110, Harvard Apparatus, USA), a device that allowed the passage of only one liquid at each time, was used to change from one solution to another. The direct delivery of CNO into the POA

and the use of a liquid switch required no immobilization of the animal during sampling, therefore this strategy avoided the stress involved in handling the mouse for an injection and prevented air bubbles from entering into the sampling system. In total, twelve samples, of 20 minutes each, were collected. Control mice were littermates that did not express cre (WT-like mice), therefore no DREADDs-Gq was expected to be expressed. In exception of this, the experiments of control (WT) and Vglut2-cre (CRE) mice were performed exactly in the same way. During experiments, the room temperature was 22±1°C.

Ambient temperature stimulation

The *in vivo* sampling done together with ambient temperature stimulation experiments is explained in chapters 5 and 6. To allow mice to habituate, animals were put in the experimental cage, a homemade thermal chamber, one day before the experiment. The thermal chamber was composed of a cylindrical metallic bin, with 16.7 cm of diameter x 23.5 cm of height (Luna 3 liters stainless steel, EKO, Germany), surrounded by a silicone hose (Precision Pump Tubing, Platinum-Cured Silicone, L/S 16, Masterflex®, Germany), which was connected to a circulating thermal bath (Heating circulator bath, Haake, USA or ARCTIC A10 Refrigerated circulator, ThermoFischer). The bin was covered with a rubber net (Non-Slip Carpet Stopper, TROP), to avoid the animal from escaping the cage, a behavior described in the literature during heat stress (figure 2.3-C)[120]. This assemble was put inside a styrofoam box and enclosed with a homemade transparent plexiglass lid, which contained small holes to allow air entry while still maintaining the temperature settings (figure 2.3).

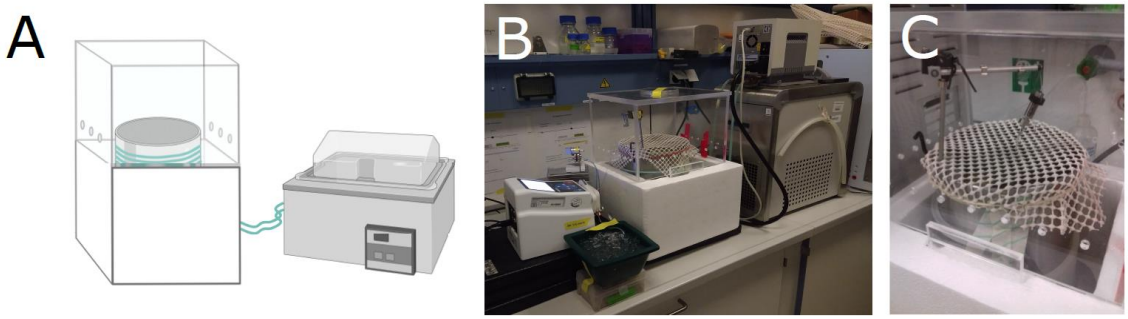

Figure 2.3: Homemade thermal chamber used for ambient temperature stimulation.

A: Scheme representing the thermal chamber. Figure created with BioRender.com[116]. B: Picture of the homemade thermal chamber during an *in vivo* sampling experiment. C: The net covering the metallic bin is shown in detail.

a. Warm

In the warm ambient temperature stimulation experiment (5.2.1), samples were collected from two groups: one experimental (warm group) and one control (control group). In the warm group, first, microperfusates were sampled for two hours under the baseline condition, in which the thermal chamber temperature was kept at 24±0.5°C. In sequence, the thermal chamber temperature was increased to 36±0.5°C and samples were collected also for two hours. In the control group, the chamber temperature was kept at 24±0.5°C throughout the entire experiment. The samples collected during these experiments were analyzed by two different methods, namely LC-MS/MS and enzyme linked immunosorbent assay (ELISA). For the LC-MS/MS analysis, in total, six 40 minute microperfusates were sampled, from both groups. While for the ELISA assay, four samples were collected for 1 hour and 20 minutes each, for a total of 40 µL per sample.

b. Cold

For the cold ambient temperature stimulation experiment (section 5.2.3), microperfusates were sampled from the same cohort of animals twice, one during experimental conditions, and one during control conditions. Under experimental conditions, firstly, samples were collected during baseline, with the thermal chamber at 24±0.5°C, for two hours. Later, the

microperfusates were sampled for 2 hours and 40 minutes, while the chamber was cooled down to 5±0.5°C. Under control conditions, the whole sampling was performed at 24±0.5°C. Similarly to the warm experiment, the microperfusates collected during cold stimulation were analyzed with LC-MS/MS and ELISA. For the former, seven microperfusates of 40 minutes each were collected from both conditions, and for the latter, four samples were collected for one hour and 20 minutes each during the two conditions.

2.2.13 Injection of orexin receptors' antagonists into the POA

Before experiments described in section 5.2.2.4, mice were adapted to another light ON/OFF cycle. In these experiments, antagonists of orexin receptors were injected into the POA. According to the literature[77], the peak of orexin release happens at the end of the dark phase, at the last three hours (05:00-08:00). Thus, to deliver the antagonists while orexin is assumed to be mostly released[77], the circadian rhythm of the mice was delayed by six hours (new light ON/OFF cycle: ON at 14:00 – OFF at 02:00), so the experiment could happen during working hours. As it takes around one day to delay one hour of the circadian rhythm of mice[121], the animals were allowed to adjust to the new light ON/OFF cycle for at least one week prior to the POA infusion of orexin receptors' antagonists experiments.

One day before the experiment, mice were habituated to the experimental setup, and put in test cages (72-0016, Harvard Apparatus, USA) placed inside a ventilated cabinet (Cooling incubator, Binder, Germany). On the day of the experiment, after probe insertion, done similarly to what is described in section 2.2.12, animals were allowed to habituate to the tubings attached to their heads for one hour to decrease stress levels. Antagonists of orexin receptors, OX1R and OX2R, were injected directly into the POA through the OFM probe (cOFM-P-6-2, Joanneum Research, Austria). The injections happened either at 24±0.5°C or at cooling, from 24°C to 12°C. On day one, the OX1R antagonist SB-334867 (50μM, 1μL, dissolved in DMSO:saline (1:1000)), was injected into the POA at 24±0.5°C, using a dose previously described in the literature[122]. On the following day, the vehicle

(DMSO:saline (1:1000)) was injected at 24±0.5°C. At least one day later, SB-334867 (50μM, 1μL, dissolved in DMSO:saline (1:1000)) was injected at cooling, followed by injection of the vehicle on the next day also at cooling. At least two days later, the OX2R antagonist 20 μM seltorexant (4 μL, dissolved in DMSO:saline (8:1000)) was injected into the POA at 24±0.5°C. In sequence, vehicle injection occurred on the next day at 24±0.5°C. One day later, 20 μM seltorexant (4 μL, dissolved in DMSO:saline (8:1000)) was injected at cooling, followed by vehicle injection at cooling on the next day. Two cohorts of animals were used for the injections of both antagonists at both temperature settings.

2.2.14 Measurement of food and water consumption

Food and water consumption were measured during ambient temperature stimulation experiments (sections 5.2.1 and 5.2.3) and drug injections (section 5.2.2.4). Water was given in the format of a gel, which was sterile and contained 97% of water (Solid Drink®, Triple A Trading, The Netherlands). Animals had *ad libitum* access to food and solid water before and during the experiment. To compare how much mice ate and drank, food pellets and the solid water were weighted before and after the experiment.

2.2.15 Perfusion and brain sectioning

Transcardial perfusion was performed to evaluate the cannula implantation and AAV injection site of experiments explained in chapters 4, 5, and 6, and to prepare brains for immunohistochemistry (chapters 4 and 5). For this, first, animals were perfused with phosphate buffer saline (PBS), followed by perfusion with 4% paraformaldehyde (PFA). For the cannula implantation and AAV injection check, mice were decapitated and their heads were postfixed for four days in 4% PFA at 4°C. On the fifth day, the brains were dissected out of the heads and cryoprotected with 20% sucrose. After the brains sank in this solution, 30 μm brain sections were cut using a microtome (Leica SM 2010R, Leica Biosystems, Germany). To prepare brains for immunostainings, right after the perfusion, brains were removed from mice heads and put in 4% PFA at 4°C overnight. On the next

day, brains were placed in 20% sucrose solution for cryoprotection. Once brains were fully sank in the sucrose solution, they were stored in TissueTek® (Sakura Finetek, The Netherlands) until cryostat sectioning. For immunofluorescence, 20 μm sections were cut in a cryostat (Leica CM3050S, Leica Biosystems, Germany).

2.2.16 Bicinchoninic acid (BCA) assay

BCA assay was used to quantify total content of protein in samples collected *in vivo* with 1000 kDa and OFM probes, as described in chapter 3. Pools of two samples per animal (final volume 20 μL) were divided in replicates (10 μL each). To measure the samples, a commercial kit (Pierce™ BCA Protein Assay Kit, Thermo Fischer Scientific, USA) was used, following the instructions of the manufacturer. Briefly, after the preparation of the standard dilution series, the standards and the samples were pipetted to a 96-well plate. Next, kit working reagent was added and mixed in the plate on a shaker for 30 seconds. In sequence, the plate was covered and incubated at 37°C for 30 minutes. After this, the absorbance was measured at 256 nm using a plate reader (Infinite M200 PRO, Tecan, Switzerland).

2.2.17 Silver staining

The silver staining was to evaluate the efficiency of the 1000 kDa and OFM probes to collect peptides and proteins, as described in chapter 3. For this, samples collected *in vivo* were mixed with Laemmli buffer (2% SDS, 5% β-mercaptoethanol, 10% glycerol, 62.5 mM Tris-HCl (pH 6.8) and 0.002% bromophenol blue) and loaded into a 4-12% Bis-Tris polyacrylamide gel (4-12% NuPAGE® Bis-Tris Mini Gels, Thermo Fisher Scientific, USA). For protein separation, it was performed an electrophoresis for 30 min at 200 V in MES buffer (50 mM MES, 50 mM Tris Base, 0.1% SDS, 1 mM EDTA, pH 7.3) using Xcell SureLock TM mini-cell electrophoresis system (Thermo Fisher Scientific, USA). After this, the gel was fixed for 45 min at RT with acetic acid:methanol:ddH_2O (10:40:50) and later washed for 1 hour and 30 minutes in ddH_2O, with changes occurying every 15 minutes.

In sequence, the gel was incubated with 0.02% (w/v) sodium thiosulfate for 3 minutes at RT and washed twice with ddH_2O for 1 minute each wash. Next, the gel was stained with 0.1% (w/v) silver nitrate at 4°C for 30 minutes in the dark and washed again twice with ddH_2O for 1 minute each. Later, the staining was developed in 0.04% formaldehyde in 2% (w/v) sodium carbonate until proteins became visible. Finally, the reaction was stopped with 5% acetic acid and the gel was washed with ddH_2O. For image acquisition, the gel was wrapped on a plastic foil and scanned.

2.2.18 ELISA

ELISA was used to measure the levels of orexin-A and adiponectin in samples collected *in vivo* with OFM probe during warm and cold stimulation, respectively. For the warm experiment, samples were analyzed with a competitive ELISA kit for orexin-A (Mouse Orexin A ELISA Kit, MyBioSource, USA), following the procedures recommended by the manufacturer. Briefly, after preparing the standard dilution series, the samples and the standard were added in duplicates to a 96-well ELISA plate pre-coated with mouse orexin-A. In sequence, the biotinylated detection antibody was pipetted into the plate, which was incubated for 45 minutes at 37°C. After washing and, in sequence, drying the wells, avidin conjugated to horseradish peroxidase (HRP) was added to the plate, and incubated for additional 30 min at 37°C. Next, the substrate of HRP was pipetted to each well and incubated for 15 minutes at 37°C in the dark. Finally, the reaction was finished with the stop solution and the optical density (O.D.) was measured with a plate reader (Infinite M200 PRO, Tecan, Switzerland) set to 450 nm. The sensitivity of this ELISA kit is 37.5 pg/mL. To measure the levels of orexin-A in the samples, the R package drc[123], which estimates the concentration based on the standard curve, was used (figure 2.4).

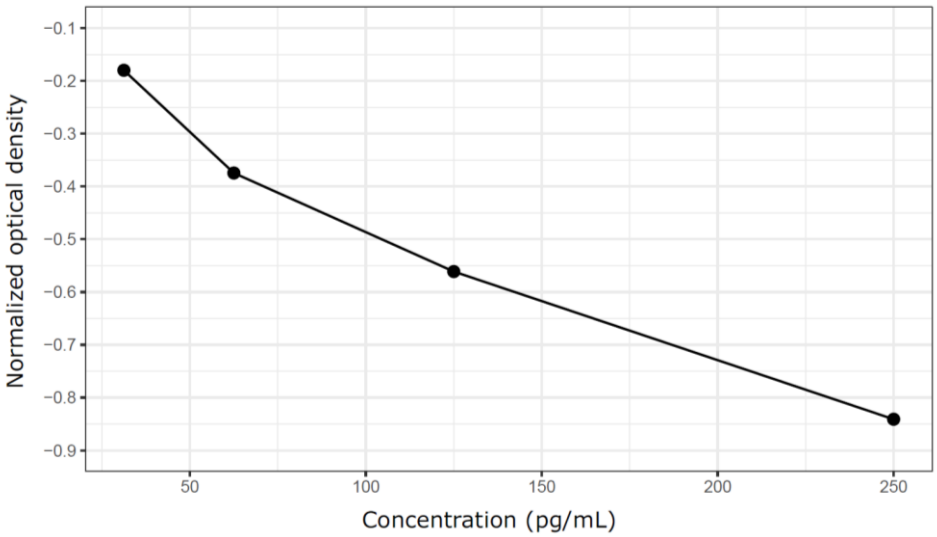

Figure 2.4: Standard curve of orexin-A ELISA assay kit

Each standard was normalized by the blank.

For the cold experiment, the levels of adiponectin were measured with a sandwich ELISA kit (Quantikine® ELISA Mouse Adiponectin/Acrp30 Immunoassay, R&D systems, USA), following the steps determined by the manufacturer. The steps were similar to the orexin-A ELISA, but in the adiponectin kit, the 96-well plate was pre-coated with monoclonal antibody specific for mouse adiponectin. The sensitivity of the adiponectin ELISA kit is 0.003 ng/mL. To estimate adiponectin levels in the samples, the R package drc[123] was also used.

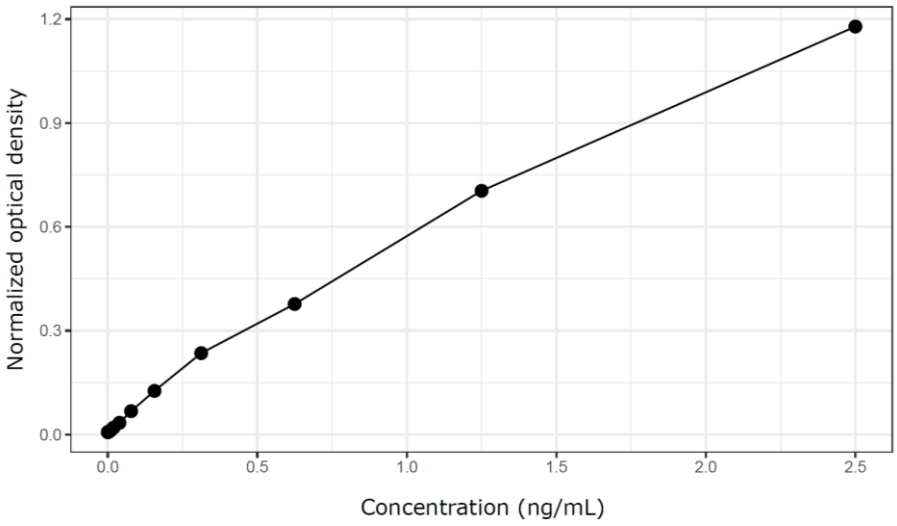

Figure 2.5: Standard curve of adiponectin ELISA assay kit

Each standard was normalized by the blank.

2.2.19 Immunohistochemistry

The tissue for immunohistochemistry was prepared as explained in section 2.2.16. For the staining, first the brain sections were surrounded with a water-repellent pen (Dako Pen, Dako-Agilent, USA). Then, the slides were blocked with blocking solution (5% goat serum, PBS containing 0.1% Triton X-100 (PBST), 0.4% fish skin gelatin, 0.02% sodium azide and 13.3 mM glycine) or with 3% BSA in PBS containing 0.1% Triton X-100 (PBST) for two hours at RT. In sequence, the slide was incubated with the primary antibody diluted in the blocking solution or 3% BSA in PBST overnight at 4°C. On the following day, after washing the slides with PBST four times of 15 minutes and with PBS twice of five minutes, the slides were incubated with the secondary antibody and DAPI for two hours at RT. Finally, after four washes of 15 minutes with PBST and one with PBS, the slides were mounted with Immu-Mount (FisherScientific, UK). The following primary antibodies were used: rabbit anti-mCherry (1:2000, Abcam, UK), rabbit anti-Orexin-A/B (1:100, Santa Cruz Biotechnologies, USA), rabbit anti-OX2R (1:250, Millipore, USA), and chicken anti-GFP (1:1000, Novus Biologicals, USA). As secondary antibodies, the following were used: goat anti-rabbit IgG conjugated to Alexa-647 (1:1000, Life

Technologies, USA) and donkey anti-chicken IgG conjugated to Cy3 (1:1000, Jackson Immuno Research, USA).

2.2.20 Image acquisition

To capture fluorescent images, a C2+ confocal microscope (Nikon, Japan) or a Ni-E wide field microscope (Nikon, Japan) were used. For bright field images, the acquisition was performed on a Ni-E wide field microscope (Nikon, Japan). Both microscopes were accessed at the Nikon Imaging Center of Heidelberg University. The NIS-Elements AR (Nikon, Japan) and ImageJ/Fiji[124] were used to process and analyze the images.

2.2.21 LC-MS/MS and proteomics data analysis

This part of the thesis was done in collaboration with Dr. Daniele Colombo, a former postdoc researcher from the laboratory of Prof. Dr. Jeroen Krigjsveld at the German Cancer Research Center (DKFZ). Dr. Colombo and I performed the sample preparation together, while he was the only one responsible for the LC-MS/MS analysis.

As described in chapters 3, 4, and 5 the samples were collected *in vivo* either during experimental or control conditions (explained in section 2.2.12) were analyzed by LC-MS/MS.

Sample preparation

For the optimization of sample processing described in chapter 3, three different conditions were tested. For these tests, it was prepared a pool containing samples collected from five animals implanted with the OFM probe. Then, this pool was divided into three parts for the next steps. The three conditions are referred here as A, B, and C, and were processed in duplicates. Conditions A and B were only used in experiments described in chapter 3 and condition C was used in experiments of chapters 3, 4, and 5.

In condition A, a 3 kDa filter was used to refine the samples. In sequence, samples were reduced and alkylated, respectively, with 5 mM tris (2-carboxyethyl)phosphine (TCEP) and 20 mM chloroacetamide (CAA) for five minutes at 95°C. Next, samples were desalted and cleaned using a magnetic-bead based method, called single-pot solid-phase-enhanced sample preparation (SP3), as previously described[125]. Briefly, washed SP3 magnetic beads (50 μg/μL) were added to the samples in a ratio of 1:10 (beads' solution volume:sample volume) and the mix was completed to 100 μL final volume. Then, acetonitrile (ACN) was added to a final concentration of 95% and samples were incubated at RT for 18 minutes. In sequence, the tubes were put on a homemade magnetic rack for two minutes. After removing the supernatant, beads were washed with ACN twice while tubes remained on the magnetic stand. At the end of the second wash and discard of the supernatant, the beads were air dried. In sequence, beads were reconstituted in 18 μL of digestion buffer (50 mM ammonium bicarbonate containing 50 ng of Trypsin/Lys-C mixture (Trypsin/Lys-C Mix, Mass Spec Grade, Promega, USA)) and incubated overnight at 37°C. On the following day, the reaction was stopped by the addition of 2 μL of 10% formic acid (FA) and beads were removed using magnetic separation.

In condition B, a solid phase extraction was performed with the samples using a commercial kit (OASIS, Waters, USA), following the recommendations of the manufacturer. Briefly, to prepare for loading, the well sorbent was washed with 100 μL of ACN, then with 100 μL of solvent B, which contained 60% MeOH and 1% FA in ddH_2O, followed by a wash with 100 μL of solvent A (1% FA in ddH_2O). Next, samples were loaded on the sorbent, washed three times with solvent A, with decreasing volumes, from 300 μL to 100 μL. Finally, proteins and peptides were eluted by applications of 50 μL, then 25 μL of solvent B.

In condition C, used in experiments of chapter 3, 4, and 5, microperfusates were reduced and alkylated, respectively, with 5 mM TCEP and 20 mM CAA for five minutes at 95°C. Next, samples were desalted and cleaned using the SP3 method[125] explained above.

Chromatography

For the optimization of LC-MS/MS workflow described in chapter 3, four combinations of LC-MS/MS parameters were tested on samples treated with condition C, referred here as methods 1, 2, 3, and 4. The samples consisted of duplicates of a pool prepared mixing samples collected *in vivo* from five animals implanted with the OFM probe. The LC parameters of the four LC-MS/MS combinations were different in regard to the run duration and mixing of solvents A and B, as explained below. The methods 1, 2, and 4 were only used in experiments of chapter 3, and the method 3 was used in chapter 4.

In regard to the liquid chromatography, peptide separation was done using the Easy NanoLC 1200 with a trapping (Acclaim PepMap C18, 5µm, 100Å, 100µm x 2cm) and an analytical column (Waters nanoEase MZ Peptide BEH C18, 130Å, 1.7µm, 75µm x 25cm). The solvent A was 0.1% (v/v) formic acid (FA) in ddH2O and solvent B was 80% ACN, 0.1% (v/v) FA in ddH2O. Samples were loaded onto the trapping column with a constant flow of solvent A at a maximum pressure of 800 bar. Peptides were eluted at 0.3 µL/minute at a temperature of 55°C, kept using HotSleevePlus column oven (Analytical Sales and Services, USA).

Method 1 was performed similarly to a previous study[126]. Briefly, a 120 min gradient was applied with 0–103 min, 1–38% B; 103–104 min, 38–100% B; 104–109 min, 95% B; 109–110 min, 95–0% B; 110–120 min, 100% A. Method 2 and 3 used the same LC parameters, only differing in the MS/MS settings (explained below). In both methods, after 10 min of equilibration, a 45 min gradient was employed with 0–4 min, 3–8% B; 4–6 min, 8–10% B; 6–23 min, 10–32% B; 23-26 min, 32–50% B; 26–27 min, 50-100% B; 27–34 min, 100% B; 34–35 min, 100-3% B; 35-45 min, 3% B. Finally, the method 4 was performed similarly to what was previously described[127]. After 10 min equilibration, buffer B increased from 4-10% B from 0-5 min, 10-25% B in 5-55 min, 25-45% in 55-73 min, and a steep increase to 95% in 74 min.

The analysis of samples collected during POA^{VGLUT2} neuron activation experiments was performed using method 3. While samples from the ambient temperature experiments

were analyzed with a gradient similar to method 3, with 3-8% B from 0-4 min, 8-10% from 4-6 min, 10-40% from 6-58 min, 40-85% 58-78 min, and from 85-100% in 79. At last, 100% solvent B was kept for 15 min, followed by 97% solvent A for 11 minutes.

MS/MS and proteomics data acquisition

For the MS methods, it was used different combinations of m/z ratio ranges and charge exclusion for MS2 fragmentation, with MS2 meaning the second MS analysis in MS/MS. The four LC-MS/MS combinations differed in the MS parameters regarding the m/z ratio ranges and charge exclusion used in the MS2 fragmentation. The methods 1, 2, and 4 were only used in experiments of chapter 3, while the method 3 was used in experiments of chapter 3 and 4. After separation in the LC, peptides were introduced into the MS via a Pico-Tip Emitter 360 μm OD x 20 μm ID; 10 μm tip (New Objective, USA) set at 275°C. Samples were analyzed on a Q-Exactive HF Orbitrap mass spectrometer (Thermo Fisher Scientific, USA) with a spray voltage of 2 kV.

In the method 1, full scan MS spectra ranging from 350 to 1500 m/z, were acquired in the Orbitrap with a resolution of 120000 FWHM (full width at half maximum). The filling time was configured to a maximum of 32 ms with an automatic gain control (AGC) target of $3x10^6$ ions. The 20 ions that were most abundant per full scan were selected for MS/MS acquisition with dynamic exclusion of 25 seconds. Unassigned, one or more than seven charges were excluded. During the MS/MS scans, the normalized collision energy (NCE) was set to 26. Additionally, the resolution was configured to 15000 FWHM with automatic gain control of $2x10^4$ ions and maximum fill time of 50 ms. The isolation window was configured to m/z 2, with a fixed first mass of 110.

In the method 2, MS spectra were acquired with an m/z scan range of 240 to 1800, with a resolution of 60000 FWHM. The filling time was configured to a maximum of 32 ms with an AGC target of $3x10^6$ ions. The 20 ions that were most abundant per full scan were selected for MS/MS acquisition with dynamic exclusion of 15 seconds. Ions with charge unassigned and 1 were excluded. During the MS/MS scans, the NCE was set to 40.

Additionally, the resolution was configured to 15000 FWHM with automatic gain control of $5x10^4$ ions and maximum fill time of 50 ms. The isolation window was configured to m/z 2, with a fixed first mass of 110.

The MS spectra of method 3 were acquired with 300 to 3000 m/z scan range, with a resolution of 60000 FWHM. The filling time was configured to a maximum of 32 ms with an automatic gain control target of $3x10^6$ ions. The 20 ions that were most abundant per full scan were selected for MS/MS acquisition with dynamic exclusion of 10 seconds. Ions with unassigned charge were excluded. During the MS/MS scans, the normalized collision energy (NCE) was set to 30. Additionally, the resolution was configured to 15000 FWHM with automatic gain control of $2x10^4$ ions and maximum fill time of 50 ms. The isolation window was configured to m/z 1.4, with a fixed first mass of 110.

The method 4 was based on a previous study[127]. It was set to acquire MS spectra with 400 to 1600 m/z scan range, with a resolution of 70000 FWHM. The filling time was configured to a maximum of 256 ms with an automatic gain control target of $3x10^6$ ions. The top 10 most abundant ions per full scan were selected for MS/MS acquisition with dynamic exclusion of 10 seconds. Ions with one or more than six charges were excluded. During the MS/MS scans, the NCE was set to 30. Additionally, the resolution was configured to 17500 FWHM with automatic gain control of $1x10^5$ ions and maximum fill time of 64 ms. The isolation window was configured to m/z 3, with a fixed first mass of 110.

The MS spectra obtained from samples collected during POA^{VGLUT2} neuron activation experiments were acquired using the same parameters as method 3, except the NCE, as a stepped configuration of 30-35-40 was used, and the isolation window, which was set to m/z 2. For the ambient temperature experiments, full scan MS spectra was acquired similarly to method 3, with the exception of mass range, set at 450 to 4500 m/z, resolution, set at 120,000 FWHM, and dynamic exclusion, set for 40 seconds. In addition, ions with single charges were also discarded. And in the MS/MS scans, the NCE was set to 26, with automatic gain control of $1x10^5$ ions.

Proteomics data processing

The acquired MS/MS data from all experiments was processed using MaxQuant (version 1.6.2.6)[128,129]. The proteome data was searched against the reference mouse proteome (20180523_Uniprot_mus-musculus_canonical) obtained from the Uniprot database[130] and an updated version of Neuropep mouse database[85], a compilation of all neuroactive peptides present in the mouse. Proteins and peptides were quantified with the label-free quantification (LFQ) algorithm of MaxQuant, MaxLFQ. LFQ normalization was omitted and MS/MS spectra were not required for the LFQ comparison. In addition, intensity-based absolute quantification (iBAQ) intensities were calculated with a log fit enabled. Identification transfer between runs via the matching between runs algorithm was allowed with either 0.5 or 10 minute time window or default parameters. As variable modifications, trypsin digestion with up to 2 missed cleavages per enzyme (total of 5 missed cleavages), carboxypeptidase, and fixed C-Carbamidomethyl modification were included. Additionally, Oxidation (M), Acetyl (Protein N-term), Gln->pyro-Glu, Glu->pyro-Glu, Amidated (C-term), Sulfation (Y), Phospho (STY) were also selected as variable modifications. Minimal peptide length was set at five amino acids. Dependent peptides were searched at a false discovery rate (FDR) of 1%. FDR for peptides and protein was set to 5%. The reversed sequences of the target database were used as a decoy database. All the other parameters remained as the default MaxQuant settings.

Data analysis

This part was done in collaboration with Dr. Silvia Calderazzo, biostatistician from DKFZ, Dr. Colombo, and by myself.

LFQ values were extracted from MaxQuant protein group and peptide output tables and log2-transformed for further analysis. To avoid that a peptide sequence that is common among two or more different proteins, MaxQuant assigns peptides to protein groups. Such groups contain one or more protein, depending on the peptide sequences found. Data was analyzed at the peptide level and at the protein group level, as illustrated in figure 2.6. The analysis at the peptide level had the potential to inform about individual

peptides, with the downside of lacking robustness. On the other side, the protein group analysis is more robust but lacks the information regarding individual peptides. Proteins and peptides that were only identified by a modification site, the contaminants, as well as the reversed sequences were removed from the data set. All further analysis was performed in the R environment (version 3.3.3)[131] using packages available through BioConductor[132]. Particularly, the differential analysis was performed using the package Limma (R package version 3.30.1)[133]. Benjamini-Hochberg correction was applied to calculate adjusted p-values.

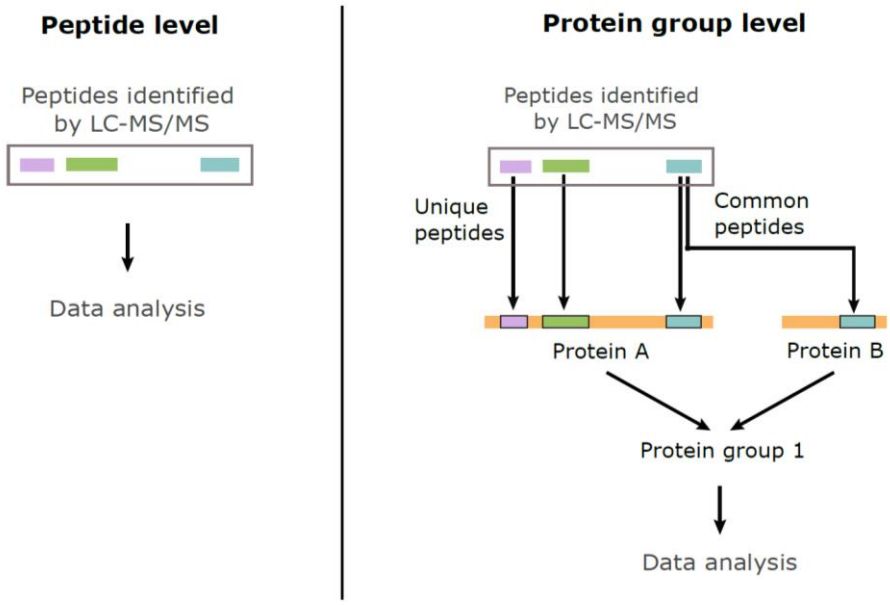

Figure 2.6: Datasets used in the analysis.

The scheme illustrates the two datasets used in the analysis, namely the peptide and the protein group, which were obtained after the data processing using MaxQuant.

2.2.22 Targeted mass spectrometry

This part of the thesis was done in collaboration with Dr. Max Sauter from the laboratory of Prof. Dr. Walter Haefeli at the Heidelberg University Hospital.

List of peptides used

This experiment is mentioned at the chapter 6. It was done to verify, if neuroactive peptides previously detected in the unbiased screening could also be found in *in vivo* samples with another MS-based technique. For that, the list of neuroactive peptides detected during the LC-MS/MS was narrowed to a few candidates (table 2.13). Such peptides included bioactive peptides and tryptic peptides. They were synthesized by Chempeptide Limited (Shangai, China) upon request and were used to define the m/z and mass transitions.

Table 2.13: List of neuroactive peptide candidates selected for targeted MS.

Peptide	**Sequence**	**Modifications**	**Peptide type**
Adiponectin (116-125 aa)	SAFSVGLETR	Unmodified	Tryptic
Secretogranin 1	KELENLAAMDLELQK	Unmodified	Tryptic
DBI (53-60 aa)	AKWDSWNK	Unmodified	Tryptic
Orexin (100-112 aa)	AGAELEPHPCSGR	Unmodified	Tryptic
Orexin A	QPLPDCCRQKTCSCRLYE LLHGAGNHAAGILTL	N-terminal pyroglutamyl residue; C-amidation; Two disulfide bridges between Cys6 - Cys12, Cys7 - Cys14	Bioactive
Orexin B	RPGPPGLQGRLQRLLQA NGNHAAGILTM	C-amidation	Bioactive
Neuropeptide Y (29-64 aa)	YPSKPDNPGEDAPAEDM ARYYSALRHYINLITRQRY	C-amidation	Bioactive
Nucleobindin 1 (189-199 aa)	YLESLGEEQRK	Unmodified	Tryptic
Somatostatin-28	SANSNPAMAPRERKAGC KNFFWKTFTSC	Disulfide bridge Cys17-Cys28	Bioactive

Peptide solution preparation

Peptides were weighted into glass vials and dissolved in ACN/water (1/1, v/v) including 0.1 % formic acid (FA) at a concentration of approximately 0.25 mg/mL. These solutions were diluted 1000-fold in ACN/water (1/1, v/v) including 0.1 % FA to a combined spike solution. Solutions were kept at 4 °C.

Sample preparation

Samples were prepared by addition of 10 µL of combined spike solution to 990 µL of buffer containing 0.2 % BSA and withdrawal of 20 µL from this stock. Peptides were either extracted by protein precipitation with a 2-fold excess of ACN + 0.1 % FA followed by centrifugation at 13200 × g for 5 min. Or peptides were extracted by solid phase extraction using HLB µ-elution plates (Waters, Milford, MA, USA) operated with an overpressure unit (Waters). Samples were loaded onto the plates and subsequently washed with water + 0.1 % FA. Peptides were then eluted with 2 times 25 µL of ACN/H2O/MeOH (2/1/1) + 0.1 % FA. Extracts were transferred to 96-well collection plates (Waters) and diluted with water:FA (2:0.1).

Instrumental analysis parameters

A LC-MS/MS system (Waters) consisting of a triple stage quadrupole mass spectrometer (Xevo TQ-XS with Z-spray source) equipped with an Acquity classic UPLC® system (Waters) was used for mass spectrometric detection. Chromatographic separation was performed on a Waters Acquity BEH C18 peptide column (300 Å, 1.7 µm, 2.1 x 50 mm) heated to 60 °C using a flow rate of 0.5 mL/min and an injection volume of 20 µL. The eluent consisted of 0.1 % (v) aqueous FA with 5 % ACN (aqueous eluent; A) and ACN including 0.1 % FA (ACN eluent; B). The initial eluent composition of 85 % solvent A/15 % solvent B was kept for 0.1 min. The ratio was then changed to 40 % solvent A/60 % solvent B within 2.9 min and subsequently changed during 0.2 min to 2 % solvent A/98 % solvent B, which was held for an additional 0.5 min. Finally, the ratio was returned to starting conditions during 0.3 min, and maintained for equilibration for an additional 0.2 min and while the subsequent injection was prepared (1 min). The Z-spray ionization parameters were manually optimized to fit all investigated peptides. The resulting parameters are shown in Table 2.14.

Table 2.14: Optimized MS parameters for the detection of the peptides using heated ESI in the positive ion mode.

MS/MS parameter	
Spray voltage	1000 V
Cone voltage	20 V

Source temperature	150 °C
Desolvation gas flow (N_2)	1,000 L/h
Desolvation temperature	600 °C
Dwell time	20 ms
Collision gas flow (Ar)	0.15 mL/min

ESI: Electrospray ionization.

Selected reaction monitoring (SRM) measurements were performed utilizing Ar for collision-induced dissociation in positive ion mode and optimized for each peptide using the integrated IntelliStart procedures of the MassLynx V4.2 system software (Waters, Milford, MA, USA). For each peptide all abundant multiply charged precursor were evaluated. Table 2.15 shows the resulting mass transitions obtained during optimization.

Table 2.15: Optimized SRM parameters for the detection of the peptides.

Peptide	Monitored mass transitions [m/z]	Collision energy [V]
Orexin-Pro	442.0 → 377.3	12
	442.0 → 519.4	20
Nucleobindin	451.3 → 249.1	14
	451.3 → 538.5	12
DBI	517.9 → 261.1	24
	517.9 → 835.7	17
Adiponectin	534.0 → 455.0	12
	534.0 → 575.5	15
Secretogranin-1	582.5 → 201.0	40
	582.5 → 745.7	18
Neuropeptide Y	611.2 → 601.2	14
	713.0 → 751.2	21
Somatostatin-28	630.5 → 748.5	13
	630.5 → 892.4	22
Orexin-A	713.2 → 706.3	10
	713.2 → 854.3	15
Orexin-B	735.1 → 616.3	24
	735.1 → 693.7	21

SRM: selected reaction monitoring.

2.2.23 *Ex vivo* calcium imaging

This part of the thesis was done in collaboration with Dr. Gretel Kamm, a postdoc researcher who also works at the Siemens Lab. I injected the mice with AAV encoding the calcium indicator GCamp6 and prepared the orexin-A solution. Dr. Kamm was responsible for the tissue preparation and the calcium imaging.

Tissue preparation

As described in section 5.2.2.2, *ex vivo* calcium imaging was performed to evaluate the effect of orexin-A on POA neurons. For this, mice injected with AAVs coding for iCre-hSyn1 and cre dependent GCaMP6 (explained in detail in section 2.2.9) were euthanized with an overdose of ketamine and xylazine. Following the dissection, 300 μm thick brain slices were done in chilled carbogen-bubbled NMDG-HEPES solution (93 mM NMDG, 2.5 mM KCl, 1.2 mM NaH_2PO_4, 5 mM L(+)ascorbic acid, 2 mM thiourea, 3 mM sodium pyruvate, 10 mM $MgSO_4$, 0.5 mM $CaCl_2$, 20 mM HEPES, 30 mM $NaHCO_3$, 25 mM glucose and 10 mM N-acetyl-L-cysteine, pH 7.3). with a vibratome (HM 650V; Themo Scientific, USA). Three coronal slices covering the POA region (approximately at Bregma AP: +0.24 to -0.16 mm) were collected per animal per brain. In sequence, slices were incubated for 15 min in carbogen-bubbled NMDG-HEPES solution at 32 °C. Next, brain slices were kept in a chamber at RT containing carbogen-bubbled ACSF (125 mM NaCl, 2.5 mM KCl, 25 mM NaHCO3, 1.25 mM NaH2PO4, 1mM MgCl2, 2 mM CaCl2, and 25 mM glucose), for up to four hours, until imaging.

Ex vivo calcium imaging

Calcium imaging was performed using an upright microscope (BX51W; Olympus, Japan) connected to a motorized base plate (SliceScope SS-1000-00; Scientifica, UK), a 20X objective (XLUMPLFLN 20XW Plan Fluorit; Olympus, Japan), 470 nm excitation illumination (pE-2; CoolLED, UK) and a digital CCD camera (ORCA-R2 C10600-10B; Hamamatsu, Japan). The frequency acquisition of the camera was configured at 10 Hz. During imaging, brain slices were constantly perfused with ACSF, gassed with 95% O_2 and 5% CO_2 at 3 ml/min, with the bath temperature being monitored by a thermistor (TA-

29; Warner Instrument, USA) and kept at 32±0.5°C. MetaFluor 7.1 (Molecular devices, USA) was used for the image acquisition. Baseline was recorded while only ACSF was perfused in the bath. After four minutes, 500 nM orexin-A in ACSF (Tocris, USA) was applied on the bath for three minutes. After washout, slices were perfused with high potassium ACSF (ACSF described above with 40 mM KCl and 85 mM NaCl).

Data analysis

Image acquisition was performed using MetaFluor 7.1 (Molecular devices, USA). These images were concatenated with ImageJ/Fiji[124] to prepare an .avi video file, which was used to detect the regions of interest (ROIs), i.e. neurons, and extract their calcium signals over time. For this, using the CaImAn package[134], run in an online Jupyter notebook (demos/notebooks/demo_online_cnmfE.ipynb), the data was motion corrected and ROIs were retrieved with the Constrained Nonnegative Matrix Factorization (CNMF) algorithm[135], followed by manual curation. ROIs with unusual shapes (e.g. square) were removed from the analysis. Extracted calcium signals were baseline corrected using the 'baseline' package[136] in R, and were used to calculate the zscore, in which the mean and standard deviation of the baseline period were used to normalize the whole dataset. Finally, the mean of the baseline and the orexin-A periods were compared for each ROI using Wilcoxon signed-rank test, as previously described[137]. ROIs for which the p-value ≤ 0.05 and the calcium fluorescence signal peak occurred during the orexin-A period were considered to have their activity 'increased'. On the other hand, the ROIs in which the p-value ≤ 0.05 and the calcium fluorescence signal peak occurred during the baseline period were labeled as having 'decreased' activity.

2.2.24 Statistical analysis

The statistical analysis was performed in GraphPad Prism for Windows v5.00 and in R (R versions R-3.3.3 and R-4.0.3)[131] and RStudio version 1.3.1093, with packages used in certain experiments specified in the previous sections. Statistical tests are indicated in the respective figures. One star '*' means $p < 0.05$, three starts '***' mean $p < 0.001$, and 'n.s.'

means non-significant. Normality was tested with D'Agostino & Pearson omnibus test and Shapiro-Wilk test.

CHAPTER 3: OPTIMIZATION OF NEUROACTIVE PEPTIDE SAMPLING AND DETECTION

3 OPTIMIZATION OF NEUROACTIVE PEPTIDE SAMPLING AND DETECTION

3.1 Introduction

While searching for body sources of acetylcholine, Ulf von Euler and John Gaddum, in 1931, serendipitously found a new molecule that became history. Substance P, discovered by the duo, was the first peptide described to be produced in the brain and involved in cell-cell communication, in other words, the first neuropeptide. Since then, more than 100 peptides that participate in the regulation of neural activity have been included in the same category[45]. In addition, some peptide hormones also act in the CNS[45]. Thus, as explained in more details in section 1.6 of the introduction, I refer to neuropeptides and peptide hormones that act in the brain as neuroactive peptides.

Neuroactive peptides play an important role in the regulation of different physiological and behavioural processes, being relevant in healthy and diseased contexts[2,45]. Because of that, there is much interest in studying them. However, they are challenging to investigate, due to low extracellular concentration, rapid degradation, adhesive nature, and complex synthesis, release, and action[90,91]. In spite of this, several technical advances have been made to probe these molecules through three main aspects: structure, location, and function (more details in section 1.8.1 of Introduction). The application of each of these approaches depends on the experimental question.

With this thesis, I aimed to unbiasedly study neuroactive peptides putatively implicated in thermoregulation. For this, an approach that would allow the detection of multiple molecules collected in parallel to thermal manipulations would be well suited. Thus, in this chapter I will present the optimization of the *in vivo* sampling protocol (section 3.2.1) and of the sample preparation and LC-MS/MS screening scheme (section 3.2.2). The latter was performed by me and my collaborator, Dr. Daniele Colombo, a former postdoc at the lab of Dr. Jeroen Krigjsveld at the German Cancer Research Center (DKFZ), Heidelberg.

3.2 Results

3.2.1 Sampling optimization

3.2.1.1 *In vitro* characterization

Two different sampling techniques could be used for the collection of neuroactive peptides, namely microdialysis and OFM (more details in section 1.8.1). To evaluate the feasibility of any of the probes used in these techniques in collecting a peptide of interest, I started testing these devices *in vitro*[138]. My first aim was to compare the efficiency of the 1000 kDa microdialysis and the OFM probes in collecting proteins and peptides. In order to decide which probe to use, I mimicked the *in vivo* situation by testing both probes placed in a solution containing BDNF. This peptide was chosen because its expression has been found enriched in the POA upon warm peripheral stimulation[35]. Assuming that BDNF would be released at the POA during a thermal challenge, it could presumably be collected during the *in vivo* sampling. Thus, BDNF was one of the molecules that I expected to be present in *in vivo* samples, and testing if the probes are able to collect this peptide was an important quality control step.

In the *in vitro* sampling approach, the probe was connected to the sampling system in the same way as it would be in the *in vivo* setup, but in this case, it was placed in a tube containing BDNF solution (55 μM rBDNF) diluted in 0.1% BSA in Ringer, instead of being implanted in an animal's brain. After this, the samples collected with the 1000 kDa and cOFM probes were analysed using western blot for BDNF. As shown in figure 3.2-A, the OFM outperformed the 1000 kDa probe, nearly reproducing what was detected in the BDNF solution used as the input (BDNF total in the figure 3.2-A).

3.2.1.2 *In vivo* characterization

The next step was to evaluate if the 1000 kDa and OFM probes could be used to collect neuroactive peptides from the POA *in vivo*. To increase the surface area of the

exchangeable part of both probes and improve collection, I used devices with 2 mm length exchangeable surfaces. It is important to highlight that this comes with the expense of sampling molecules from non-POA regions in the close vicinity (Figure 3.1).

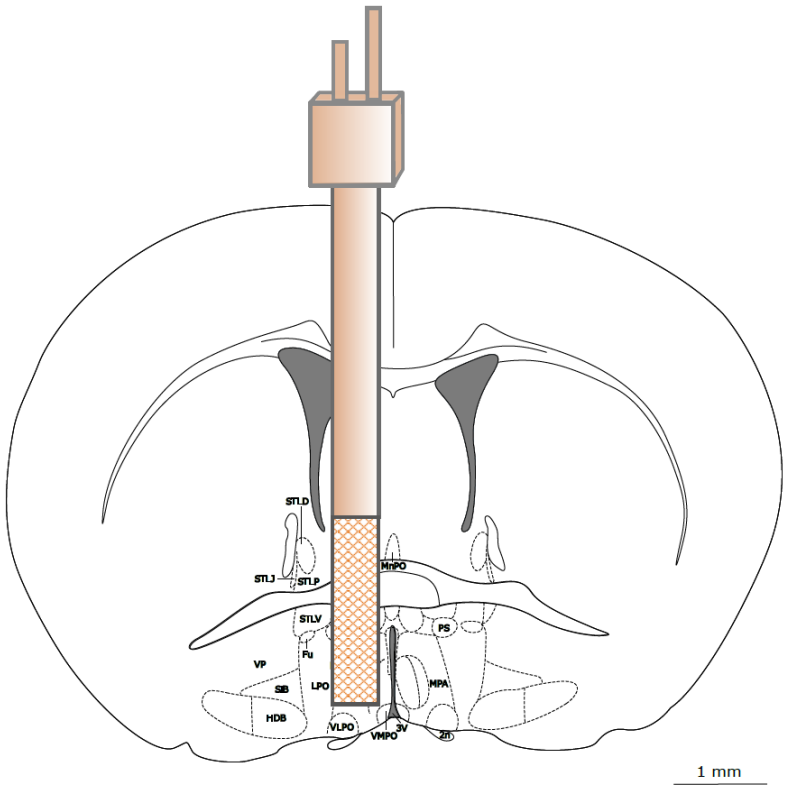

Figure 3.1: Mouse coronal brain section with a sampling probe

The scheme represents a sampling probe implanted in the POA coordinates. In filled orange is the probe shaft and in chess orange is the exchangeable surface, where the exchange of molecules occur (Adapted from Franklin and Paxinos, 2007). aca: anterior commissure, Fu: bed nucleus of stria terminalis, fusiform part; Hy: Septohypothalamic nucleus; LPO: lateral preoptic area; LV: lateral ventricle; MnPO: Median preoptic nucleus; MPA: medial preoptic area; PS: parastrial nucleus; STLV: lateral bed nucleus of stria terminals; STMV: medial bed nucleus of stria terminalis; VLPO: ventrolateral preoptic nucleus; VMPO: ventromedial preoptic nucleus; 3V: third ventricle.

For the *in vivo* sampling with the 1000 kDa and OFM probes, the respective probe was inserted in a cannula previously implanted in the animal brain. The two probes were

always tested in different animals. To evaluate the samples collected with these probes, I performed silver staining and bicinchoninic acid (BCA) assay.

To evaluate the sample protein diversity, I performed a silver staining with samples collected with the 1000 kDa and OFM probes. The staining was used to visualize the collected proteins and peptides in a gel. With this, for example, I could check if smaller molecules were present in the samples. Figure 3.2-B shows the silver stained gel loaded with samples coming from animals implanted with 1000 kDa and OFM probes. As shown in the figure 3.2-B, proteins and peptides of different sizes were collected with both probes. The picture also shows variability among these samples regarding the amount of proteins – indicated by the different shades of brown.

The total protein concentration of samples coming from the probes was estimated using BCA assay. For this, two samples collected from each animal were pooled together and each pool (20 µl in total) was quantified separately. Figure 3.2-C shows the estimated sample concentration of samples collected with both probes. Based on these results, it is possible to infer that there is a high variability in the same group concerning protein amounts for both probes, but no significant difference was found comparing the means of samples collected with both probes (figure 3.2-C).

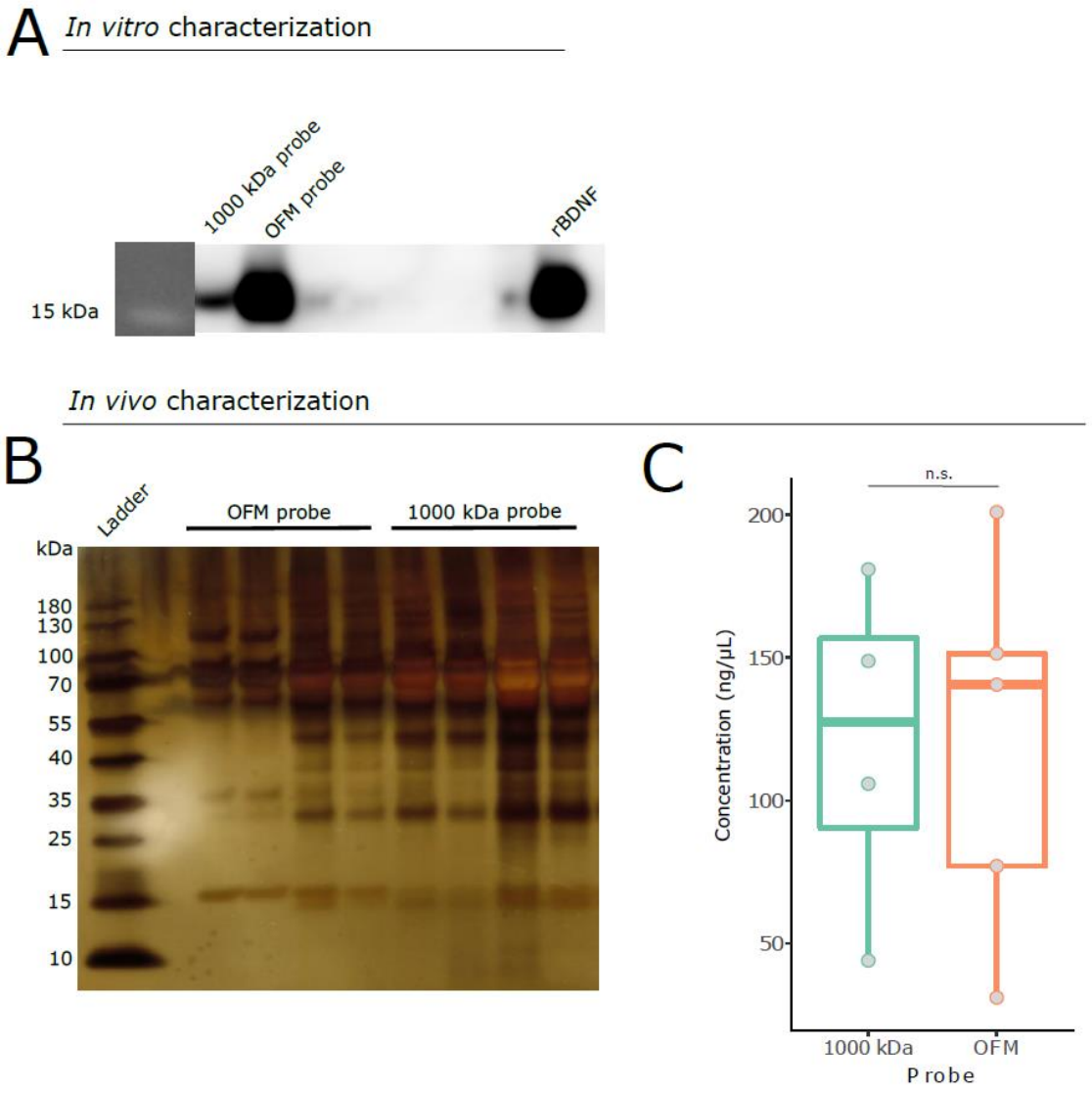

Figure 3.2: ***In vitro* and *in vivo* characterization of microperfusates.**

A: Western blot for BDNF of samples collected *in vitro*. rBDNF (expected size: 15 kDa) was either collected using the 1000 kDa probe or the OFM probe. The rBFNF solution from which rBDNF was collected from, during the *in vitro* microperfusion, was loaded on the extreme right side of the blot for comparison. B-C: Characterization of samples collected from freely behaving mice. B: Protein silver staining of samples collected with OFM probe (n = 4 samples, 2 mice) and 1000 kDa probe (n = 4 samples, 2 mice). C: Total protein BCA quantification of samples collected with 1000 kDa probe and OFM probe. The box plot shows the median (thick line), interquartile range (box) and full range (whiskers). Each dot represents one animal. Two-tailed Mann-Whitney test, mean 1000 kDa probe = 119.90±59.15 (n = 4 mice), mean OFM probe = 120.20±66.50 (n = 4 mice), p-value = 1.000. 'n.s' = non-significant.

In addition to the *in vitro* and *in vivo* characterization of the 1000 kDa and OFM probes, I also took into consideration other aspects to decide between these two. By visual inspection, the tissue damage due to cannula and probe implantation was similar comparing the two approaches (data not shown). Nevertheless, the OFM probe is cheaper and can be reused. Thus, after considering all aspects analyzed (summarized in table 3.1), I decided to continue the sampling experiments with the OFM probe.

Table 3.1: Comparison between the 1000 kDa and open probes.

	1000 kDa	**OFM**
In vitro recovery of BDNF	+	+++
Sample concentration	=	=
Tissue damage	=	=
Reusability	No	Yes
Price	+++	+

3.2.2 Optimization of neuroactive peptide detection

To overcome the challenges of detecting neuroactive peptides in microperfusates (detailed in section 1.8.1 of introduction), the samples were analysed with LC-MS/MS, a high-throughput and highly sensitive approach[106]. However, the first attempts of proteomics analysis of POA microperfusates only detected 8 neuroactive peptides (data not shown). Thus, my next aim was to improve the detection of neuroactive peptide in microperfusates. For that, together with Dr. Colombo, we tested different sample processing conditions and LC-MS/MS parameters in order to define a better workflow for the enrichment of neuroactive peptide detection in microperfusates. For these tests, I made a pool composed of samples collected from five animals implanted with the OFM probe. Then, this pool was divided into three parts for the next steps (figure 3.5-B).

3.2.2.1 Sample processing optimization

We tested three sample processing conditions, summarized in figure 3.5-A. The three conditions are referred here as A, B, and C. In A, the samples were refined with a 3 kDa filter. With the 3 kDa filter used in condition A, we aimed to simplify the samples and filter for molecules smaller than 3 kDa, a molecular size range that would fit several neuroactive peptides. Thus, we expected to only observe peptides smaller than 3 kDa in these samples. For the removal of salts from the sample, an important step before analyzing samples in a mass spectrometer, we compared two methods, the magnetic beads clean-up (adapted from Hughes et al., 2014) (used in conditions A and C) and the solid phase extraction (used in B). In A, the magnetic beads clean-up occurred after the refinement with the 3 kDa filter. In B, a solid phase extraction was performed in the samples with a commercial kit (OASIS, Waters, USA). And in C, the magnetic beads clean-up was followed by trypsin treatment, in order to test if applying trypsin digestion could enhance peptide detection, given that tryptic peptides are standardly searched in proteomics. Of note, the trypsin digestion came with the expense of also digesting neuroactive peptides (as illustrated in figure 3.3). Following the preparation, the samples were run in replicates in the LC-MS/MS and analyzed with four different LC-MS/MS methods explained in section 3.2.2.2 (figure 3.6-A).

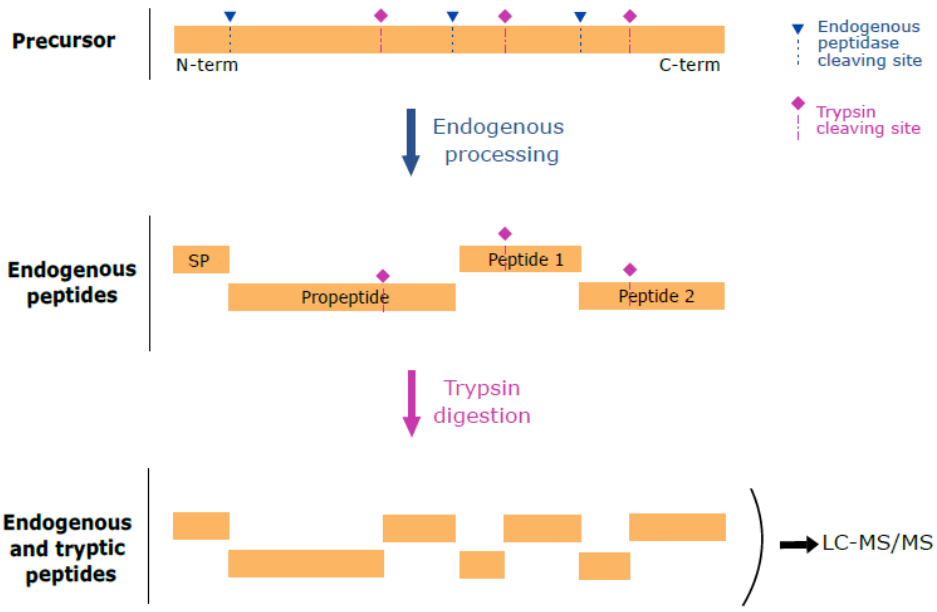

Figure 3.3: Natural processing of neuroactive peptides and subsequent trypsin digestion used in condition C

'SP' stands for signal peptide.

The three sample processing conditions were evaluated based on the amount of proteins and neuroactive peptides detected in the samples processed with each of the conditions. The acquired MS data was processed using MaxQuant (version 1.6.2.6)[128,129]. Protein quantification was performed using the label-free quantification (LFQ) algorithm of MaxQuant, MaxLFQ, which compares the intensity of the same peptide across samples from different runs[139]. To avoid that a peptide sequence that is common among two or more different proteins, MaxQuant assigns peptides to protein groups. Such groups contain one or more protein, depending on the peptide sequences found (figure 3.4)[129].

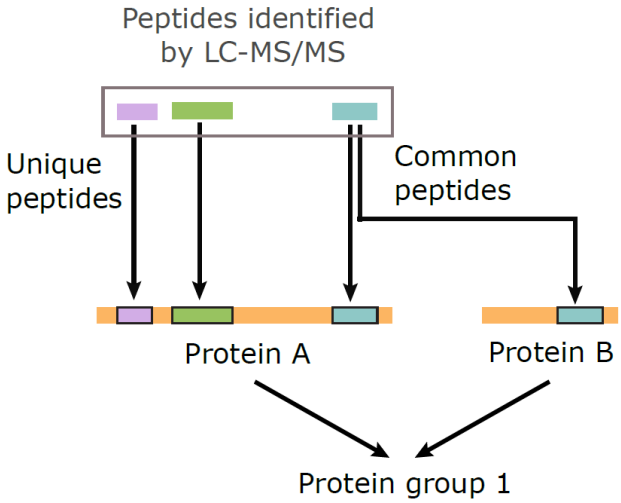

Figure 3.4: Protein groups as they are assembled by MaxQuant.

Figure modified from Tyanova et al, 2016.

The total amount of protein groups found in each condition is shown in figure 3.5-C. As it can be appreciated in this figure, the sample processing condition C (magnetic beads clean-up with trypsin treatment) outperformed the other conditions, leading to the detection of up to 570 protein groups in the samples tested. Interestingly, the number of neuroactive peptide was also remarkably higher in condition C (Figure 3.5-D and E). Specifically, among the 19 neuropeptides identified in total, two were detected in samples processed with condition A, three were detected with condition B, and all 19 were detected with condition C. Therefore, considering the best performance of condition C in terms of total protein and neuropeptide detection, we concluded that this was the best condition tested.

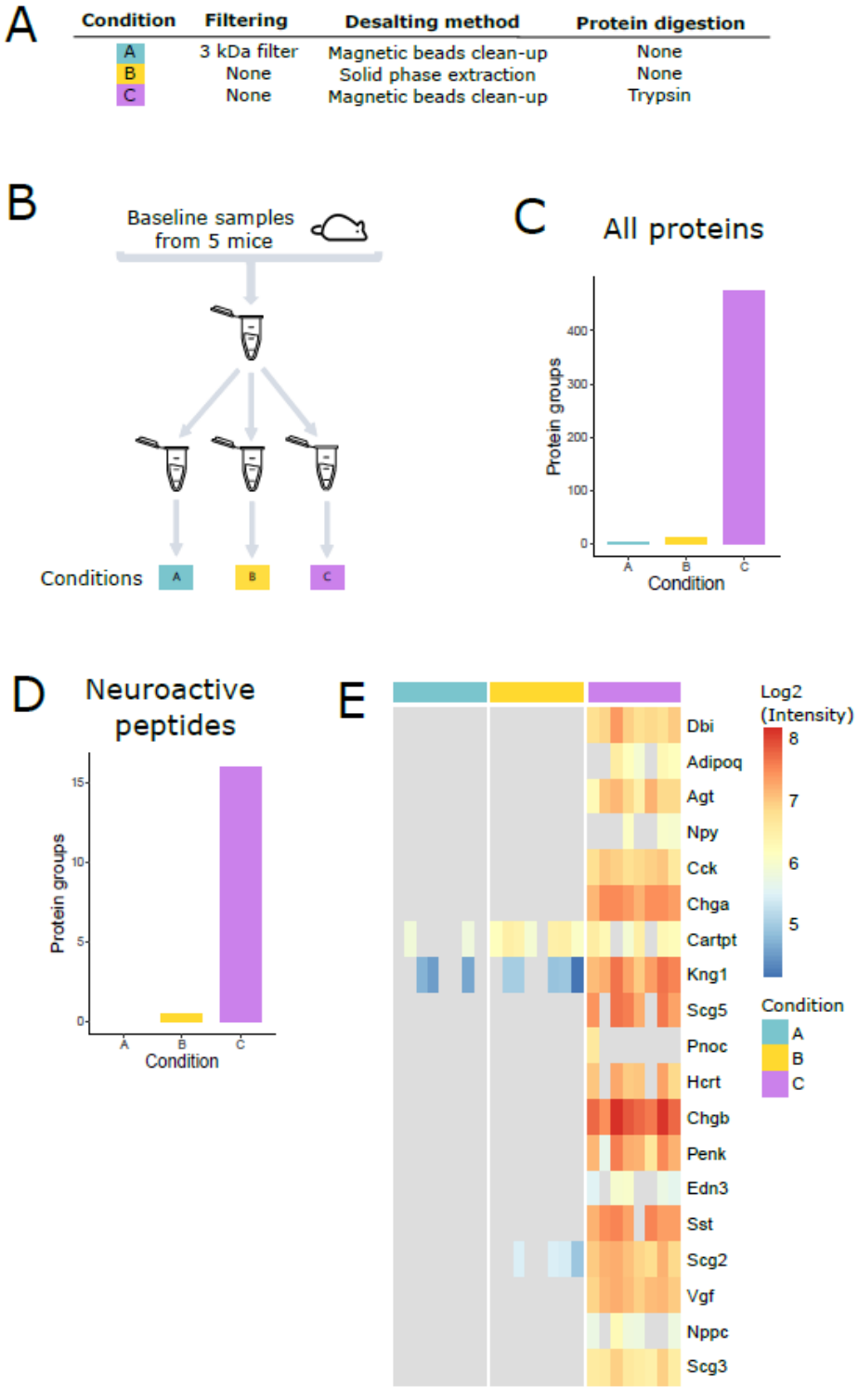

Figure 3.5: **Optimization of sample processing conditions to enhance the detection of neuroactive peptides in microperfusates.**

A. Summary of sample processing conditions tested in microperfusates. B. Summary of sample preparation for the optimization. In total, samples from five mice were pooled together. The pool

was divided into three aliquots and each aliquot received a different treatment. Each sample processing condition was run in duplicate. Duplicates were run using four different LC-MS/MS parameters explained in the next section and in figure 3.6-A. C. Total amount of protein groups from all proteins detected in the microperfusates treated with the different sample processing conditions. D. Total amount of protein groups from all neuroactive peptides detected in the microperfusates treated with the different sample processing conditions. E. Heatmap showing the log10 of intensity of all neuroactive peptides identified in the microperfusates treated with the different sample processing conditions. Columns in the heatmap represent the three processing conditions run in duplicate and analyzed with four different LC-MS/MS methods explained in the next section and summarized in figure 3.6-A. Missing values in the heatmap are shown in light grey.

3.2.2.2 LC-MS/MS workflow optimization

The next step was to find a LC-MS/MS workflow that could efficiently detect a good number of different neuroactive peptides in microperfusates. For that, we tried four combinations of LC-MS/MS parameters, referred here as methods 1, 2, 3, and 4, summarized in figure 3.6-A. The LC parameters were chosen based on previous studies investigating neuropeptides in microdialysates collected from the crab hemolymph[140] and the neuropeptidome of the *Tsetse* fly[127], as well as the human plasma peptidome[126]. The LC gradient applied in methods 1 and 4 had slower increments of buffer B (hydrophobic) into buffer A (hydrophilic), enabling better separation of hydrophilic and hydrophobic peptides. On the other hand, the LC gradient of methods 2 and 3 was shorter, theoretically providing a less precise but faster separation of peptides. For the MS methods, it was used different combinations of m/z ratio ranges and charge exclusion.

To compare the different LC-MS/MS methods, we focused the analysis on the samples processed with condition C. As done previously, we evaluated the different methods based on the amount of protein groups and neuroactive peptides detected in each sample. Figure 3.6-C shows the total amount of protein groups found in each sample run with different LC-MS/MS parameters. Comparing the four different methods, the method 4 was the one that enabled the detection of more protein groups, followed by methods 1

and 3, with the second method performing the worst. Focusing on the neuroactive peptides (figure 3.6-D and E), among all 19 peptides detected, 18 were found with method 1, 16 by method 2, 18 by method 3 and 18 by method 4.

Therefore, among all LC-MS/MS methods tested, method 4 was the one in which more protein groups and neuroactive peptides were detected. Nevertheless, considering that method 3 had a shorter LC run, the detection of 15 peptides in both replicates out of 18 peptides detected in total showed good reproducibility rate. Taking into consideration the time efficiency, the shorter run of method 3 represented a good advantage. Thus, among methods 3 and 4, considering the similar performances in terms of neuroactive peptide detection, and that method 3 had the advantage of being faster, we rationalized that method 3 was more beneficial for the purposes of this thesis.

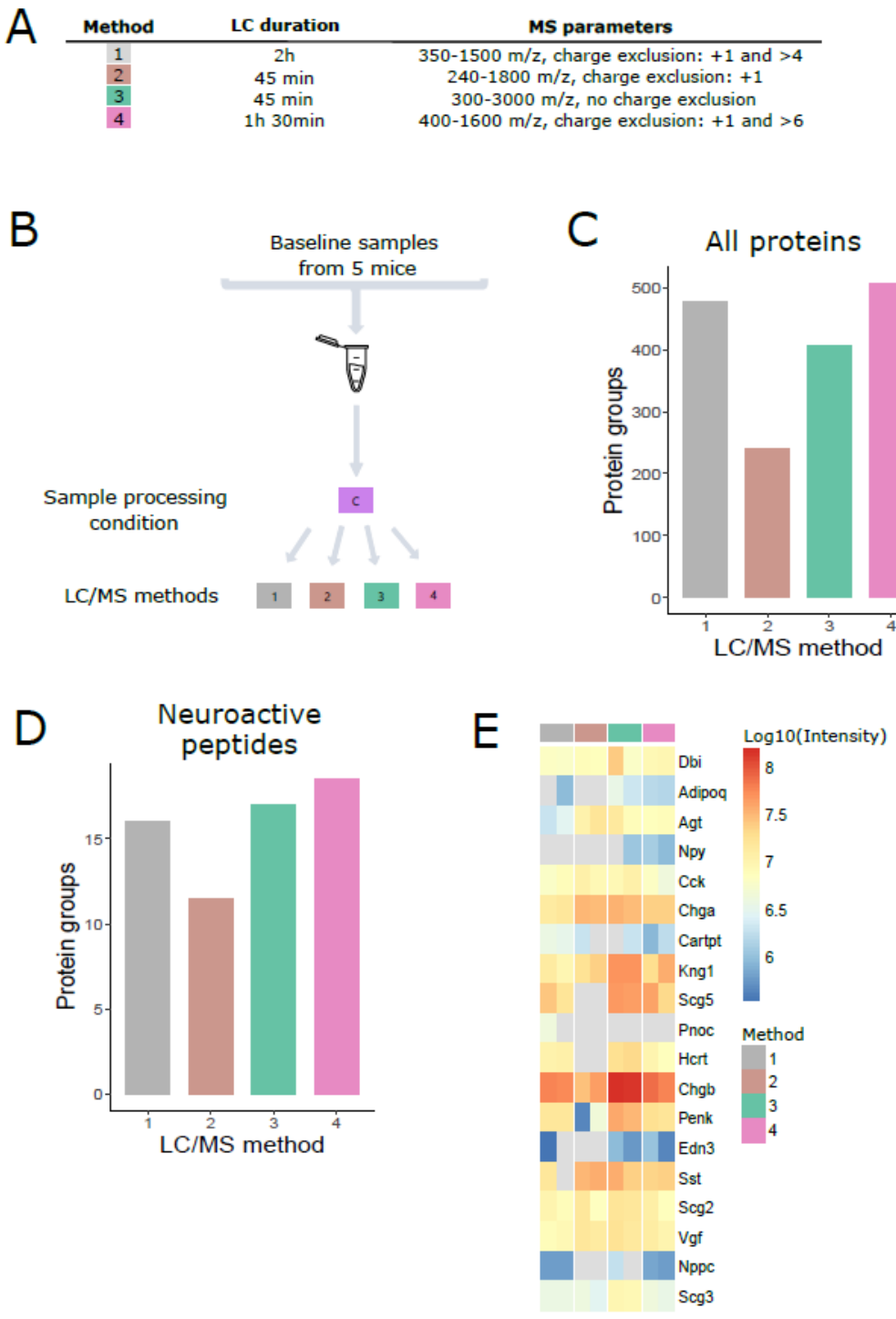

Figure 3.6: **Optimization of LC-MS/MS methods to improve the detection of neuroactive peptides in microperfusates.**

A. Summary of LC-MS/MS methods tested in microperfusates. B. Summary of sample preparation for the LC-MS/MS tests. After being processed with the condition C, explained in figure 3.5, the samples were divided into four aliquots, and each aliquot was run with a different combination of

LC-MS/MS methods. C. Total amount of protein groups from all proteins detected in the microperfusates tested with the four different LC/MS methods. D. Total amount of protein groups from all neuroactive peptides detected in the microperfusates tested with the four different LC/MS methods. E. Heatmap showing the log10 of intensity of all neuroactive peptides identified in the microperfusates tested with the four different LC-MS/MS methods. Missing values in the heatmap are shown in light grey.

3.3 Discussion

The regulatory role of neuroactive peptides in healthy and diseased states make them molecules of great interest. Despite the technical advances that enabled better investigation of these substances, their *in vivo* measurement still remains challenging. Thus, my goal with this first set of experiments was to define an optimized workflow to collect and detect neuroactive peptides from freely behaving animals. Based on the parameters tested here, the most optimized sampling and screening scheme was the combination of OFM *in vivo* sampling with the sample processing performed with magnetic beads clean-up and trypsin treatment. Additionally, the most efficient LC-MS/MS combined 45 min of LC run and 300-3000 m/z range and no charge exclusion.

We tested three different processing conditions (A, B, and C). With the 3 kDa filter used in condition A, our aim was to simplify the samples collected with OFM probe. Given the membrane-free nature of these probes, there is the possibility of collecting almost all molecules present in the extracellular space around the probe. This has the disadvantage of adding more complexity to the sample analysis, as many proteins and peptides can potentially be collected. For instance, the detection of highly abundant proteins could be favoured instead of lowly abundant neuroactive peptides[100]. Thus, we expected that the 3 kDa filter would make the LC-MS/MS analysis easier. However, samples treated with condition A performed too poorly, and no neuroactive peptide was detected.

We also tested if adding trypsin to the samples after desalting by magnetic beads clean-up would improve the detection of neuroactive peptides. Trypsin is the most common protease used in the sample preparation for LC-MS/MS because of its cleavage specificity and high enzymatic activity[100]. Thus, one advantage of adding it to the samples is that the well-known cleavage pattern of trypsin makes tryptic peptides easily trackable in the proteome using computational methods. Therefore, considering the mouse proteome and knowing where to expect tryptic cleavage sites to occur, the tryptic peptides detected by MS/MS are more easily aligned to the reference proteome by computational approaches[100].

One difficulty of working with neuroactive peptides and trypsin digestion is that larger proteins yield more peptides than smaller ones. When the raw MS/MS data is computationally analysed, the more numerous peptides coming from larger proteins provide a more solid evidence for the presence of these proteins in the samples. In contrast to this, smaller proteins, which includes the majority of neuroactive peptide precursors, yield less tryptic peptides, thus the reliable identification of these precursors is hindered. On top of this, no clear tryptic digestion signature exists for some neuroactive peptides. Nevertheless, the use of trypsin in the samples still greatly improve the identification of neuroactive peptide precursors. We indeed observed a much higher detection of protein groups and of neuroactive peptides in microperfusates processed with trypsin (condition C) than without (conditions A and B).

The combination of processing condition C and the LC-MS/MS method 3 yielded the detection of nearly 400 proteins groups, including 18 neuroactive peptides. Thus, neuroactive peptides represented around 4.5% of the all protein groups. The neuroactive peptide database that we used as reference[85] contained 115 neuroactive peptide precursors. Assuming that all these precursors can be detected by LC-MS/MS and comparing this amount to a mouse hypothalamus proteome[141], which detected 7718 protein groups, neuroactive peptide precursors would correspond to roughly 1.5% of the whole proteome. Taking this into consideration, our results suggest that the combination

of *in vivo* sampling and our optimized LC-MS/MS workflow provided a three-fold enrichment in the detection of neuroactive peptides.

To conclude, in comparison to the first attempts of performing proteomics on microperfusates, in which only 8 neuroactive peptides were detected (data not shown), the subsequent optimized workflow largely surpassed these results. In the tests performed here, up to 18 neuroactive peptides were detected in the samples, showing a substantial improvement in the identification of these peptides in microperfusates. Additionally, comparing these results to another unbiased analysis of microdialysates, our sequential optimization protocol allowed us to markedly increase the number of detected peptides in samples from rodent brain from 85[111] as found before, to more than 400 in the tested samples. Therefore, our workflow not only was suitable for the unbiased screening of secreted peptides, but also greatly improved the recovery of peptides and proteins in general.

CHAPTER 4: CHARACTERIZATION OF NEUROACTIVE PEPTIDES RELEASED DURING ACTIVATION OF PREOPTIC GLUTAMATERGIC NEURONS

4 CHARACTERIZATION OF NEUROACTIVE PEPTIDES RELEASED DURING ACTIVATION OF PREOPTIC GLUTAMATERGIC NEURONS

4.1 Introduction

Despite the cellular and anatomical efforts in characterizing the POA in the context of thermoregulation (more details in section 1.4 of introduction), molecular mechanisms that act in the region and modulate the activity of its neurons during thermal challenges remain elusive. However, a good hint came from brain injection studies of neuroactive peptides and DE analyses (more details in section 1.7 of introduction). Together, these studies have proposed that some peptides could decrease Tcore, such as NPY[63], or increase, such as TRH[51,60]. Although important, these studies had limitations, as discussed in section 1.7, therefore it is still unclear if neuroactive peptides are naturally released at the POA in order to adapt to thermal challenges.

Among several thermoregulatory neuron populations (described in more detail in section 1.4 of introduction), POA^{VGLUT2} neurons appear as one of the major subgroups[20,29,37]. The artificial stimulation of these and other thermoregulatory neurons, with methods as chemogenetics (explained in detail in section 1.8.2 of introduction)[29,35,38], is one way to target these populations. The activation of thermoregulatory neurons with chemogenetics represents an artificial and strong stimulation of these neurons[112]. Therefore, it is important to highlight that chemogenetics activation is not expected to faithfully represent what happens *in vivo* during a natural stimulation. Nevertheless, it is a good tool to target and stimulate a given cell population. In this context, the stimulation of a neuronal thermoregulatory population with chemogenetics makes it possible to access the central control of Tcore, with the advantage of targeting a specific neuron group.

The POA^{VGLUT2} neuronal population has been shown to partially overlap with neurons expressing the peptides BDNF, PACAP, and QRFP. Thus, I hypothesized that upon the

activation of preoptic glutamatergic neurons, among other neuroactive peptides, I would be able to detect these molecules in the samples. To investigate if these or other neuroactive peptides are differentially released upon themoregulatory neuronal population, I used chemogenetics to activate POA^{VGLUT2} together with an *in vivo* sampling technique. With this, the goal of this chapter was to unbiasedly investigate the neuroactive peptides secreted at the POA upon thermoregulatory neurons activation. To my knowledge, this was the first attempt to unbiasedly characterize the secretome (set of proteins and peptides secreted into the extracellular space) during thermoregulatory neuron stimulation. Here, I present the results obtained with this experiment.

4.2 Results

4.2.1 Chemogenetic activation of preoptic Vglut2+ neurons led to hypothermia

To identify the neuroactive peptides released at the POA that could modulate thermoregulation, I artificially activated a population of themoregulatory neurons using chemogenetics in parallel to OFM. After collection, the samples were analysed by LC-MS/MS in an unbiased way, in order to detect which peptides were released at the POA and collected by this approach. The samples were analysed in a collaboration with Dr. Daniele Colombo, in the laboratory of Dr. Jeroen Krijgsveld at DKFZ, and with Dr. Silvia Calderazzo, a biostatistician from DKFZ.

I used chemogenetics to artificially activate a particular set of thermoregulatory neurons expressing VGLUT2. For this, I injected Vglut2-cre male adult mice in the POA with a viral construct coding for a cre-dependent engineered muscarinic receptor coupled to protein Gq (DREADDs-hM3d-Gq). This receptor is activated upon binding of the inert ligand clozapine-N-oxide (CNO), that initiates the Gq protein signaling cascade and ultimately leads to more neuronal excitability[112]. This AAV was coupled to mCherry, which allowed the visualization of injected cells. It was also fused to the human synapsin promoter, thus I expected to observe mCherry+ cells only in Vglut2+ neurons that

expressed the receptor (Figure 4.1-B). Control animals, which were littermate mice negative for cre, were injected with the same virus. Following the injection, in the same day, the animals were implanted with an OFM cannula in the POA for *in vivo* sampling. At least one week later, I implanted the animals with a telemetry probe in the peritoneal cavity for core temperature measurement.

Two weeks after AAV injection and cannula implantation, microperfusates were collected at 0.5 µl/min flow rate. During the first two hours, microperfusates were collected under baseline (only vehicle, Ringer), and then under the perfusion of a solution containing CNO (10 µM CNO in Ringer) for additional two hours (figure 4.1-A). Both solutions were delivered directly into the POA via the OFM probe, in parallel to the sampling. A liquid switch, a device that allows the passage of only one liquid at each time, was used to change from one solution to another. The direct delivery of CNO and the use of a liquid switch required no immobilization of the animal during sampling, therefore this strategy avoided the stress involved in handling the mouse for an injection.

Specific POA^{VGLUT2} activation was measured following changes in core temperature. Change in Tcore was calculated subtracting the body temperature on the day of microperfusion comparing to the averaged Tcore measured on the day before. Chemogenetic activation of POA^{VGLUT2} neurons elicited robust hypothermia in Vglut2-cre positive mice, which persisted during the whole *in vivo* sampling, while no influence on Tcore of control mice was observed (fig. 4.1-C and D). These results were in agreement to what was previously described in the literature[20,29,37].

I also measured the ambulatory activity of mice within the cage throughout the experiment, quantified in the figure 4.1-E as the cumulative sum of activity. Of note, the Vglut2-cre already started the experiment showing lower activity in comparison to WT-like counterparts. The decreased activity was observed during baseline and during CNO stimulation, in the opposition to the Tcore, which only decreased upon the drug administration.

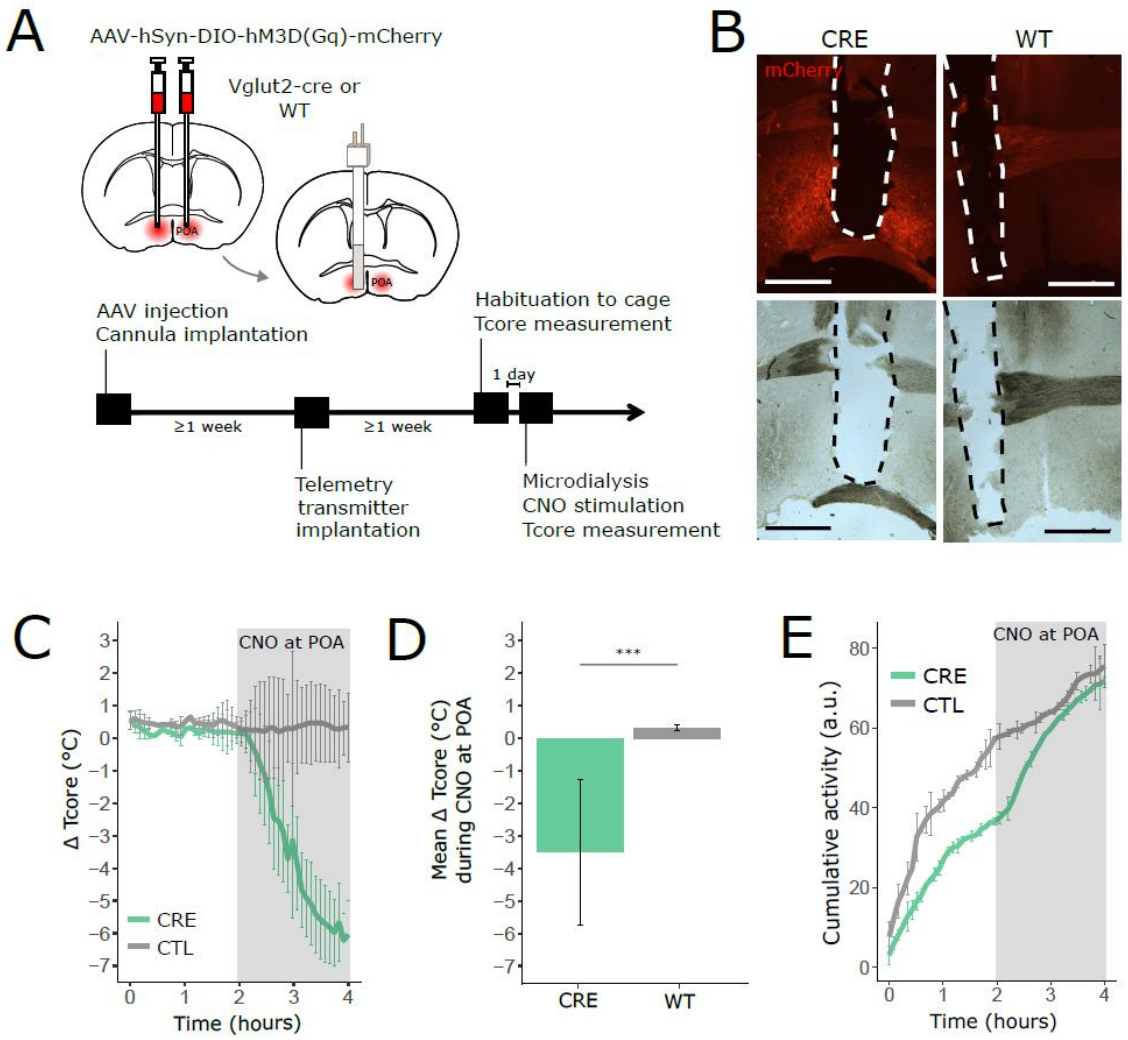

Figure 4.1: Chemogenetic activation of POA^{Vglut2} neurons

A: Scheme showing the experimental strategy to the AAV-mediated chemogenetic activation (Gq-DREADDs) of Vglut2-cre neurons in POA. B: Representative microscopy images of coronal microtome brain sections showing the injection and the implantation sites. On the left side, one Vglut2-cre (CRE) positive animal expressing Gq-DREADDs-mCherry. On the right side, one littermate, WT-like, Vglut2-cre negative mouse, in which mCherry signal is absent. The dashed lines delimit the area where the cannula was implanted. C: Changes in Tcore temperature in Vglut2-cre (n = 5) and WT (n = 4) male mice during microperfusion sampling, before and after CNO stimulation at POA (mean ± s.d.). D: Comparison between mean values of Tcore change after CNO arrived at POA (light grey highlight in C) in CRE and WT groups (two-tailed Mann-Whitney test, mean CRE = -3.485±2.234 (n = 5), mean WT = 0.321±0.085 (n = 4), p-value <0.0001). '***' means < 0.0001. E: Cumulative activity (relative movement of mice within the cage) in Vglut2-

cre (n = 5) and WT (n = 4) male mice during microperfusion sampling, before and after CNO stimulation at POA (mean ± s.d.).

4.2.2 POA^{Vglut2} neurons activation led to differential release of neuroactive peptides

The microperfusion sampling occurred in parallel to chemogenetic activation of POA^{VGLUT2} neurons. Both groups received vehicle during baseline and CNO afterwards (figure 4.2-A). For LC-MS/MS analysis, Dr. Colombo and I used the optimized sample processing workflow described in chapter 3. In sequence, the samples were analysed by Dr. Colombo on a Q Exactive Orbitrap mass spectrometer (Thermo Scientific, San Jose, CA, USA), online coupled to EASY-nLC nano flow ultra-high performance liquid chromatography (UHPLC) instrument (Thermo Scientific, San Jose, CA, USA). Data analysis was performed in Max Quant.

Two different data analysis approaches were used to evaluate the samples, namely, the group and the temperature analysis. The data analysis was performed by Dr. Calderazzo, Dr. Colombo, and by myself. Dr. Calderazzo and Dr. Colombo wrote most of the R script used to analyze the data, and I wrote part of the code for the group analysis. Each approach is explained in the next sections.

4.2.2.1 Group analysis

In this data analysis approach the Vglut2-cre (CRE) and control (WT) groups were analyzed comparing before and after CNO stimulation. For that, averaged baseline intensities were subtracted from averaged CNO stimulation intensities. The resulting values were then used to calculate the fold change of CRE in comparison to WT samples using the R package Limma[133].

In total, 552 protein groups (this concept is illustrated in figure 3.4) were found. From these, 42 were found significantly different in the CRE group in comparison to WT ($p \leq$

0.05, adjusted by Benjamini-Hochberg correction) (figure 4.2-C). The top 29 protein groups are shown in the heatmap in figure 4.2-B.

In regard to neuroactive peptides, in total, we were able to detect 20 protein groups of neuroactive peptide precursors, referred here as neuroactive peptide – protein level. Among these, one neuroactive peptide precursor, namely proSAAS, was found significantly increased between the CRE and WT groups ($p \leq 0.05$, adjusted by Benjamini-Hochberg correction) (figure 4.2-D). In addition to the protein groups of neuroactive peptide precursors, we also quantified the data based on individual detected peptides. With this, we aimed to cover the endogenous and tryptic peptides (illustrated in figure 3.3). Following this approach, we were able to identify 115 individual peptides derived from the 20 protein groups mentioned above. From these, 7 peptides were found significantly different in samples from the CRE group in comparison to WT ($p < 0.05$, adjusted by Benjamini-Hochberg correction) (figure 4.2-F). These seven peptides are shown in a heatmap for visualization of their intensity in individual samples (figure 4.2-E). The peptides found increased upon CNO stimulation in the CRE group come from the following precursors: diazepam binding protein (DBI) (one peptide), Kininogen-1 (KNG1) (one peptide), and ProSAAS (two peptides, shown in the heatmap as ProSAAS-A and ProSAAS-B). The peptides found decreased come from Secretogranin-1 (SCG1) (three peptides, shown in the heatmap as Scg1-A, Scg1-B, and Scg1-C).

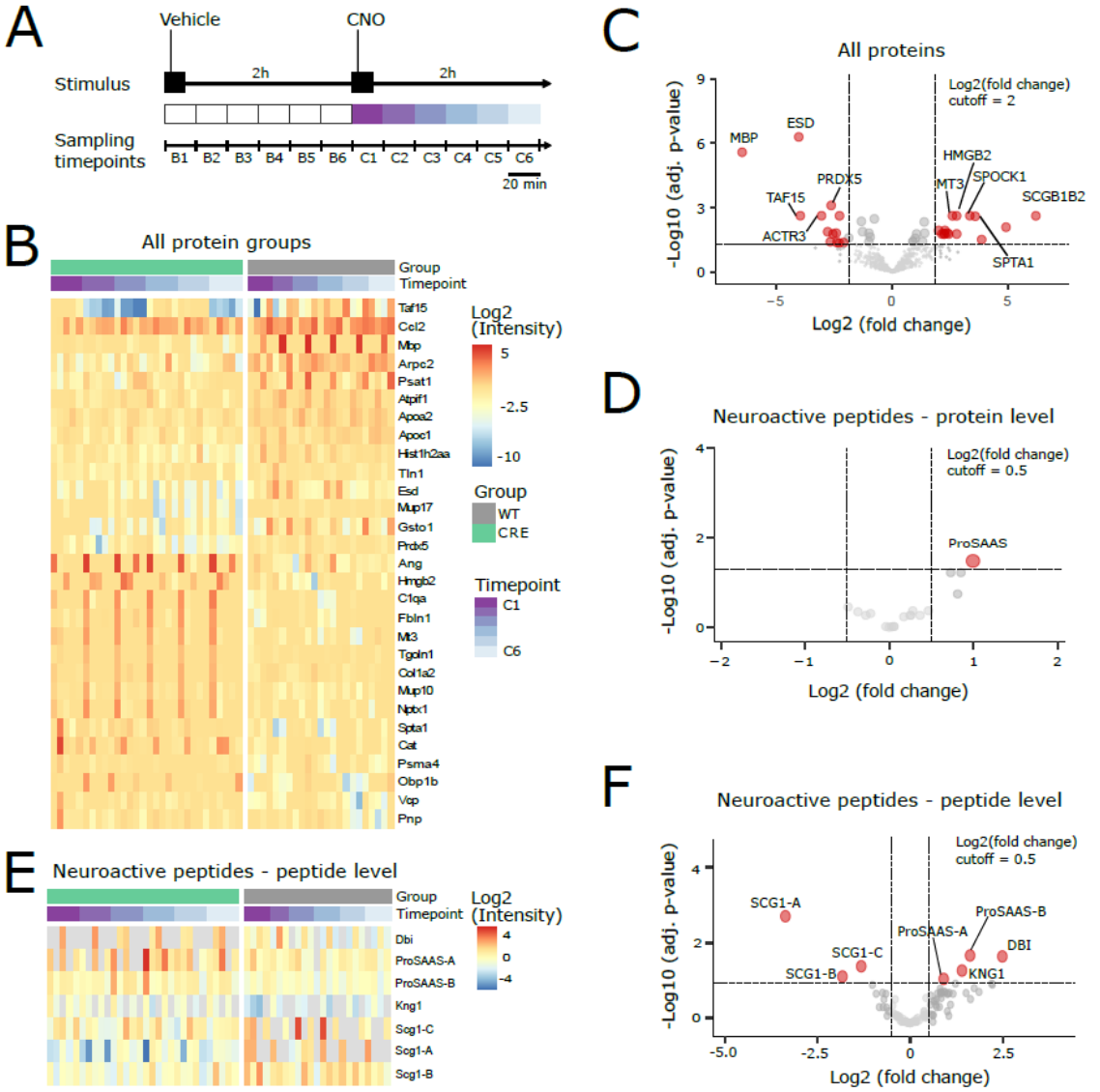

Figure 4.2: **Preoptic glutamatergic activation led to differential release of proteins and neuroactive peptides in the CRE group**

A: Sampling and stimulation scheme used in the experiments performed with each group. B-C: All protein groups found in the analysis. D: Protein groups of neuroactive peptide precursors detected in the analysis. E-F: Individual peptides from neuroactive peptide precursors found in the analysis. B and E: Heatmaps show the protein groups or peptides significantly changed in the CRE group (n = 5 mice) in comparison to WT (n = 4 mice). The plot shows the log 2 of the intensity of these molecules in samples collected during CNO stimulation normalized by averaged baseline intensities of each corresponding group. From each mouse, a maximum total of 6 samples are shown and color labeled based on different timepoints referred in A. The group and timepoint annotation of B also applies to E. Missing values in the heatmaps are shown in light

grey. C, D and F: Volcano plots show the log2 of fold change and the adjusted p-value of samples from the CRE group in comparison to the WT group. The fold change cutoff used in C was 2, and in D and F was 0.5. Each red dot represents a significant protein or peptide found in the analysis. In grey dots are all the other proteins or peptides. Dots of significant hits were expanded in size for better visualization purposes only.

4.2.2.2 Temperature analysis

In the temperature data analysis approach, the core body temperature of each animal was correlated with the intensity of protein group or peptide, regardless of the experimental group. However, as shown in figure 4.1-C, only the CRE group changes the Tcore robustly throughout the experiment. The comparison was done based on increments of 1°C, i.e., the fold change represents how much the intensity of a protein or peptide is changing with differences of 1°C in temperature. For instance, a given peptide intensity shows 0.5 increase with every decrease of 1°C in Tcore.

In total, 552 protein groups were detected. From these, 21 were found significantly changed based on differences in the Tcore ($p \leq 0.05$, adjusted by Benjamini-Hochberg correction) (figure 4.3-B and C). All of them are shown in the heatmap in figure 4.3-C. From all 522 protein groups detected, 20 of them were of neuroactive peptide precursors. From these, one was found significantly different according to the Tcore ($p \leq 0.05$, adjusted by Benjamini-Hochberg correction) (figure 4.3-D and E). This precursor, namely somatostatin (SMS), was found positively correlated to body temperature, showing increased intensity with increments of 1°C. SMS intensity in individual samples according to the Tcore is shown in a scatter plot (figure 4.3-D). In agreement to the protein group analysis, using the analysis based on individual peptides, we also found one peptide from somatostatin significantly different based on the correlation with Tcore (figure 4.3-F and 4.3-G).

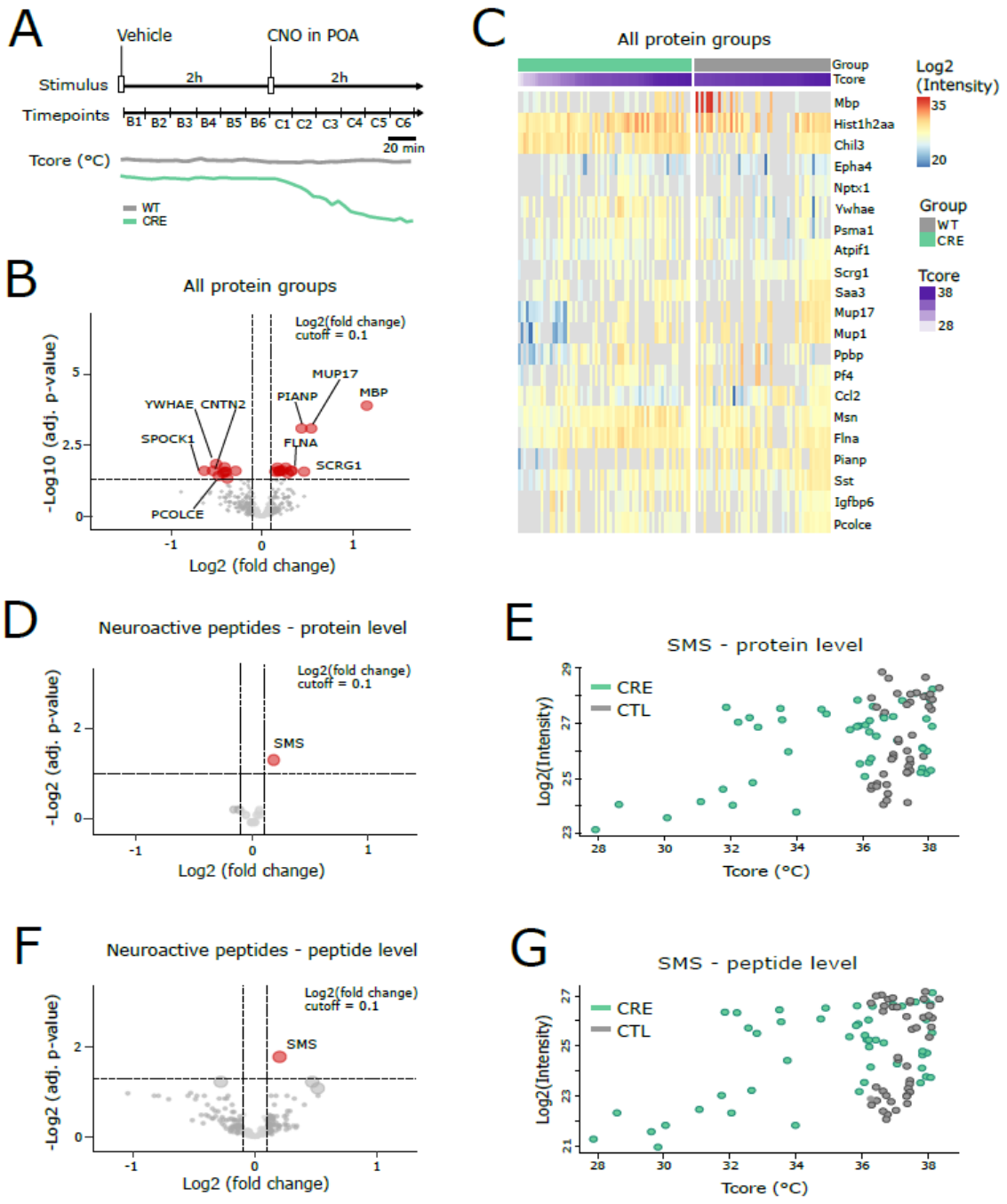

Figure 4.3: **POA^{VGLUT2}-activation induced hypothermia correlates with differential release of proteins and neuroactive peptides in the CRE group**

A: Scheme showing the sampling and stimulation timeline used in the experiments performed with each group. Below, a representative Tcore (°C) trace of each group. B-C: All protein groups found in the analysis. D: Protein groups of neuroactive peptide precursors detected in analysis. F: Individual peptides from neuroactive peptide precursors detected in the analysis. C: Heatmap

shows the log 2 of the intensity of protein groups significantly changed in agreement with Tcore. The plot is divided into the two groups, with the CRE samples shown on the left side and labeled in green, and WT samples shown on the right side and labeled in dark grey. Each column represents a sample from a mouse of the respective group which correlates with a certain temperature (color labeled in the purple gradient). Missing values in the heatmaps are shown in light grey. B, D, F: Volcano plots show the log2 of fold change and the adjusted p-value of samples and represent the change in intensity that correlates with increments of 1°C in Tcore. The fold change cutoff used in all plots was 0.1. Each red dot represents a significant protein or peptide found in the analysis. The top 10 significant hits are labeled on the plot in B. In grey dots are all the other proteins or peptides. Dots of significant hits were expanded in size for better visualization purposes only. E-G: The log2 of intensity of the somatostatin protein group (E) and peptide (G) according to the Tcore. Each dot represents one sample coming either from the CRE group (green) or control (CTL) group (dark grey).

4.3 Discussion

As the thermoregulatory centre in the brain, the POA is the target of many peripheral and central modulatory actions[36]. Nevertheless, to date, little is known about the molecules released at the POA during temperature challenges. To investigate this, here I combined *in vivo* sampling with the stimulation of POA^{VGLUT2} thermoregulatory neurons. This was done to collect molecules arriving at the POA in parallel to the manipulation of these neurons and its consequent hypothermia. The samples were processed and the molecules detected using an unbiased LC-MS/MS approach.

Based on the results presented in this chapter, using two different data analysis approaches, in total, my colleagues and I were able to detect 20 protein groups of neuroactive peptide precursors in microperfusates. From these, based on the group analysis, one precursor was found statistically significant in the CRE group upon POA^{VGLUT2} activation, namely proSAAS. And through the temperature analysis, the precursor of somatostatin was found significantly changed based on increments of 1°C in Tcore. Taking into consideration the nature of neuroactive peptide synthesis, which

are translated as precursors and cleaved into smaller bioactive peptides after translation, we also performed data analysis at the peptide level. With this approach, with the group analysis, we were able to find peptides from four precursors significantly changed in the CRE group: proSAAS, KNG1, DBI, and SCG1. And using the temperature analysis, a peptide from somatostatin was also found enriched, in agreement with the protein levels.

When facing a warm challenge, preoptic thermoregulatory neurons of mammals coordinate physiological and behavioural adaptations, with the goal of avoiding excessive warming of the body and keeping the Tcore balanced, a requirement for homeostasis in these animals. For instance, heat loss is promoted by cutaneous blood vessels dilation and sweating, and a decrease in heat production comes from the inhibition of the BAT thermogenesis[1]. In agreement with that, physiological adjustments, such as vasodilation and BAT thermogenesis inhibition, have been observed upon artificial thermoregulatory neuron activation in mice[35]. The artificial activation of thermoregulatory neurons that I used in my experiments is one manner to access and modulate a population of thermoregulatory neurons. However, it is important to highlight that the strategy I used, chemogenetics-DREADDs, is a very artificial modulation, provided that this stimulation imposes the simultaneous activation of any cell that express the engineered receptor, in this case, roughly all VGLUT2 positive neurons. Accordingly, other cells unrelated to thermoregulation could also be activated. Taking this into consideration, the chemogenetic stimulation was used as a tool to strongly and specifically stimulate neurons that, at least part of them, play a role in thermoregulation.

Independently of being artificially or naturally driven, the activation of POA^{VGLUT2} thermoregulatory neurons induces a decrease in Tcore to reach thermal balance[20,29]. Such hypothermia could either be the consequence or the cause of changes in release of neuroactive peptides at the POA. If the decrease in Tcore is a consequence of a peptide acting at the POA, an increase in peptide secretion in this region would be driving hypothermia, while a decrease would indicate that such peptide could be thermogenic

and its function is perhaps lowered by a negative feedback. If the hypothermia stems from a causal relation, the decrease in Tcore could lead to less cellular activity in any tissue, thus decreasing the secretion of any molecule by these cells. Also, because of the lower temperature, diffusion of molecules, in general, is likely compromised. This could prevent the arrival of peptides in the POA either via synaptic inputs, volume transmission (wide spread of neuroactive substances for cell communication through the ISF and the CSF[47,48]), or the bloodstream.

While my results allow the correlation of the peptide release at POA with changes in Tcore and activation of glutamatergic preoptic neurons, more experiments would be needed to infer that a peptide is in fact modulating thermoregulation. Nevertheless, based on my results, the peptides' pattern of expression, the presence of their receptors in the POA, and their functions previously described in the literature, I can hypothesize the role of the neuroactive peptides I found in the modulation of body temperature.

Peptides deriving from SCG1 were detected statistically decreased with our analysis at the peptide level in the CRE group in comparison to WT. On the other hand, other precursors and peptides of neuroactive peptides were detected significantly increased with our approach, namely proSAAS, KNG1, DBI, and somatostatin.

SCG1

Three peptides deriving from SCG1 were found decreased with our analysis at the peptide level. SCG1 is a neuroendocrine secretory granule protein, involved in the packing of peptides into secretory vesicles, and it is hypothesized to give origin to biologically active peptides. However, a physiological role for SCG1 peptides found to be processed *in vivo*, PE-11 and CCB peptide, remains elusive. On top of these two, still unknown peptides could stem from this precursor[142].

ProSAAS

The neuroactive peptide precursor ProSAAS was found changed at the peptide level, with two peptide sequences being significantly increased. This precursor is thought to

be involved in controlling the neuroendocrine secretory pathway. According to the curation of Uniprot database (https://www.uniprot.org (last accessed on 17.01.2022)), ProSAAS gives rise to nine smaller peptides, whose physiological functions are still unclear. One report has suggested a role in thermal balance. In this study, after exposing mice to cold, the authors observed increased levels of one of ProSAAS peptides, PEN, in the hypothalamus of female mice[143]. The two peptides from ProSAAS found increased in our analysis do not cover the PEN sequence though (figure 4.4). The results from Chakraborty et al (2006) and ours suggest that ProSAAS and peptides that derive from it could contribute to thermoregulation. However, additional studies are needed to better analyze this relation.

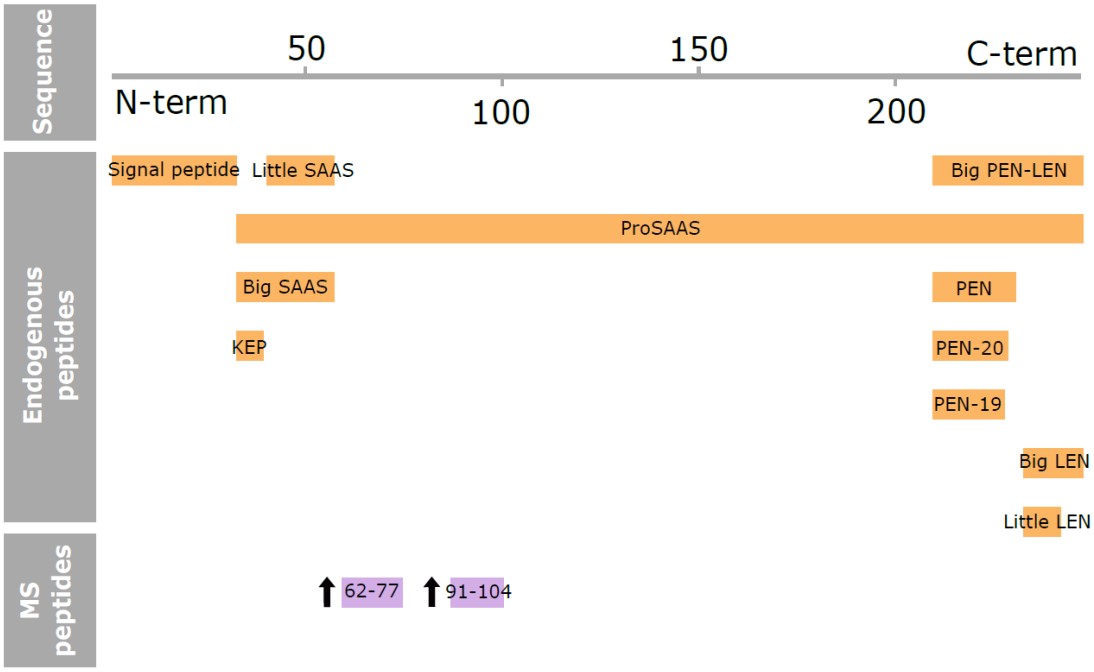

Figure 4.4: **Coverage plot of ProSAAS, its derived peptides, and the peptides found significant upon POA^{VGLUT2} activation**

The plot shows the precursor sequence length, the endogenous peptides in orange, and the peptides found significant upon POA^{VGLUT2} activation in lilac. The arrows next to the peptides indicate the direction of the change detected in the analysis. The annotations for the precursor processing were retrieved from Uniprot.

KNG1

KNG1 precursor processing gives rise to one bioactive peptide, bradykinin. This peptide likely has no effect on thermoregulation, since its injection in the ventricles showed no effect on Tcore[144]. The peptide sequence from this precursor found increased in our analysis covers another region of KNG1, which also has no description of being involved in thermal balance.

DBI

In our cause, peptides from the DBI precursor were found increased in the CRE group during hypothermia. DBI is a peptide that has two distinct functions inside and outside of cells. Intracellularly, it interacts with Acyl-CoA molecules and plays a role in lipid metabolism, and extracellularly, it binds to the benzodiazepine site of gamma-aminobutyric (GABA) type A receptor and regulates its activity[145]. Recently, it has been shown that this protein plays a role in energy homeostasis, with plasma levels found increased in human obesity, a disorder in which there is a lower metabolism rate[145]. As in our analysis, peptides from DBI were detected increased in the CRE group during hypothermia, a condition in each metabolism is also reduced. Together, these two lines of evidence could suggest that DBI is involved with hypometabolic states.

Somatostatin (SMS)

In our analysis, somatostatin was found positively correlated to body temperature at the protein and peptide level. Thus, during the reduction in Tcore induced by POA^{VGLUT2} neuron activation, the levels of somatostatin were also found decreased. The somatostatin precursor is synthesized in the hypothalamus and encodes two neuropeptides, somatostatin-28 and somatostatin-14. Classically, somatostatin has been implicated in the regulation of the growth hormone (GH) release by the anterior pituitary. Nevertheless, its five receptors, somatostatin receptor 1-5, are expressed in several tissues, including the POA, and several other physiological roles have been related to this neuropeptide, including the inhibition of insulin release by the pancreas and of renin by the kidneys[146]. Reports also suggest that somatostatin is also be involved

in thermoregulation. The infusion of somatostatin and one agonist of the somatostatin receptor 2 leads to increase in Tcore[49,147], while the intraperitoneal injection of a substance that depletes somatostatin decreases body temperature[148]. In addition, exposure to a cold stimulus (8°C) and a warm stimulus (30°C), increases and decreases somatostatin concentration in the hypothalamus, measured by RIA[148]. Taken together, these studies suggest a thermogenic role for somatostatin. Accordingly, the reduced intensity found by our analysis could mean that the reduction of somatostatin contribute to the hypothermic effect of chemogenetic stimulation of glutamatergic preoptic neurons.

Conclusions

Altogether, our unbiased analysis of the POA secretome upon the activation of thermoregulatory neurons detected peptides from five neuroactive precursors differentially released during stimulus, namely proSAAS, KNG1, DBI, SCG1, and somatostatin. These results suggest that such peptides are differentially released in the POA during the chemogenetically-driven hypothermia. Interestingly, somatostatin, a neuroactive peptide that was previously regarded as hyperthermic, i.e. inducing hyperthermia, was found to be reduced upon the activation of POA^{VGLUT2} neuron and strong Tcore reduction. This could suggest that the decrease of peptide(s) derived from somatostatin could be contributing to hypothermia induced by preoptic glutamatergic stimulation. In a natural scenario, it is possible that such peptide(s) act in the POA and help this structure coordinate thermoregulation. To conclude, our unbiased identification of neuroactive peptides released in the POA upon glutamatergic activation then provides a list of candidates to start investigating the roles of these molecules in thermoregulation.

CHAPTER 5: INVESTIGATION OF NEUROACTIVE PEPTIDES SECRETED DURING PERIPHERAL THERMAL STIMULATION

5 INVESTIGATION OF NEUROACTIVE PEPTIDES SECRETED DURING PERIPHERAL THERMAL STIMULATION

5.1 Introduction

In homeothermic animals, Tcore is maintained by the thermoregulatory circuitry and orchestrated by the POA (more details in sections 1.3 and 1.4 of the Introduction). The POA is located in the hypothalamus, at the base of the brain. This position enables this region to receive multiple modulatory inputs, including neural projections and molecules from the CSF and the blood (detailed in section 1.4 of the introduction)[1,3].

The exposure to warm and cold environments in mammals leads to physiological and behavioral adaptations, which intend to preserve the body temperature, keeping it around a balance point regardless of the external temperature[1,4]. Despite the efforts to better understand the role of POA in the control of these adaptive responses (more details in section 1.4 of the introduction), it is still elusive how this area is molecularly modulated during a thermal challenge.

One hypothesis is that neuroactive peptides could participate in preoptic thermoregulation by acting in the POA, through the modulation of the activity of part of its neurons during thermal challenges (more details in section 1.7 of the introduction). To investigate this, first I combined peripheral warm and cold thermal stimulation with an *in vivo* sampling technique. After collection, the samples were analysed by LC-MS/MS in an unbiased way, in order to detect which peptides were released at the POA and collected by this approach. The samples were analysed in collaboration with Dr. Daniele Colombo.

In this chapter, I will present the results of the warm- and cold-induced secretome at the POA in sections 5.2.1 and 5.2.3, respectively. In addition to the unbiased screening of thermoregulatory peptide candidates, I narrowed the list of significant hits and further verified those using different analytical methods, which I will present in the sections

5.2.2, for the warm candidate, and 5.2.4, for the cold. To my knowledge, this was the first attempt to unbiasedly characterize the POA secretome induced by peripheral thermal stimulation.

5.2 Results

5.2.1 Warmth-stimulation led to differential release at the POA

5.2.1.1 Thermal chamber reached warm stimulation temperature in 30 minutes

To investigate neuroactive peptides released at the POA during a warm challenge, I performed *in vivo* sampling during exposure to warmth. Specifically, I collected the interstitial fluid from the POA of male C57 BL/6 mice using OFM *in vivo* sampling. Only mice with correct cannula implantation were included in the analysis (figure 5.1-B). I collected the microperfusates in Ringer solution at 0.5 μl/min sampling rate in parallel to ambient temperature stimulation, which occurred in a homemade thermal chamber (described in more details in the methods section 2.2.12). The chamber was able to reach 36°C from 24°C in 30 minutes (figure 5.1-C and D). During baseline, for two hours, the thermal chamber temperature was kept at 24°C, and during the two hours of stimulus, the temperature was increased to 36°C. The control group, in which another cohort of mice was used, was exposed to 24°C throughout the entire experiment (figure 5.1-A).

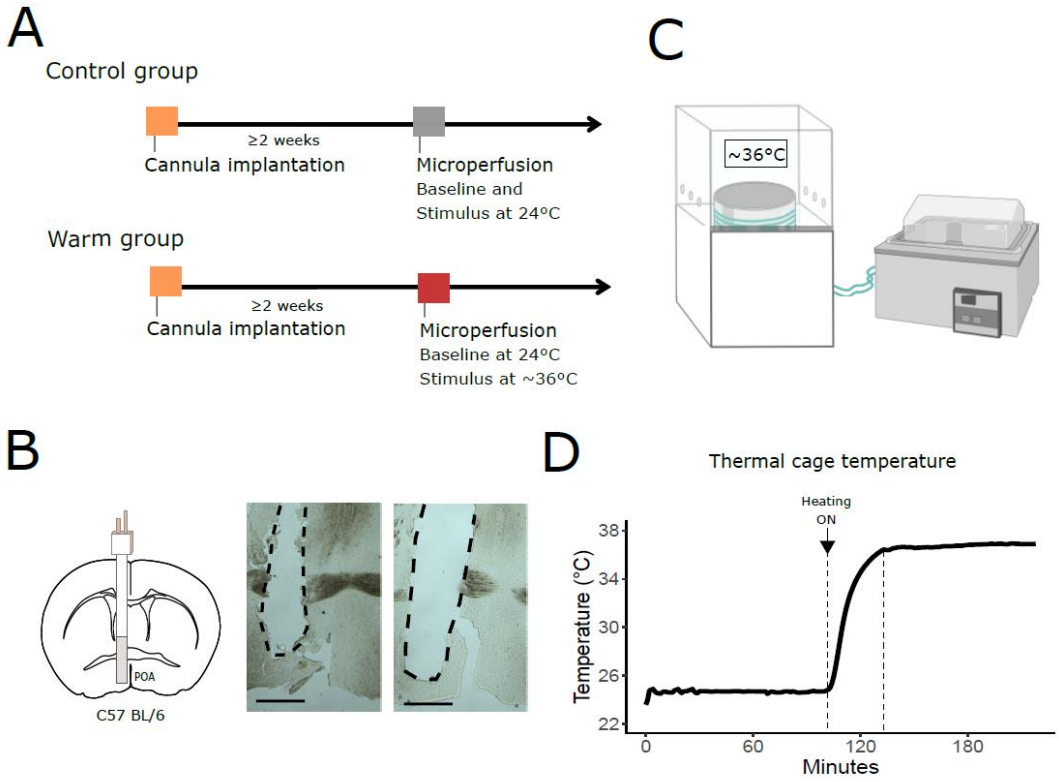

Figure 5.1: Warm stimulation setup and *in vivo* microperfusion implantation check

A: Experimental timeline of the control and the warm groups. B: The scheme represents the location of OFM cannula implantation. Representative bright field microscopy images of the implantation of two animals are shown. Scale bar: 100 µm. The dashed lines define the area where the cannula was implanted. C: Scheme depicting the thermal chamber built for the ambient temperature stimulation. Figure created with BioRender.com[116]. D: The plot shows the thermal cage temperature before and after the heating coming from the circulating water bath was turned on. The dashed lines delimit the time needed to reach the desired stimulation temperature of 36°C.

5.2.1.2 Peripheral warm stimulation changed the protein groups released at the POA

To investigate neuroactive peptides differentially released in the POA upon warm stimulation, samples were analyzed using LC-MS/MS. For this, Dr. Colombo and I used the optimized LC-MS/MS workflow described in chapter 3, with few modifications only in the LC-MS/MS parameters. The data analysis was performed by Dr. Calderazzo, Dr.

Colombo, and by myself. The data was analyzed with Max Quant. Proteins and peptides were quantified with MaxLFQ (MaxQuant quatification algorithm).

Samples from the warm and control groups were compared based on the normalized intensities of peptides collected during the stimulus period of each group (figure 5.2-A). The stimulus period corresponded to the second half of the experiment, in which the warm-group mice were exposed to 36°C, while the control-group mice continued being exposed to 24°C, as they were during the baseline period. In total, 662 protein groups (concept illustrated in figure 3.4) were found. From these, 118 were found significantly different in the warm group in comparison to the control group ($p \leq 0.05$, adjusted by Benjamini-Hochberg correction) (figure 5.2-E). All these protein groups are shown in the heatmap in figure 5.2-D.

Because feeding and water intake could create confounds in the analysis, as these two parameters influence metabolism and homeostasis, I measured the food and water consumption before and after the stimulus. Comparing the control and warm groups, there was no significant difference between warm-stimulated and control mice in terms of food and water consumption (figure 5.2-B and C). Of note, these were not the same animals used in the proteomics analysis, however they received the same stimulus as described above for each group.

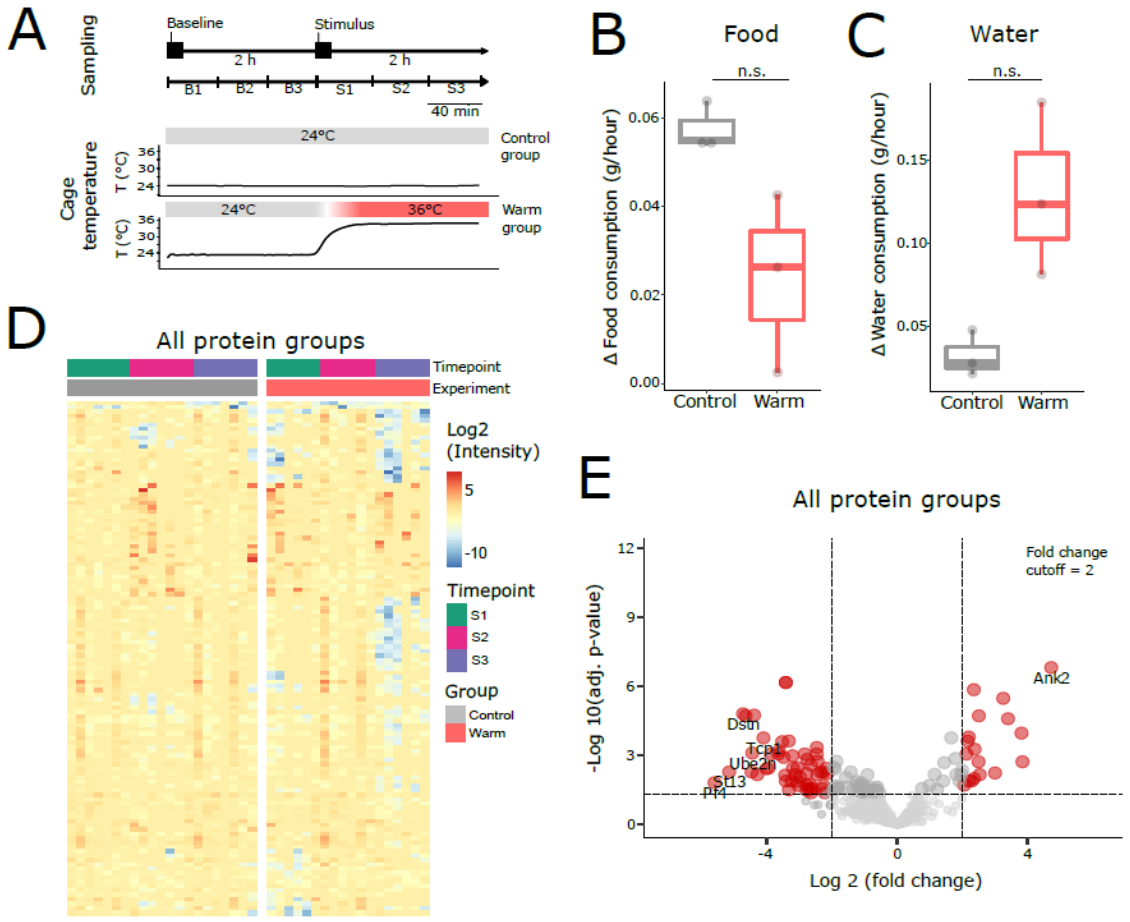

Figure 5.2: Warm stimulation led to differential release of protein groups and alterations in food and water intake.

A: Sampling and stimulation scheme used in the experiments performed with the control and warm groups. Three samples were collected during baseline (B1-3), and three were collected during stimulus (S1-3). B and C: Box plots showing the change in food (B) and water (C) consumption for each group. Each dot represents one mouse. The box plot shows the median (thick line), interquartile range (box) and full range (whiskers). B: Two-tailed Mann-Whitney test, mean control = 0.023±0.020 (n = 3), mean warm = 0.057±0.005 (n = 3), p-value = 0.100. C: Two-tailed Mann-Whitney test, mean control = 0.032±0.013 (n = 3), mean warm = 0.130±0.052 (n = 3), p-value = 0.100. D: Heatmap showing all the protein groups significantly changed in the warm group (n = 6 mice) in comparison to control (n = 7 mice). The plot shows the log 2 of the intensity of samples collected during the stimulus period normalized by averaged baseline intensities. The plot is divided into the two groups, with control samples shown on the left side and labeled in grey, and the warm samples shown on the right side and labeled in red. A different color is assigned to each time point. E: Volcano plot with all the protein groups found in the analysis. The plot shows

the log2 of fold change and the adjusted p-value of samples from the warm group in comparison to the control group. The fold change cutoff used in this plot was 2. Each red dot represents a significant protein found in the analysis. In grey dots are all the other proteins. Dots of significant hits were expanded in size for better visualization purposes only.

5.2.1.3 Peripheral warm stimulation induced changes in the release of neuroactive peptides arriving at the POA

Regarding the precursors of neuroactive peptides, what I refer here as the protein level of neuroactive peptides (more details in the introduction section 1.6), the analysis was the same as done for all protein groups (illustrated in figure 3.4). In total, we were able to identify 17 protein groups of neuroactive peptide precursors. Among these, three precursors were found statistically different in the warm group, in comparison to the control. Among these, the precursor of orexin/hypocretin (OREX) was found decreased, while pronocipeptin (PNOC) and the insulin-like growth factor II (IGF2) were found increased upon warmth ($p \leq 0.05$, adjusted by Benjamini-Hochberg correction) (figure 5.3-A). All the 17 precursors are shown in a heatmap for visualization of their intensity in individual samples (figure 5.3-B).

As explained in section 1.6 of introduction, after being synthesized as precursors, neuroactive peptides, after translation, are cleaved into smaller bioactive peptides (figure 1.2). Since we added trypsin during our sample processing, on top of the endogenous peptides, the samples contained tryptic peptides of all proteins present, including the neuroactive peptide precursors (illustrated in figure 3.3). Thus, to investigate all peptides in the samples, endogenous and tryptic, we performed a search in MaxQuant based on the cleavage pattern of trypsin and peptidases involved in the processing of neuropeptides and peptide hormones (shown in table 1.1).

Based on this approach, we were able to identify 175 peptides coming from the 17 protein groups mentioned above. From these, seven peptides from seven precursors were found significantly different in warm samples in comparison to control samples (figure 5.3-C).

These seven peptides are shown in a heatmap for visualization of their intensity in individual samples (figure 5.3-D). The peptides found decreased upon warm stimulation come from the following precursors: orexin/hypocretin (OREX) and secretogranin 2 (SCG2). While the peptides found increased came from the precursors of secretogranin-1 (SCG1), secretogranin-3 (SCG3), nucleobindin 1 (NUCB1), neurosecretory protein VGF (VGF), and proenkephalin (PENK).

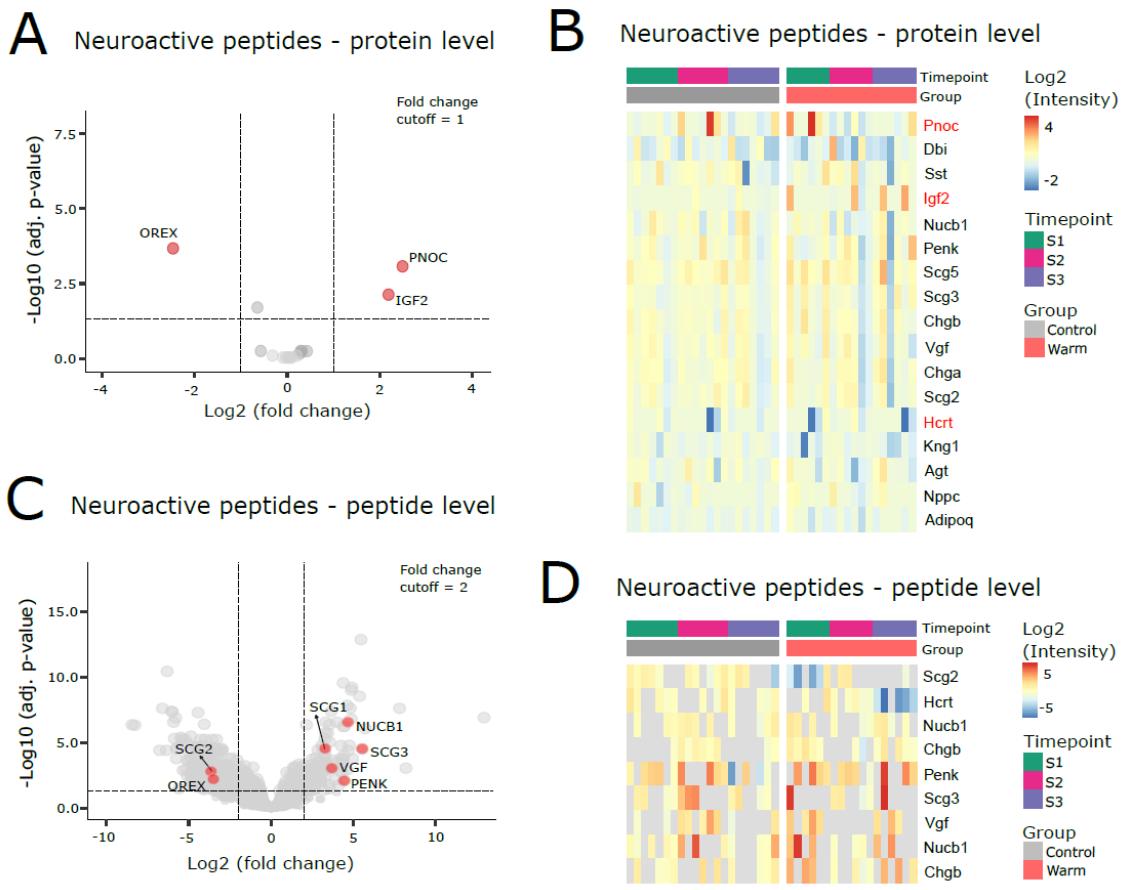

Figure 5.3: Warm stimulation led to differential release of neuroactive peptides arriving at the POA

A and B: Volcano plot (A) and heatmap (B) with all the protein groups of precursors of neuroactive peptides found in the analysis. In B, the red text represents the protein groups found significantly changed in the warm group. C: Volcano plot with all the peptides detected in the analysis, with significant peptides derived neuroactive peptides highlighted in red. D: Heatmap with all the peptides coming from precursors of neuroactive peptides found in the analysis. In A

and C: The volcano plot shows the log2 of fold change and the adjusted p-value of samples from the warm group in comparison to the control group. Each dot comes from proteins in A and peptides in C. The red dots represent the significant hits, while grey dots represent all the other protein groups (A) or peptides (C). Dots of significant hits were expanded in size for better visualization purposes only. The fold change cutoff used in the plots was 1 in A and 2 in C. In B and D: Heatmaps show the log 2 of the intensity of samples collected during the stimulus period normalized by averaged baseline intensities. The plot is divided into the two groups, with control samples shown on the left side and labeled in dark grey, and the warm samples shown on the right side and labeled in red. A different color is assigned to each time point. Missing values are colored in light grey in the heatmap. A-D: 7 mice were used in the control group and 6 mice the in warm group.

5.2.2 Verification of warm-induced secretome

5.2.2.1 Orexin was detected in microperfusates by two different analytical methods

In order to verify our unbiased screening of neuroactive peptides differentially regulated in warm-exposed animals, I selected OREX from the list of candidates for further investigation. The list was filtered based on the fold change, the availability of methods to investigate the peptide and its precursor, and on literature support. Based on these criteria, my next steps focused on studying the role of orexins on preoptic thermoregulation.

The Hcrt gene encodes a precursor that is further processed into the mature peptides Orexin-A and Orexin-B. With LC-MS/MS analysis, we found OREX to be decreased at the precursor protein level (figures 5.3-A and B, and 5.4-A), as well as at the peptide level (figures 5.3-C and D, and 5.4-B). Of note, the peptide found significant matched to a sequence that is part of the OREX precursor but outside of the sequences of the biologically active forms of orexin (figure 5.4). None of the orexins, orexin-A or orexin-B, were found with our analysis. And given the protein groups include all the peptides of one or more proteins found by MaxQuant, the orexin protein group did not have any

of the biologically active orexins included. Therefore, all the results of orexin, either at protein or peptide level, come from a sequence part of the propeptide (Figure 5.4). Nevertheless, the peptide found might indicate that bioactive orexins could had been present in the samples as well.

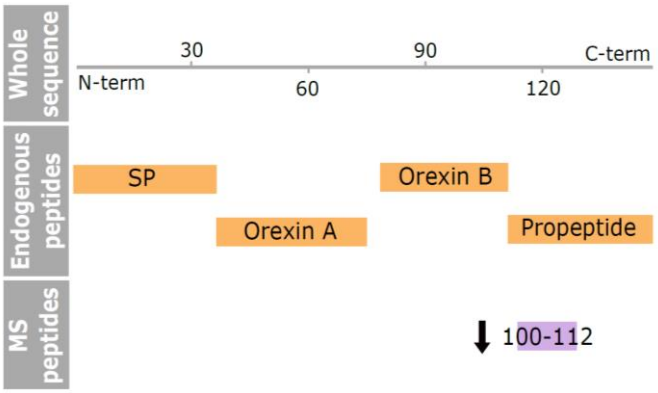

Figure 5.4: Coverage plot of the precursor of orexin, its derived peptides, and the peptide found significant upon warm stimulation

The coverage plot represents the whole amino acid sequence of the precursor of orexins, with the middle part showing the endogenous peptides produced by enzymatic cleavage in orange, and the lower part showing the peptide that was found significant in the analysis, represented in lilac. The peptide covers the amino acids from the position 100 to 112 in the precursor sequence. The arrow next to it represents the direction of the change found in the analysis. The annotation information was retrieved from Uniprot.

To test if orexin-A could be detected in microperfusates with another analytical method, I collected samples from an additional cohort of mice and used ELISA to measure orexin-A in the samples. The sampling occurred similarly to what I described above, but for this experiment, I collected samples during the control condition (at 24°C) and at warm condition (~36°C) from the same group of mice (n = 3), in different days (as shown in the scheme in figure 5.5.A). After collection, I analyzed the samples with an ELISA kit for orexin-A (Mouse Orexin A ELISA Kit, MyBioSource, USA). From a total of 12 samples collected (four samples from three mice), orexin-A could be detected above the ELISA

kit detection limit in four samples (figure 5.5-B). Because of this, it was not possible to perform a statistical comparison of the baseline and the stimulus, nor of control against warm samples. Nevertheless, the ELISA results, together with the LC-MS/MS results, further suggest the presence of orexins in the samples, but only the proteomics data was used to quantify and compare the levels of orexins, precisely part of its propeptide sequence (pro-orexin), in the samples.

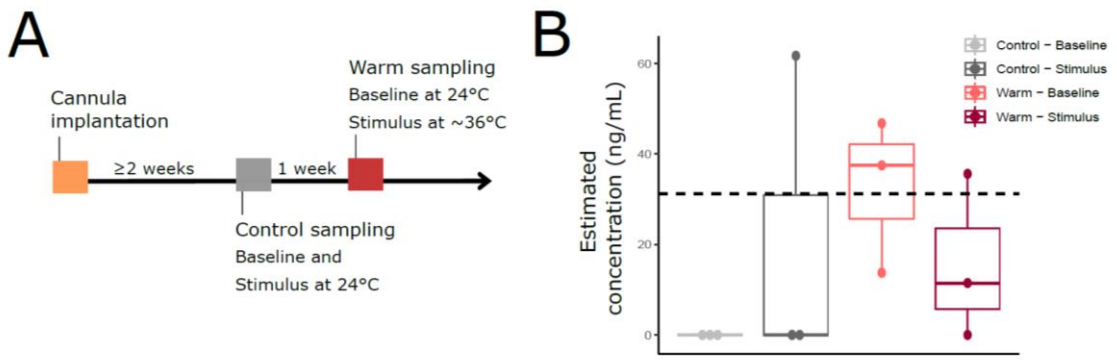

Figure 5.5: Orexin levels in microperfusates measured by ELISA.

A: The scheme represents the microperfusion sampling used to collect samples for the Orexin-A ELISA. B: The estimated concentration of orexin-A in microperfusates. Each dot represents one mouse. The dashed line indicates the detection limit of the ELISA kit used for quantification. Samples detected below the limit were considered not reliable.

5.2.2.2 Portion of POA neurons was modulated by orexin-A

Our LC-MS/MS and ELISA results suggest that orexin precursor is released into the POA. Orexins are exclusively synthesized in LHA and perifornical area neurons[74,75]. To verify the presence of orexinergic fibers projecting to the POA, I performed an immunohistochemistry on cryostat brain slices for orexin-A/B. Using a slice covering the region of LHA as a positive control for an antibody against orexin-A/B (figure 5.6-A), I was able to also visualize orexin-A fibers in the POA, reproducing what was previously observed[76] (figure 5.6-A).

To investigate if orexins modulate neuronal activity on preoptic neurons, I performed an experiment in collaboration with Dr. Gretel Kamm, a postdoc also working in the Siemens Lab. Together, we evaluated the effect of orexin on preoptic neurons using calcium imaging on POA slices. With this approach, calcium was used as an indicator of neuronal activation, with the advantage of recording from multiple cells simultaneously. Variations in calcium signals were measured *ex vivo*, before and after orexin-A was applied on top of the slices. As shown in figures 5.6-E-G, considering 388 neurons expressing the calcium indicator GCaMP6s (explained in detail in 2.2.23 of methods) (n = 5 slices from 2 mice), after orexin-A was added on POA slices, an increase in neuronal activity, as indicated by elevations in calcium signals, was observed in 12% of these neurons. On the other side, orexin-A application was accompanied by decreased neuronal activity, as measured by calcium signals, in 5% of neurons expressing GCaMPs. Thus, the presence of orexin-A fibers in the preoptic region, the expression of orexin receptors in the POA described in the literature[82], and the changes in neuronal activity on preoptic neurons induced by orexin-A suggest that the POA could be one of the target regions of orexins.

5.2.2.3 Orexin receptor 2 co-localized with a marker of a thermoregulatory subpopulation

Based on my results and on the literature, the POA is presumably one of the regions where orexin can exert its influence. Nevertheless, it is still unknown if orexins could modulate preoptic thermoregulatory neurons. To investigate this, I analyzed if the OX2R co-localized with Lepr, a marker of a subpopulation of thermoregulatory neurons in the POA[38]. For this, I collected brains of transgenic mice expressing the reporter GFP in nuclei of Lepr-cre cells (LepR^{cre}-HTB). Then, I did an immunohistochemistry for OX2R with these slices to evaluate if there was an overlap between the orexin and the leptin receptors (figures 5.6-B-D). As it can be appreciated in figure 5.6-C, the Lepr subpopulation has a triangular pattern of distribution in the POA, around the ventricles, while OX2R is spread all over the region, with overlap with Lepr+ neurons. Thus, these results suggest that if orexins are released into the POA during warm stimulation, they

could potentially act on Lepr+, which are, at least a portion of them, thermoregulatory neurons.

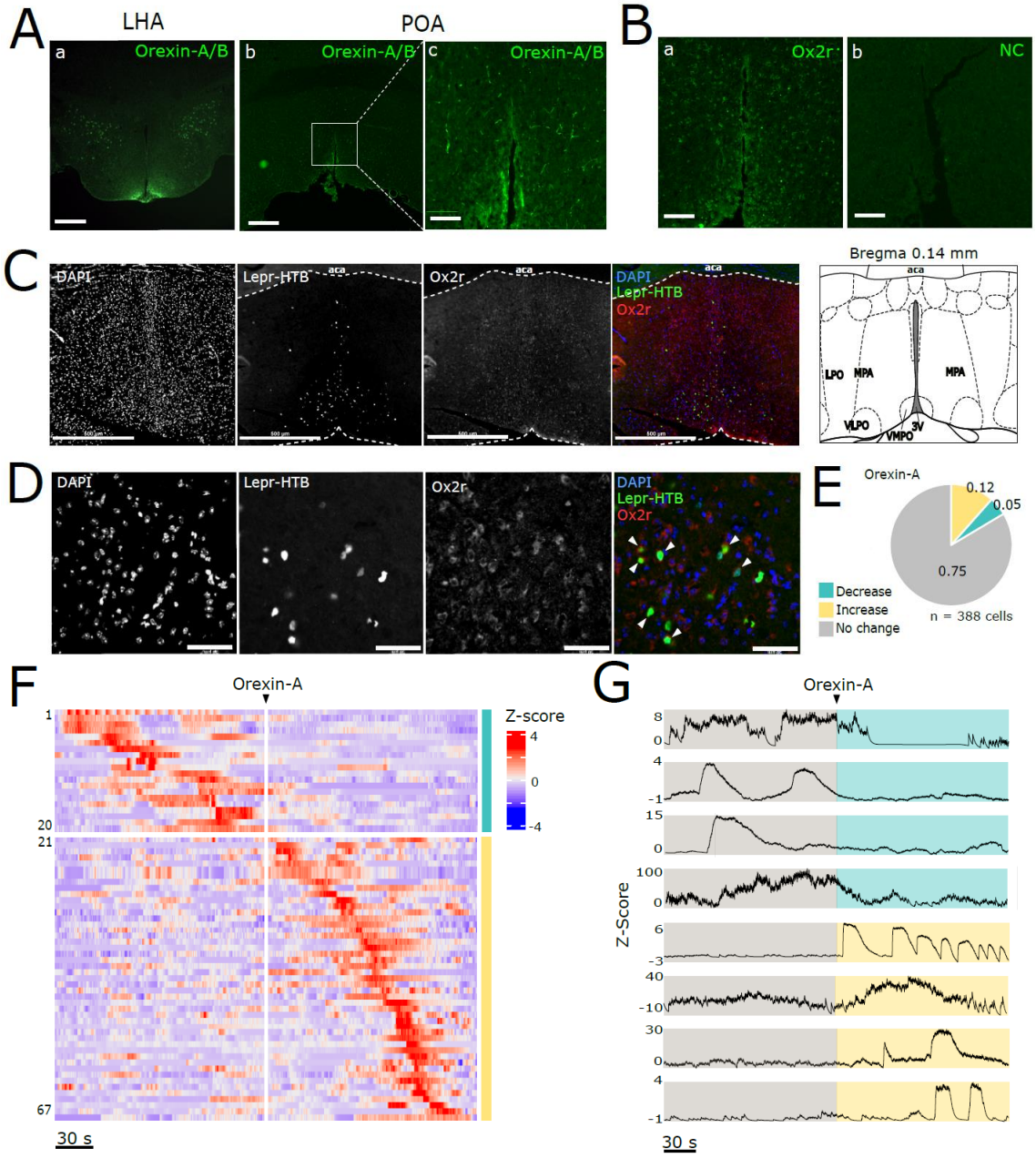

Figure 5.6: Pattern of orexin receptor 2 in POA and effect of orexin-A on POA neurons.

A and B: Photomicrographs of immunofluorescence performed on cryostat brain sections for (A) orexin-A in (a) the lateral hypothalamus (LHA) and in the POA (b and c), and for (B) OX2R in the POA. B-a shows the staining with OX2R and B-b shows the negative control, in which no primary

antibody was added. Scale bar in A-a and A-b: 300 μm, and 100 μm in A-c, B-a, B-b. C: Immunoflurescence staining for OX2R (in red) on POA brain slice of $LepR^{cre}$-HTB reporter mouse line, which expresses GFP in nuclei (in green). DAPI is shown in blue. A separate image for each channels is shown. Scale bar: 500 μm. D: Higher magnification of the same images shown in C. The arrow heads indicate the colocalization of Lepr-cre with OX2R. Scale bar: 50 μm. E: Distribution of the effect of orexin-A in POA neurons. F: Heatmap depicting the z-score of POA neurons that showed a significant response to application of orexin-A in perfusion bath. Each row corresponds to an individual neuron. The upper part (turquoise bar) and the lower part (yellow bar) show the neurons with a decreased and increased response, respectively, while orexin-A was present. Scale bar: 30 seconds. G: Representative calcium traces of neurons that showed decreased (turquoise bar) and increased (yellow bar) responses. Scale bar: 30 seconds.

5.2.2.4 Effects of orexin receptor antagonists on the preoptic area

The next step was to evaluate, *in vivo,* if the inhibition of orexinergic modulation at the POA had an effect on Tcore. For this, I injected antagonists of the two orexin receptors, into the POA of male and female mice, using the OFM microperfusion system, one drug at each time, in different days. In parallel, I measured the Tcore using a telemetry probe implanted intraperitoneally. According to the literature, the peak of orexin release occurs at the last three hours into the dark phase, when the animals are most active[77]. Thus, to maximize the antagonism of orexin receptors when orexin would be mostly released, I delayed the circadian rhythm of the mice by six hours and injected the antagonists between the last three hours of the dark phase.

First I wondered if an acute interference with the orexin signaling affects basal thermoregulation. To answer this question, I injected the antagonists SB334867 (OX1R antagonist) and seltorexant (OX2R antagonist) while mice were present in a ventilated cabinet with constant temperature at 24°C (figure 5.7-A). As shown in figures 5.7-B and C, a small, but significant difference was seen when comparing the mean of Tcore change after the injection of the OX1R antagonist and the vehicle. On the other side, OX2R

antagonist had no significant effect on Tcore at 24°C in comparison to the vehicle (figures 5.7-D and E).

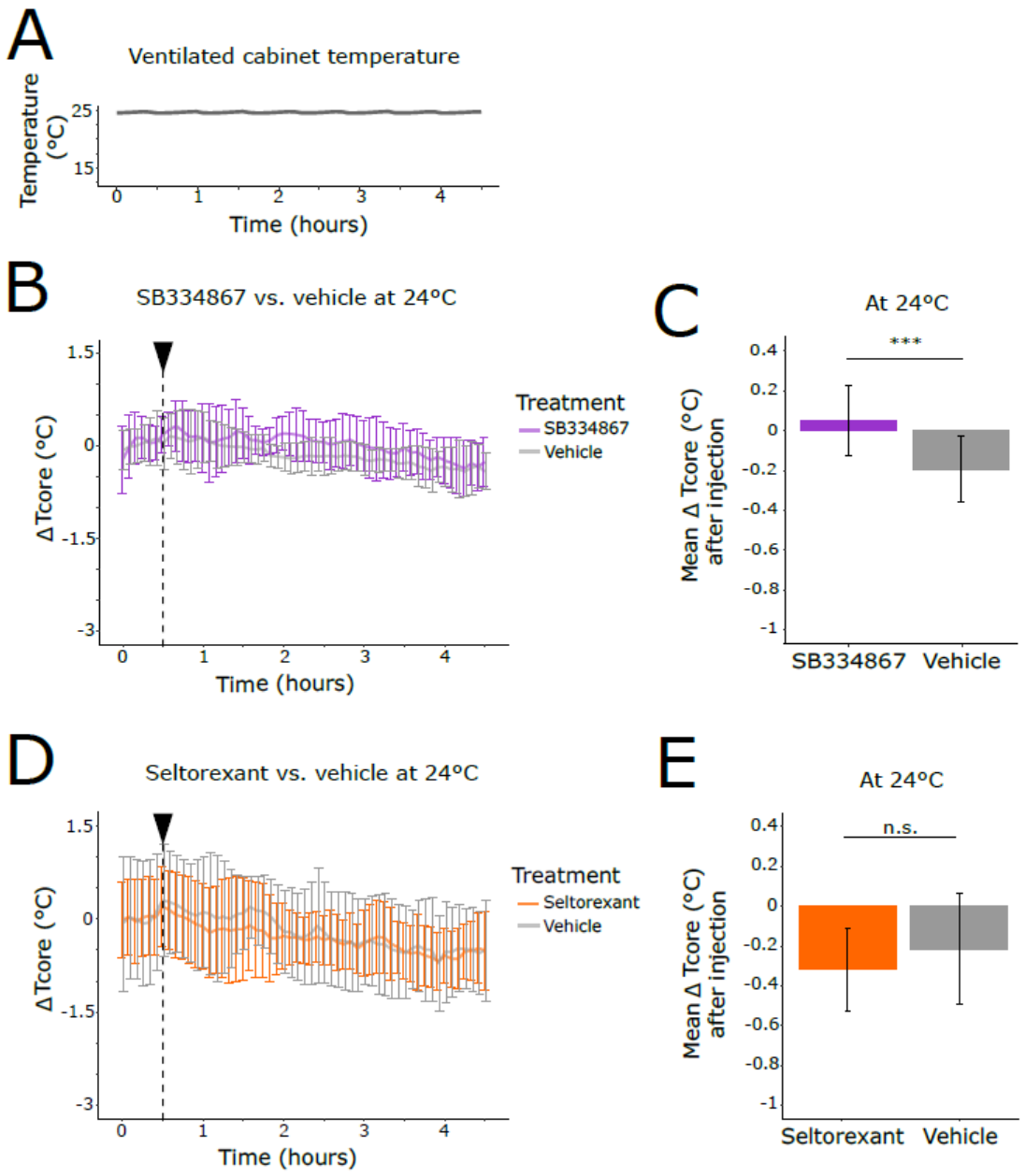

Figure 5.7: Effects of orexin receptor antagonists injected into the POA on core body temperature at 24°C.

A: The temperature of the ventilated cabinet during the experiment. B and C: Change in Tcore upon injection of SB334867, an OX1R antagonist. D and E: Effect of seltorexant, an OX2R antagonist, injection in Tcore. In B and D, the dashed line indicates when the drug or the vehicle

started to be injected. Mean ± s.d. is shown. C: Comparison of the mean of Tcore change after the injection of SB334867. Two-tailed Mann-Whitney test, mean SB334867 = 0.055±0.173 (n = 6), mean vehicle = -0.189±0.164 (n = 6), $p < 0.001$ (***). E: Comparison of the mean of Tcore change after the injection of seltorexant. Two-tailed Mann-Whitney test, mean seltorexant = -0.312±0.208 (n = 8), mean vehicle = -0.212±0.270 (n = 8), $p = 0.138$.

The LC-MS/MS analysis suggested that the orexin precursor levels may be decreased upon warm stimulation (figure 5.3). On the other side, preventing the effect of orexin at the POA with an OX1R antagonist suggested a small, but significant, increase in Tcore (figure 5.7). This made me question if orexins either increase or decrease Tcore, and how they affect body temperature in a cold challenge scenario. Thus, to check if antagonizing orexins' actions at POA interferes with the ability to keep T_{core} at cooling, I also injected the same antagonists, while mice were in a ventilated cabinet that cools down to 12°C (figure 5.8-A). As it can be appreciated in figures 5.8-B and C, the antagonist of OX1R, SB334867, led to a small, but significant decrease in Tcore during the cold challenge. In opposition, the antagonist of OX2R, seltorexant, at the dose tested, led to no alteration in body temperature in comparison to the vehicle (figure 5.8-D and E).

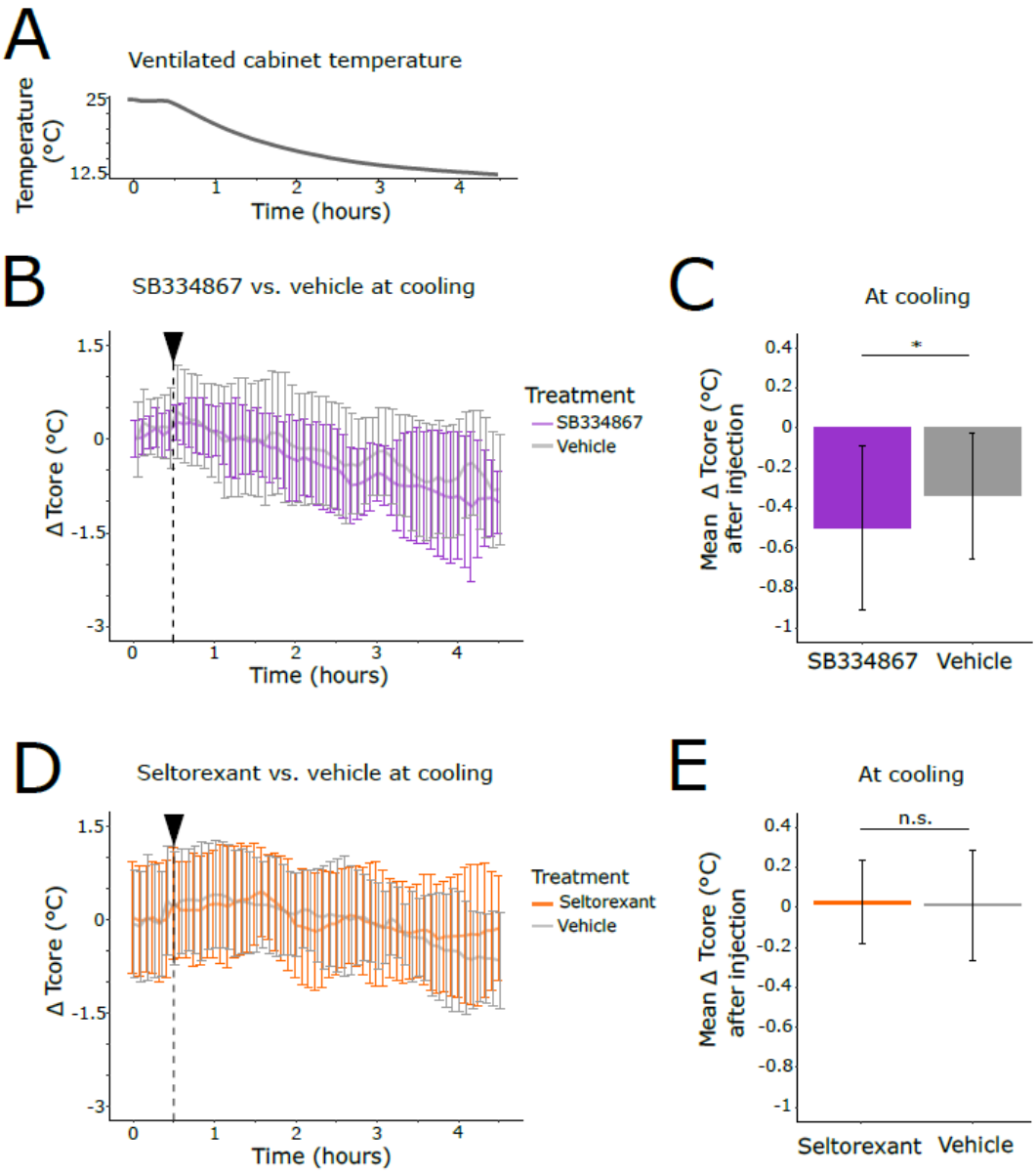

Figure 5.8: Effects of orexin receptor antagonists injected into the POA on core body temperature at cooling

A: The ventilated cabinet temperature during the experiment. The cooling to 12°C started simultaneously to drug injection. B and C: Change in Tcore upon injection of SB334867, an OX1R antagonist, during exposure to cooling. In B and D, the dashed line indicates when the drug or the vehicle started to be injected. Mean ± s.d. is shown. C: Comparison of the mean of Tcore change after the injection of SB334867 at cooling. Two-tailed Mann-Whitney test, mean SB334867 = -0.494±0.411 (n = 6), mean vehicle = -0.338±0.315 (n = 6), p = 0.037 (*). E: Comparison of the mean

of Tcore change after the injection of seltorexant at cooling. Two-tailed Mann-Whitney test, mean seltorexant = -0.014±0.206 (n = 7), mean vehicle = -0.005±0.269 (n = 7), p = 0.756.

5.2.3 Cold stimulation led to differential release at the POA

5.2.3.1 Thermal chamber reached cold stimulation temperature in 1 hour and 20 minutes

Since warming presumably induced changes in peptidergic content arriving at the POA, I wondered if the same would happen with cooling. To explore this and perform a profiling of the neuroactive peptides released at the POA during a cold challenge, I used the same *in vivo* sampling method described above, together with a similar stimulation setup, but now tuned to expose the mice to cold. However, differently from the warm stimulation, the chamber took longer to reach the target temperature, with 1 hour and 20 minutes needed to reach 5°C from 24°C in (figure 5.9-C and D). Only mice with correct cannula implantation were included in the analysis (figure 5.9-B). Similarly to the warm experiment, baseline samples were collected for two hours, while the temperature of the thermal chamber was kept at 24°C. In sequence, the chamber temperature was changed to 5°C and the sampling occurred for 2 hours and 40 minutes. For the control group, I used the same cohort of mice, and did the sampling in a week before the cold sampling. In this group, I exposed the mice to 24°C during the whole sampling (figure 5.9-A).

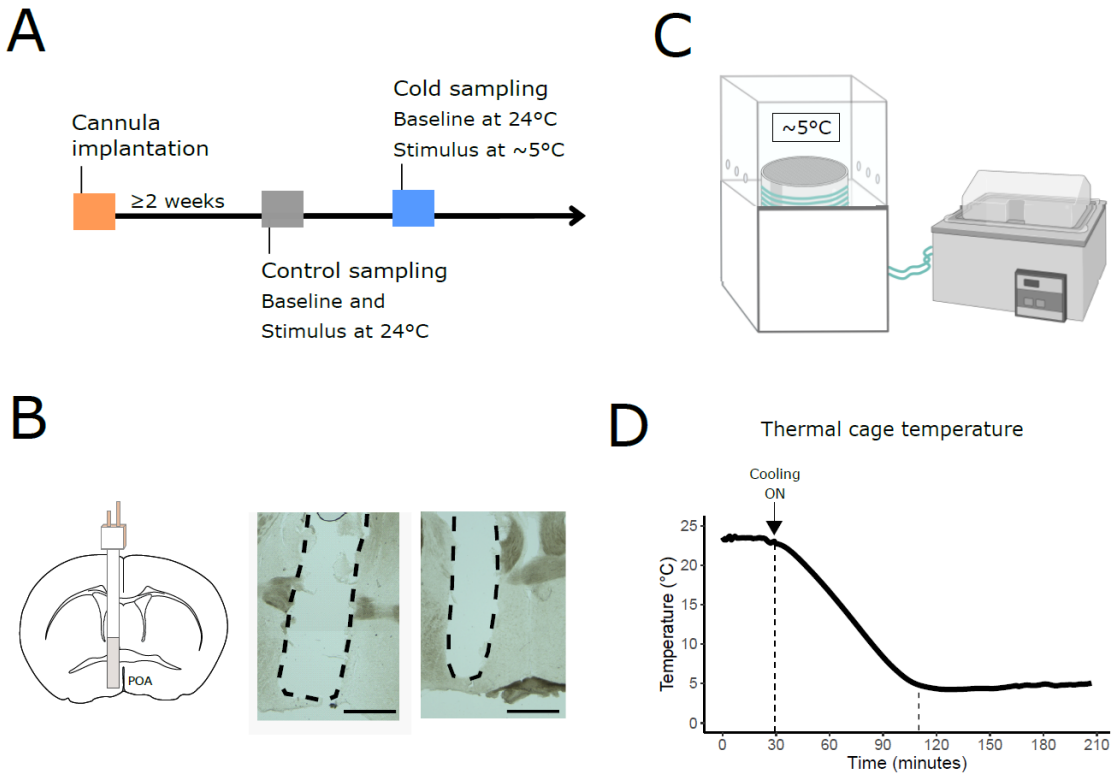

Figure 5.9: Cold stimulation setup and *in vivo* microperfusion implantation check

A: Experimental timeline of the control and the cold groups. B: The scheme indicates the location of OFM cannula implantation. Representative bright field microscopy images of the implantation of two animals are shown. The dashed line defines the area where the cannula was implanted. Scale bar: 100 µm. C: The scheme represents the homemade thermal chamber used in the cold ambient temperature stimulation. Figure created with BioRender.com[116]. D: The plot shows the thermal cage temperature before and after turning the cooling circulating water bath on. The dashed lines indicate the time needed to reach the target stimulation temperature of 5°C.

5.2.3.2 Peripheral cold stimulation led to alterations in the protein groups released at the POA

The profiling of neuroactive peptides released at the POA upon cold stimulation was performed in LC-MS/MS, in a similar manner as done with samples collected during warm challenge and using the workflow described in chapter 3, with only few modifications in the LC-MS/MS parameters. The data analysis was also conducted

likewise the warm stimulation and done in a joint effort between Dr. Calderazzo, Dr. Colombo, and myself.

For the relative quantification of samples collected during from the cold and control groups, we normalized the intensities of peptides collected during the stimulus period of each group (figure 5.10-A). In total, 939 protein groups were found, of which 533 were found significantly changed comparing samples from the cold and control experiments ($p \leq 0.05$, adjusted by Benjamini-Hochberg correction) (figure 5.10-D and E). As I did for the warm experiments, I also measured feeding and water consumption before and after the stimulus. In comparison to the control experiments, cold-stimulated mice showed no statistically significant difference of food and water intake (figure 5.10-B and C).

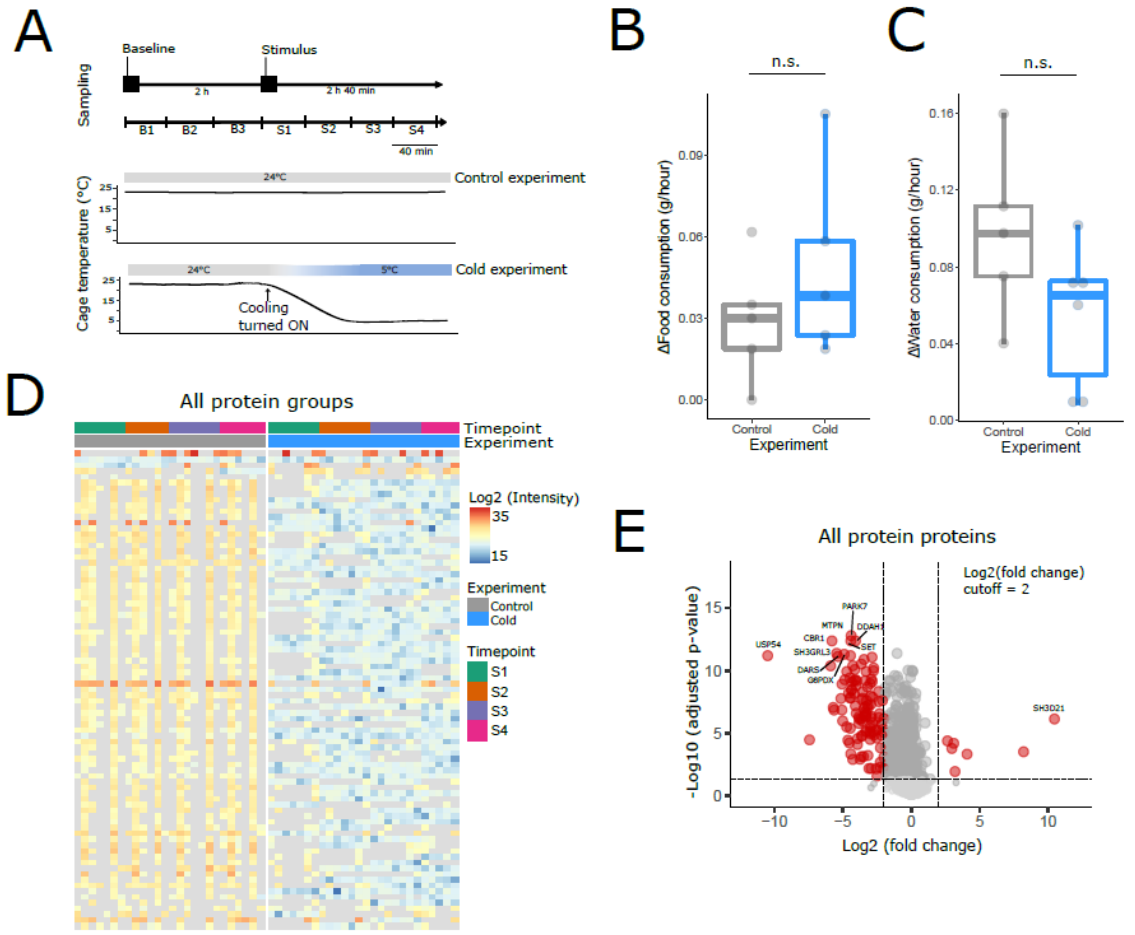

Figure 5.10: Cold stimulation induces differential release of protein groups without affecting food and water consumption

A: The scheme shows the sampling and stimulation timeline used in the control and cold experiments. Three samples were collected during baseline (B1-3), and four were collected during stimulus (S1-4). B and C: Change in food (B) and water (C) consumption during each experiment. Each dot represents one mouse. The box plot shows the median (thick line), interquartile range (box) and full range (whiskers). B: Mann-Whitney test, mean control = 0.035±0.017 (n = 4), mean cold = 0.050±0.037 (n = 5), Mann-Whitney U = 8.500, p-value = 0.801. C: Mann-Whitney test, mean control = 0.098±0.043 (n = 5), mean cold = 0.053±0.036 (n = 6), Mann-Whitney U = 5.500, p-value = 0.099. D: Heatmap with the protein groups significantly changed in the cold experiment in comparison to control (n = 7 mice, the same mice were used in both experiments). The plot shows the log 2 of the intensity of a protein group in samples collected during the stimulus period normalized by averaged baseline intensities. Each row represents a protein group and only protein groups with fold change lower than -3 or higher than 3 are shown. The plot is divided into the two experiments, with control samples shown on the left side and labeled in dark grey,

and the cold samples shown on the right side and labeled in blue. A different color is assigned to each timepoint collected either during the control or the cold experiment. Missing values are colored in light grey in the heatmap. E: Volcano plot with all the protein groups found in the analysis. The plot shows the log2 of fold change and the adjusted p-value of samples from the cold experiment in comparison to the control. The fold change cutoff used in this plot was 2. Each red dot represents a significant protein found in the analysis. In grey dots are all the other proteins. Dots of significant hits were expanded in size for better visualization purposes only.

5.2.3.3 Peripheral cold stimulation induced changes in the release of neuroactive peptides arriving at the POA

Among the 939 protein groups that we detected, in total, 21 were precursors of neuroactive peptides (figure 5.11-B). From this list of precursors, there were four protein groups statistically different in the cold experiment comparing to the control. While the precursors of DBI and KNG1 were found decreased in cold samples, the ones of ADIPO and TRH were detected increased ($p \leq 0.05$, adjusted by Benjamini-Hochberg correction) (figure 5.11-A).

We detected 301 peptides derived from neuroactive peptide precursors. Among these, 12 peptides were differentially released in the cold experiment. Cold stimulation increased the levels of peptides from the precursors of ADIPO, PENK, PNOC, chromogranin A (CMGA) and cerebellin-2 (CBLN2). On the other hand, peptides from angiotensinogen (AGT), SCG2, PNOC, and DBI were decreased during the cold challenge ($p < 0.05$, adjusted by Benjamini-Hochberg correction) (figure 5.11-C and D).

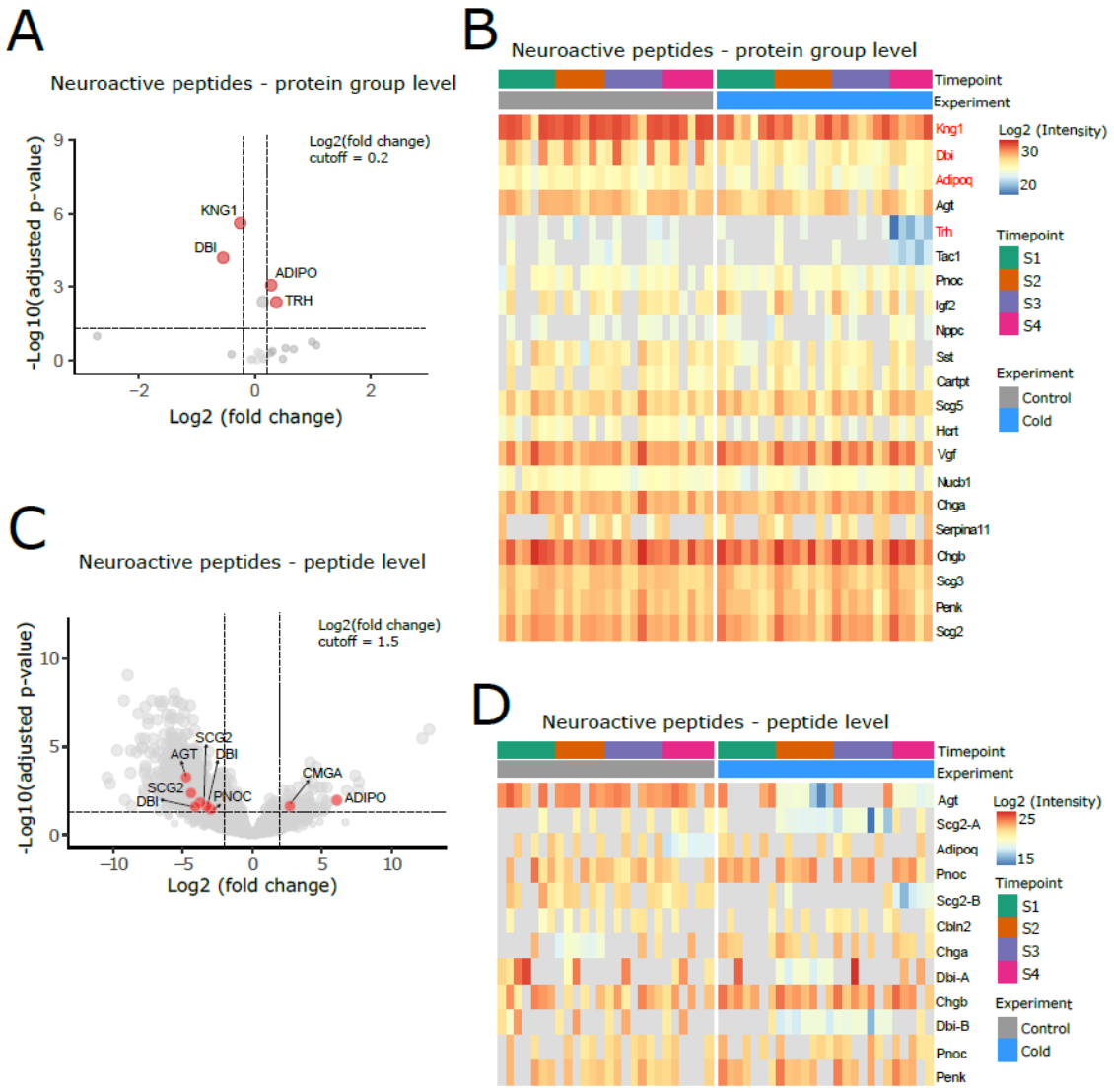

Figure 5.11: Peripheral cold stimulation induced differential release of neuroactive peptides arriving at the POA

A and B: Volcano plot (A) and heatmap (B) with all the protein groups of precursors of neuroactive peptides found in the analysis. In B, the red text represents the protein groups found significantly changed in the cold experiment. C: Volcano plot with all the peptides detected in the analysis, with the significant peptides derived from neuroactive peptide precursors, with fold change higher than 1.5, highlighted in red. D: Heatmap with significant peptides coming from precursors of neuroactive peptides found in the analysis. In A and C: The volcano plot shows the log2 of fold change and the adjusted p-value of samples from the cold experiment in comparison to the control. Each dot comes from proteins in A and peptides in C. The red dots represent the significant hits, while grey dots represent the other proteins or peptides. Dots of significant hits were expanded in size for better visualization purposes only. The fold change cutoff used in the

plots was 0.2 in A and 1.5 in C. In B and D: Heatmaps show the log 2 of the intensity of samples collected during the stimulus period normalized by averaged baseline intensities. The plot is divided into the two groups, with control samples shown on the left side and labeled in dark grey, and the cold samples shown on the right side and labeled in blue. A different color is assigned to each timepoint collected either during the control or the cold experiment. Missing values are colored in light grey in the heatmap.

5.2.4 Verification of cold-induced secretome

5.2.4.1 Adiponectin was detected in microperfusates by two different analytical methods

Among the neuroactive peptides detected by our approach, based on the same criteria used in the warm stimulation, I decided to select adiponectin (ADIPO), which was found increased at the protein group and at the peptide levels (figure 11), from the candidates coming from the cold stimulation dataset, for further verification of our results.

First, I wondered if adiponectin could be detected in microperfusates with another analytical method. For that, I sampled additional microperfusates from another cohort of mice, using the same sampling protocol as described in figure 5.10-A, and performed an ELISA for adiponectin (Mouse Adiponectin/Acrp30 Quantikine ELISA Kit, R&D systems, USA) to estimate the concentration of this adipokine in the samples. As represented in figure 5.12-B, using plasma as a positive control, I was also able to find adiponectin by ELISA in all the microperfusates tested.

Next, I speculated that the increase detected by LC-MS/MS would also be observed using ELISA. To investigate this, I compared samples collected during the control and cold experiments. I first normalized the microperfusates sampled during the stimulus period by baseline samples of each experiment, then I calculated the change as the percentage of baseline. Based on samples from 3 mice collected from each experiment, I observed no statistical significance comparing cold and control samples. Thus, differently from

the LC-MS/MS, no change was detected with ELISA comparing microperfusates from both experiments (figure 5.12-C).

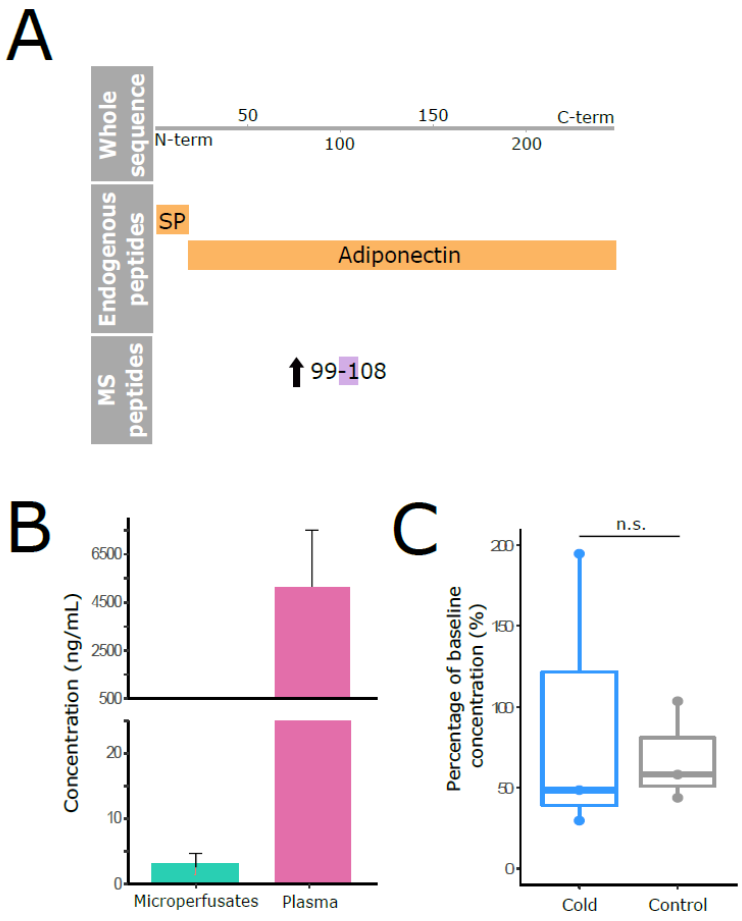

Figure 5.12: Adiponectin coverage plot and ELISA analysis of microperfusates

A: coverage plot representing the whole amino acid sequence of the precursor of adiponectin, with the middle part showing adiponectin produced by enzymatic cleavage in orange, and the lower part showing the peptide that was found significant in the analysis, represented in lilac. This peptide covers the amino acids from the position 99 to 108 in the precursor sequence. The arrow next to the peptide represents the direction of the change detected in the analysis. SP: signal peptide. The peptide processing annotation was retrieved from Uniprot. B: Concentration of adiponectin in microperfusates and in plasma measured by ELISA. C: Normalized concentration of adiponectin in microperfusates analyzed by ELISA, quantified as the percentage of baseline intensity in the control and cold groups. Each dot represents one mouse (n = 3). Two-tailed Mann-Whitney test, mean cold = 90.99±90.29 (n = 3), mean control = 68.520±31.150 (n = 3), p-value = 1.000.

5.3 Discussion

Surviving environmental challenges requires flexible neural systems. In the context of mammalian thermoregulation, constant adaptations are required to keep the Tcore balanced[1,3]. In this chapter, together with my colleagues, we investigated if neuroactive peptides play a role in the modulation of these thermoregulatory adjustments. First, we performed an unbiased profiling of neuroactive peptides released at the POA under warm and cold challenges using LC-MS/MS. Next, one significant neuroactive peptide of each dataset was selected from the list of candidates for further investigations.

As similarly discussed in the chapter 4, the results from the experiments presented in this chapter allow me to correlate peptide release at POA with a stimulus, in this case, warm or cold peripheral stimulation. However, to define a causal relationship of the peptide in modulating thermoregulation, more experiments are required. Still, I can speculate about the function of the neuroactive peptides in thermoregulation based on my results, the presence of the peptide receptor(s) in the POA, and their previously described functions.

5.3.1 Peripheral thermal stimulation induces changes in neuroactive peptides arriving at the POA

Based on the literature, I expected that, in a warm context, peptides that decrease Tcore, such as neuropeptide Y, dynorphin-A, and angiotensin II would be released in the POA, since they could potentially support heat dissipation or inhibit thermogenesis. Alternatively, the release of peptides that increase Tcore, for instance, orexin-A, somatostatin, and β-endorphin, could had been decreased, to avoid further increase in Tcore[49,50,54,58,60]. In contrast, if neuroactive peptides participate in the modulation of cold responses in the POA, I hypothesized that peptides that increase Tcore would be released in this region and that the secretion of peptides that decrease Tcore would be decreased (for more details, refer to table 1.2 in the introduction).

According to the results of the warm stimulation experiment, my colleagues and I were able to find three protein groups of neuroactive peptide precursors differentially released in the POA during warm stimulation, namely OREX, PNOC, and IGF2, in comparison to the control. An in regard to individual peptides derived from precursors of neuroactive peptides, we observed changes in peptides from OREX and SCG2, SCG1, SCG3, NUCB1, VGF, and PENK. And based on our LC-MS/MS results of cold-stimulated animals, my colleagues and I could found four precursors of neuroactive peptides differentially released in cold samples, namely DBI, KNG1, ADIPO, and TRH. On top of these, twelve individual peptides were found significant after cold stimulation, which derived from the precursors AGT, SCG2, PNOC, DBI, ADIPO, PENK, CMGA, and CBLN2.

PNOC

Comparing the warm and cold dataset, PNOC was one the neuroactive peptide precursors found in common between these two datasets. In warm samples, PNOC precursor was found increased, while in cold microperfusates two peptides from PNOC were found differentially released, with one being increased, and the other decreased (both are depicted in figure 5.13). PNOC is the precursor of the peptides nociceptin, nocistatin, and orphanin FQ2[149]. From these three, a possible role of nociceptin in thermoregulation has been suggested. I.c.v. injection of this peptide in rats led to hypothermia[66], and the knockout mouse model of its receptor, opioid receptor-like 1 (ORL1) showed increased Tcore during the light phase[150]. Additionally, ORL1 is highly expressed at the thermoregulatory center, the POA[150]. Altogether, these lines of evidence indicate that nociceptin could act as a peptide that decrease Tcore by acting at the preoptic region. Our warm results go in agreement with this. If the precursor, PNOC, is indeed increased upon warm stimulation, this could suggest that nociceptin would also be. And in case of nociceptin being a peptide that decrease Tcore, its increased levels could contribute to dissipate the heat gained from the environment during warm exposure. On the other side, the results from the cold stimulation suggest that two individual peptides from PNOC had opposite significant changes. While the peptide

covering the amino acids 32 to 42, which is part of the propetide sequence, was decreased, another peptide matching to 109 to 135 aas, part of the peptide nocistatin, was found elevated. To my knowledge, none of these peptides have been tested in the context of thermoregulation. Thus, these results could potentially suggest an involvement of these molecules in the control of Tcore.

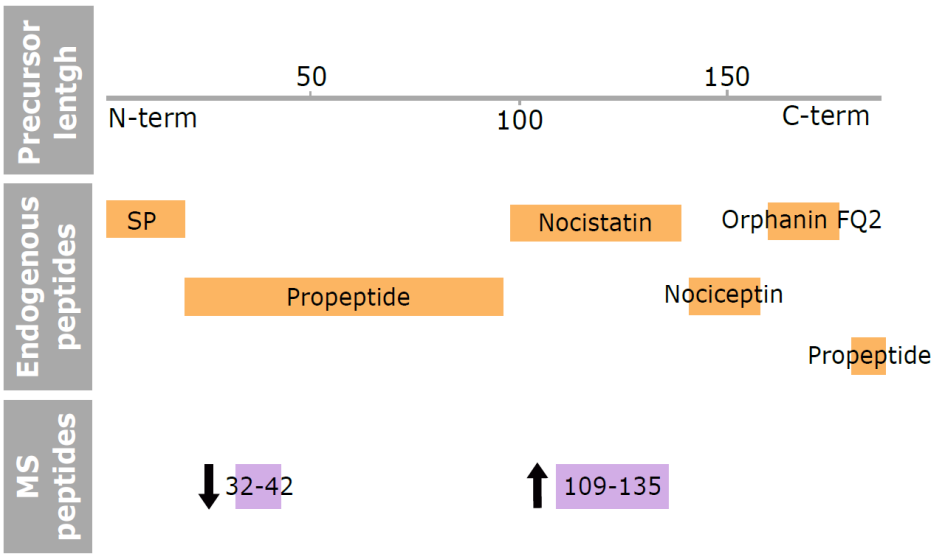

Figure 5.13: Coverage plot of PNOC.

The plot shows the precursor sequence length, the endogenous peptides in orange, and the peptides found significantly different are shown at the bottom part colored in lilac. The arrows next to them indicate the direction of the change detected in the analysis. The peptide processing annotation was retrieved from Uniprot.

PENK

In our LC-MS/MS analysis of samples collected during warm and cold stimulation, peptides derived from PENK were found increased. In the warm dataset, the sequence of the peptide found significant spans the amino acids 90 to 97. In the precursor, this sequence corresponds to part of a peptide called synenkephalin (figure 5.14), which has not been investigated in the context of thermoregulation yet. If the whole synenkephalin is indeed increased in the warm samples, it could suggest that this peptide decreases Tcore and helps dissipating the heat. In contrast, in cold samples, the significant peptide

ranged from amino acid 238 to 253, almost covering the whole sequence of the peptide PENK (238-259), whose biological function is still unexplored. In case this peptide is in fact increased in cold samples, this could mean that this molecule could help maintain the body heat during cold challenge.

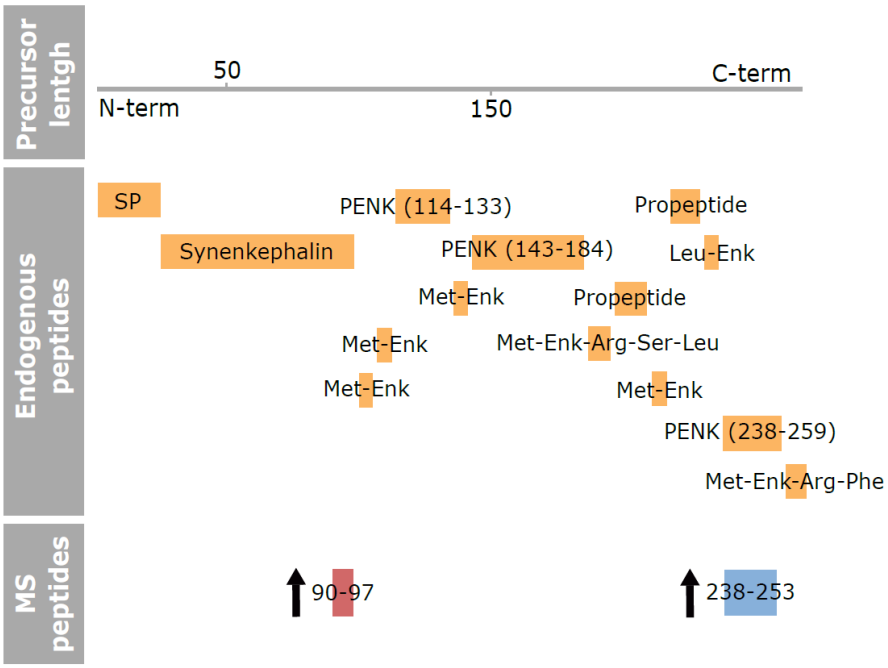

Figure 5.14: Coverage plot of PENK.

The plot shows the precursor sequence length, the endogenous peptides in orange, and the peptide found significant in warm samples in red and in cold samples in blue. The arrows next to the peptides indicate the direction of the change detected in the analysis. Met-Enk is encoded four times in the PENK sequence. The peptide processing annotation was retrieved from Uniprot[130].

5.3.2 Warm ambient temperature stimulation correlated with alterations in the secretion of neuroactive peptides

VGF

In accord with the literature, a role in thermoregulation has already been suggested for neuroactive peptides derived from the VGF. VGF is a precursor of ten peptides (figure

5.15). The VGF peptide detected differentially increased in warm samples is part of a peptide called NAPP-129[151]. While the function of this specific peptide is still unclear, a study with VGF knockout mice suggest that this protein and/or its peptides participate in energy balance. These animals showed a lower body weight and less fat content. Additionally, knockout mice showed intolerance to cold, decreasing their Tcore when exposed to 4°C[152]. However, this last result was based on an experiment done with a very small sample size (n = 2), thus the temperature of more mice should had been recorded to have a reliable conclusion.

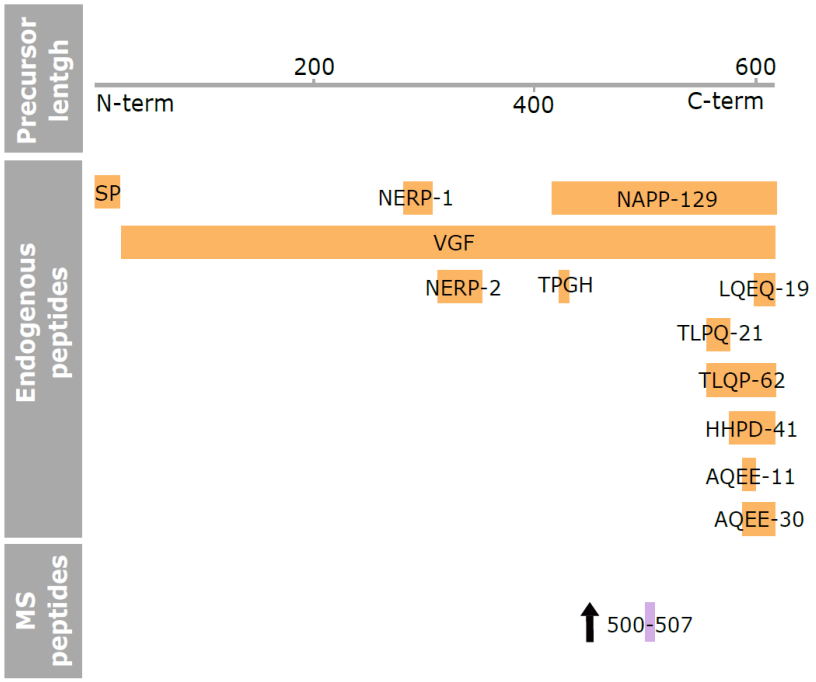

Figure 5.15: Coverage plot of VGF.

The plot shows the precursor sequence length, the endogenous peptides in orange, and the peptide found significant in warm samples in lilac. The arrows next to the peptides indicate the direction of the change detected in the analysis. The annotations for the precursor processing were retrieved from Lewis et al, 2015.

SCG1, SCG2 and SCG3

On the other side, the participation of peptides derived from the precursors SCG1, SCG2, SCG3, NUCB1, and IGF2 on thermoregulation has not been largely explored. SCG1,

SCG2 and SCG3 belong to the same protein family, the granins. In LC-MS/MS, SCG1 and SCG3 peptides were increased in warm samples, while SCG2 peptide were found decreased. As granins, these proteins are believed to participate in the formation and packing of LDCVs, the vesicles that carry neuroactive peptides in the secretory pathway[153]. In addition to this role, it has been proposed that SCG1 gives rise to two biologically active peptides, namely PE-11 and CCB peptide, although their physiological roles are still unclear[142]. As shown in figure 5.16-A, the peptide found significant (654-668 aas) is part of the CCB peptide. SCG2 is the precursor of the peptides secretoneurin and manserin. Among these, secretoneurin is the only one that has been more explored, with *in vitro* reports suggesting it to be involved in the control of neurotransmission[154,155]. For instance, a study observed an increase in dopamine release after secretoneurin was applied on rat striatum slice[155].

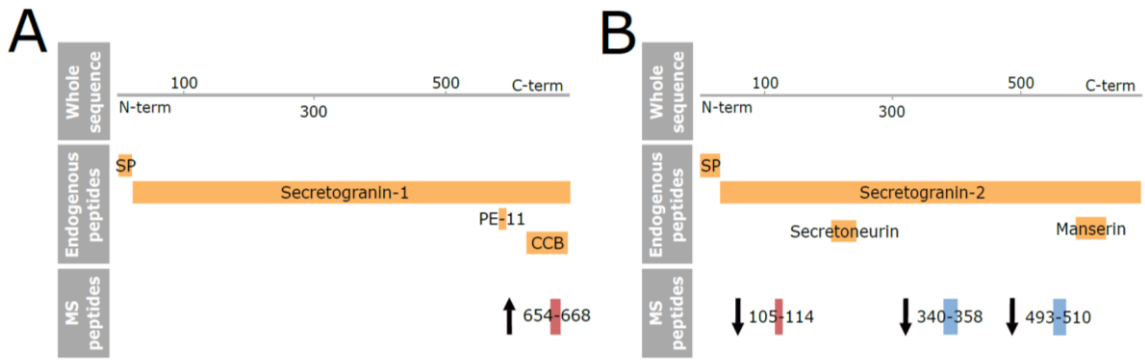

Figure 5.16: Coverage plots of secretogranin 1 and 2

The plot shows their precursor sequence length, the endogenous peptides in orange, and the peptides found significant in warm samples in lilac. The arrows next to the peptides indicate the direction of the change detected in the analysis. The peptide processing annotation was retrieved from Uniprot[130].

NUCB1 and IGF2

NUCB1 is calcium binding protein, which is proposed to give rise to the peptide nesfatin-1-like peptide (NLP)[156]. This peptide has been suggested to decrease feeding in

male rats during the dark phase, after an i.p. injection[157]. NLP sequence starts from the position 25 to 77 aas, while the peptide that was found increased in warm samples corresponds to a sequence that covers from position 193 to 203[156]. Thus, the peptide detected in the MS/MS corresponds to another part of NUCB1, whose role is unknown[156]. IGF-2, on the other side, is a growth hormone, believed to play a role in development and tissue maintenance[158]. If the levels of NUCB1 peptide 193-203 and IGF-2 are indeed increased in microperfusates collected during warm stimulation, these results could suggest an additional role for these molecules *in vivo*.

5.3.3 Cold ambient temperature stimulation correlates with changes in the release of neuroactive peptides

TRH

In our dataset, TRH protein group was detected increased during warm stimulation. TRH was originally described as a peptide hormone produced in the hypothalamus that was part of the hypothalamus-pituitary-thyroid axis, playing a role in the regulation of metabolism. Nevertheless, nowadays it is known that this neuroactive peptide also act in other regions of the brain, being associated with different functions, including the control of body temperature[159]. Supporting this notion, the injection of TRH in the POA of rats[58,59] and in the ventricles of mice[60] induced an increase in Tcore in these animals. In addition, increased release of TRH was detected in samples collected with push-and-pull perfusion (an *in vivo* sampling technique) from the PVH of male rats upon exposure to 4°C, after the animals had been acclimated to 30°C for three weeks. However, the 4°C exposure in animals kept at 22°C room temperature did not affect TRH levels. Thus, it seemed that, in this study, a higher temperature variation (from 30°C to 4°C) was required to raise TRH levels in the PVH of rats[160]. Applying a more subtle temperature variation (from 22°C to 5°C), we also observed a small, but significant elevation of TRH precursor in microperfusates of cold-stimulated mice. Together, all these lines of evidence suggest that TRH could be important for cold defense, acting as a peptide that increase Tcore.

CMGA and CBNL2

During cold stimulation, individual peptides from CMGA and CBLN2 were also detected elevated. Like SCG1-3, CMGA is also part of the granin protein family, which is important for the synthesis of LDCVs[153]. CBLN2 is also part of a protein family, the cerebellins, which are proposed to participate in the organization of synapses[161]. According to Uniprot[130], the precursor of CBLN2 only gives rise to one peptide. Thus, the peptide we found increased in cold samples covers part of CBNL2. Thus, our results could presumably suggest a role for CMGA and CBLN2 in the context of thermoregulation.

KNG1

Two neuroactive peptide precursors were found decreased in samples collected during cold stimulation, namely DBI and KNGI, whose levels were also altered upon POA^{VGLUT2} stimulation. As discussed in chapter 4, KNG1 is the precursor of bradykinin. The injection of this peptide in the ventricles elicited no effect on Tcore[144]. However, it could be that the negative results were due to the dose or the brain area injected. For instance, it could be that with different doses and/or the specific injection of one region part of the thermoregulatory circuitry, e.g. the POA, a more pronounced effect would had been observed. As also mentioned before in chapter 4, DBI has been suggested to play a role in energy homeostasis, as its plasma levels were detected increased in human obesity[145]. Therefore, if DBI and KNG1 are decreased in cold samples, they could be participating the modulation of adaptive responses to cold stimulation.

AGT

A peptide derived from the AGT precursor was found decreased in samples collected during cold stimulation. AGT is the precursor of angiotensin II (AT-II), a peptide hormone classically involved in the control of blood pressure and body fluid homeostasis[162]. In addition to these roles, it has been proposed that AT-II also participate in thermoregulation, as the i.c.v. and i.p. injection of this peptide elicited hypothermia in rats[65,163]. In our analysis, the part of AGT found significant corresponded to a peptide

covering the amino acids 470 to 477, which is not part of AT-II peptide sequence, according to the annotations of Uniprot. Nevertheless, the presence of this peptide could indicate that the AGT-derived peptide, i.e. AT-II, was also present in samples, but was not detectable by our approach. Following this reasoning, if AGT levels are decreased in microperfusates, AT-II could also be. And if this peptide indeed acts induced hypothermia, potentially decreased levels during cold exposure could suggest that its levels had been decreased to avoid the Tcore to lower further down.

5.3.4 A potential role of orexins in POA thermoregulation

In our LC-MS/MS results, OREX was detected significantly decreased at the precursor level and at the level of an individual peptide (figure 5.4-C). The significant peptide corresponds to part of the propeptide sequence, i.e. it is outside of the sequences of the biologically active forms of orexin (figure 5.4-C). Neither orexin-A nor orexin-B were detected with our approach. As detailed in section 1.6 of introduction, classical neuropeptides, like orexins, are synthesized as proneuropeptides and packed into LDCVs for secretion together with processing enzymes. Therefore, I assumed that when the content of LDCVs is released at the extracellular medium and, thus, at the interstitial fluid (ISF), other parts of the proneuropeptide are also released. Therefore, I hypothesized that if a peptide from the precursor of orexins was found, orexins themselves could also had been present, but we were unable to detect them possibly because the LC-MS/MS could have favored the detection of other peptides. In addition to this, it could also be that orexin-A and orexin-B quickly bound to their receptors and/or were rapidly degraded by extracellular peptidades[45].

In an attempt to verify the presence of orexin-A in the samples, I also performed an ELISA assay using microperfusates collected during control and experimental conditions. Using this analytical method, I was able to detected orexin-A in four out of 12 samples. This suggests that at least orexin-A could had been present in the microperfusates used in the proteomics search. Given that in the proteomic approach

peptides from many proteins are analysed, the ones coming from highly abundant proteins could hinder the detection of peptides present in low abundance, such as neuropeptides, including orexins. On the other side, provided that the ELISA assay has a good specificity, only one protein is probed. This could explain why orexin-A was not identified at all with our LC-MS/MS workflow, but was presumably found by the ELISA kit. However, it is important to highlight that orexin-A was detected close to the detection limit, and only a more sensitive approach, for example targeted LC-MS/MS could certify the presence of this peptide in the microperfusates.

Assuming that OREX release is reduced during exposure to warmth, this could suggest that such peptide is thermogenic and its secretion was lowered by a negative feedback. In agreement with that, injection of orexin A into the brain ventricles leads to hyperthermia in rats[50,54]. Orexin-B may also have an effect, but this is still unclear. While one study observed that this peptide leads to an increase in core body temperature (Tcore)[54], another found no change in Tcore[81].

Compatible with a role of orexins in the regulation of Tcore, several areas involved in thermoregulation are innervated by orexinergic neurons and express at least one of the orexin receptors, OX1R or OX2R. Among these areas, the POA, dorsal raphe, and the periaqueductal gray[76,82,83]. With immunofluorescence stainings for orexin-A and OX2R, I was also able to show the presence of orexin-A positive fibers in the POA, as well as the expression of one of orexin receptors in the same region. The colocalization of OX2R with Lepr, a marker of thermoregulatory neurons in the POA[38], suggests that if orexins are released in this area during warm stimulation, they could potentially act on Lepr+ thermoregulatory neurons. Additionally, the calcium imaging experiment further proposes that preoptic neurons are able to respond to orexin-A, in agreement to what was previously shown in the literature[76]. It is still unclear if the same happens with orexin-B. Of note, the orexin-A effect on the cells varied, with some responding quicker upon stimulus than others. Given that the injection studies mentioned above were conducted at the brain ventricles, it remains elusive where orexins could be acting in the

brain to regulate the Tcore. Altogether, the results shown in this chapter suggest that at least one of the targets of orexins could be the POA, and potentially POA^{Lepr} thermoregulatory neurons.

A differential role of OX1R and OX2R receptors has been observed in food intake and energy expenditure. While *Ox1r* knockout mice show higher food intake and lower expenditure on a normal chow diet, *Ox2r* knockout mice only have lower energy expenditure under high fat diet.[164] According to the literature, OX1R is coupled to Gq signaling and has higher affinity to orexin-A than to orexin-B. On the other side, OX2R has been suggested to use Gq and Gi cascades, depending on the cell type, and it apparently has similar affinity for both orexins[165]. These differences among orexin receptors made me hypothesize that both receptors may have different functions in the context of preoptic thermoregulation as well. Thus, in order to further investigate the contribution of both orexin receptors on Tcore maintenance by the POA, I acutely interfered with orexin signaling at this brain region by injecting antagonists for each of the two receptors, and measured the Tcore while the animal was present either at room temperature or at cold ambient temperature. Based on my results, while antagonizing OX2R had no significant effect on Tcore at room temperature, the results of the OX1R antagonist injection into the POA suggested a small but significant increase in Tcore in comparison to vehicle administration.

Since the LC-MS/MS results suggested a decrease in OREX levels upon warm stimulation, I wondered if orexin peptides increase Tcore. In this case, OREX release could had been reduced to inhibit additional heat production in the body, on top of the warmth gained from the surroundings. However, when the opposite scenario happens and a homeothermic animal is exposed to cold, heat needs to be kept in the organism and thermogenesis needs to be promoted. Thus, the next question was to investigate if OREX release into the POA was necessary to keep Tcore during cold exposure. For that, I injected the same OX1R and OX2R antagonists, while mice were stimulated with cooling starting from 24°C down to 12°C. Based on these results, the results of the OX1r

antagonist injection suggested a small but significant decrease in Tcore during the cold challenge. On the other hand, OX2R antagonist produced no change in Tcore.

Altogether, these antagonist experiments suggest that if orexins have an influence in Tcore, it potentially does so through the OX1R receptor and that this depends on the ambient temperature. At room temperature, it could be that orexins decrease Tcore at RT. However, in a cold environment, they would act increasing Tcore to maintain thermal balance, in agreement with what has been previously described in the literature[50,54]. Provided that OX1R has higher affinity to orexin-A than to orexin-B[165], it is possible that the effect observed after antagonizing OX1R stems from the inhibition of orexin-A action on this receptor. If OX1R is expressed in thermoregulatory neurons remains unclear. Additionally, it could be that a different dose of OX2R antagonist is required to oppose the influence of orexins in preoptic thermoregulation.

5.3.5 Adiponectin possibly plays a role in POA thermoregulation

In our LC-MS/MS analysis, cold exposure correlated with a small but significant increase in adiponectin precursor. In addition, an increase was observed at an individual peptide level. A role in thermoregulation for this adipose tissue hormone has been previously proposed, although conflicting results exist in regard to the effect of ADIPO on Tcore. From one side, three studies support the hypothesis that ADIPO could be a hormone that induces hyperthermia. POA injection of adiponectin in mice produced hyperthermia, without affecting locomotion[70]. ADIPO knockout mice were unable to keep the body temperature under cold challenge comparing to wild type animals[72]. And, finally, ADIPO knockout mice, after six-day exposure to 6°C, did not have the increased browning of WAT as seen in WT mice. As an important cold adaptation response, WAT browning would provide other sources of heat generation in the body[89]. Thus, together, these three different works propose adiponectin as a peptide hormone that increases Tcore, which could help in the adaptation to cold. However, this has been countered by a study that exposed another Adipoq knockout model to 4°C for four hours. In this paper, the author show that the lack of adiponectin prevented the hypothermia induced

by cold exposure observed in WT animals[71]. Provided that different knockout models have been used in the studies, this difference could possibly explain the discrepant results.

In this context, our results LC-MS/MS suggest an increase of ADIPO release in cold-stimulated mice. In order to verify with another analytical method if adiponectin was present in microperfusates, I also performed an ELISA assay with samples collected *in vivo* with OFM. Adiponectin was detected in all samples tested, in comparable levels to what was previously described in the CSF. However, in this other study CSF was collected from the cisterna magna while animals were anesthetized[166]. Thus, the collection of ADIPO with OFM presents the advantage of collecting adiponectin *in vivo.* Despite being detected with ELISA, no significant difference in ADIPO levels was observed with this other technique. This difference could be explained by technical differences between LC-MS/MS and/or by the low number of mice used in the collection of samples for the ELISA evaluation (n = 3 mice). Thus, perhaps a bigger volume or a stronger or more prolonged cold stimulation would be required for adiponectin to be differentially detected with ELISA.

Therefore, taking into consideration only the relative quantification performed with LC-MS/MS, it seemed that adiponectin was increased during cold stimulation. Such increase could mean that adiponectin is needed to protect Tcore during the cold challenge, thus further supporting the hypothesis that this hormone induces hyperthermia. According to the literature, both receptors of adiponectin, Adipor1 and Adipor2, are expressed in the hypothalamus[87]. In the POA, based on the dataset from a single cell sequencing (scRNA-Seq) of the preoptic area[88], adiponectin receptors are especially expressed in neurons and mature oligodendrocytes. Thus, altogether, ours and others results suggest that adiponectin could modulate POA thermoregulation during a cold challenge.

5.3.6 Conclusions

To conclude, our unbiased screening of neuroactive peptides during warm and cold stimulation was able to detect several peptides differentially released in the POA during each stimulus. Of note, neither the warm nor the cold stimulation were accompanied by significant changes in water and food consumption, suggesting that the results observed in our analysis are not related to these parameters. Additional investigation is required to define these peptides as modulators of preoptic thermoregulation. Nevertheless, the candidate list of thermoregulatory peptides provided by our analysis could contribute to a better understanding of the molecular control of POA during adaptation to thermal challenges. Considering the importance of maintaining the Tcore in mammals, such candidates could potentially also be implicated in healthy and diseased states.

CHAPTER 6: GENERAL DISCUSSION AND FUTURE DIRECTIONS

6 GENERAL DISCUSSION AND FUTURE DIRECTIONS

6.1 General discussion

Being the Tcore crucial for the survival of mammals, it is to be expected that several processes play a role on its control, increasing the chances of having effective thermal balance. Specifically in this thesis, I studied one of these regulatory processes, the molecular mechanisms that could modulate the activity of the thermoregulatory circuitry center, the POA, in male mice. Deviations from the Tcore balance point, elicited by thermal stimuli coming either from external (e.g. changes in ambient temperature) or internal (e.g. physical activity) sources, are recognized by the POA and, in a healthy condition, trigger autonomic and behavioral adaptations in order to keep thermal homeostasis[1,3].

My working hypothesis in this thesis was that neuroactive peptides would be released into the POA during thermal challenges. There, they could act assisting this hypothalamic region to integrate thermal information and orchestrate adaptive responses needed to keep Tcore. In agreement with this idea, different studies have previously suggested that several neuroactive peptides decrease or increase Tcore (summarized in table 1.2 and 1.3 in the introduction). In order to test this hypothesis, I performed an unbiased screening of neuroactive peptides released at the POA during three different types of stimuli, namely peripheral warm and cold stimulation, as well as central chemogenetic activation of POA^{VGLUT2} neurons. Comparing to their respective controls, in total, these three thermal challenges correlated with changes in the release of 18 neuroactive peptides (summarized in table 6.1), at the protein group and/or the peptide level. For all cases in which both, the protein and peptide levels, were statistically different, there was an agreement in the change direction. The only exception was PNOC, from which one peptide was found increased and one decreased during cold stimulation.

Table 6.1: Neuroactive peptides found significant in the screening of the secretome during chemogenetic activation of POA^{VGLUT2} neurons, warm and/or cold ambient exposure.
Each row represents one precursor that was found significant at the protein and/or the peptide level in the analysis. In green are highlighted the neuroactive peptides with previous implication in thermoregulation or energy balance. '↓ ' means found decreased in the analysis, while '↑' means increased, and '=' means no significant change or no detection. N.D. = not described.

Precursor gene	**Dataset**			**Previous evidence supporting influence in Tcore?**
	Activation of thermoregulatory neurons	**Warm**	**Cold**	
Sst	↓	=	=	• I.c.v. injection in rats and intercisternal injection in mice increase Tcore[49,57]
Adipo	=	=	↑	• POA injection in mice increased Tcore[70]; • Cold exposure increased mRNA and protein levels in WAT after 6 hours and 6 days, respectively[89]; • Cold exposure led knockout mice to hypothermia[72]; • Lack of adiponectin in another knockout mouse model prevented hypothermia after cold exposure[71]
Scg1	↓	↑	=	N.D.
ProSAAS	↑	=	=	N.D.
Dbi	↑	=	↓	• Increased plasma levels in human obese patients[145]
Kng1	↑	=	↓	N.D.
Hcrt	=	↓	=	• I.c.v. injection of orexin-A and orexin-B in rats increased Tcore[50,54]
Scg2	=	↓	↓	
Pnoc	=	↑	↓↑	• I.c.v. injections in rats led to hypothermia[66]
Vgf	=	↑	=	• VGF knockout mice have lower body weight and less fat content[152]

Igf2	=	↑	=	N.D.
Nucb1	=	↑	=	N.D.
Penk	=	↑	↑	• In rats, 100 µg i.c.v. injection led to hyperthermia and 400 µg i.c.v. injection led to hypothermia[69]
Scg3	=	↑	=	N.D.
Agt	=	=	↓	• I.c.v. injections in rats decreased Tcore[65]
Trh	=	=	↑	• POA injection in rats[59] • I.c.v. injection in mice[60] • Intraperitoneal injection in mice[58] • Increased mRNA expression upon peripheral warm stimulation in mice[35]
Cbln2	=	=	↑	N.D.
Cmga	=	=	↑	N.D.

Among the neuroactive peptides found statistically different in at least one of the secretome datasets – chemogenetics activation of POA^{VGLUT2} neurons, warm, and cold stimulation - , half of them (nine) have already been related to thermoregulation and/or energy balance (precursors highlighted in green in table 6.1). Thus, the results of this unbiased profiling further suggest the participation of these peptides in the context of energy homeostasis. The other half of neuroactive peptide precursors, to my knowledge, has not been demonstrated to play a role in Tcore control, thus our results could suggest an additional role for these molecules. As discussed in chapters 4 and 5, the outcomes of the three experiments can be used to correlate the release of certain peptides at the POA with the stimulus presented in each type of experiment. The datasets cannot, only by themselves, be used to infer causality. Still, other pieces of evidence from this thesis or from the literature help in interpreting these results and hypothesizing about a potential role in thermoregulation for the neuroactive peptides found.

6.1.1 Neuroactive peptide release during central and peripheral stimulation

One of the aims of this thesis was to investigate the differences and commonalities in regard to the neuroactive peptides secreted during central activation of POA thermoregulatory neurons and peripheral thermal stimulation. The chemogenetic activation of POA^{VGLUT2} neurons had the advantage of directly targeting cells in this hypothalamic region that participate in the regulation of body temperature[20,29,38]. Provided that POA^{VGLUT2} neurons project to other areas of the thermoregulatory circuitry[21], the chemogenetic activation indirectly stimulated these other regions as well. However, with this stimulation, other preoptic neurons that express VGLUT2 and do not play a role in Tcore control may also had been activated. Another disadvantage of this strategy is that it is an artificial activation of neurons. In contrast, the ambient temperature stimulation represents a more natural type of stimulation, when animals are exposed to variations in the environmental temperature. In this way, thermal information is assumed to go through the whole thermoregulatory system and reach the POA[3]. Nevertheless, the experiment was performed in a lab, under controlled conditions, with thermal chamber temperature varying probably more quickly than the air temperature would change in a real scenario. Therefore, taking the advantages and disadvantages of each type of stimulus into consideration, a comparison of the central versus peripheral types of stimulation could help elucidate how they affect the secretome at the POA.

Comparing specifically the cold ambient stimulation and the chemogenetic activation of preoptic glutamatergic neurons, two neuroactive peptide precursors were found in common among these two datasets, namely DBI and KNG1. Reports in the literature have suggested a participation of DBI in energy balance[145], while KNG1 has presumably no considerable effect in thermoregulation[144].

DBI has recently been proposed to play a role in energy balance, as its plasma levels were found elevated in obese human patients[145]. On the other side, the KNG1-derived peptide, bradykinin, presumably has no effect on Tcore[144]. In microperfusates sampled during

chemogenetic activation of POA^{VGLUT2} neurons, peptides derived from DBI and KNG1 were detected increased during hypothermia, whereas a decrease of DBI and KNG1 was observed in samples collected during cold stimulation at protein and peptide level. These results could suggest an additional role of these molecules in energy homeostasis.

Contrasting the central chemogenetic activation of POA^{VGLUT2} neurons to the peripheral warm stimulation, one neuroactive peptide precursor, SCG1, was common among these two datasets. One peptide derived from SCG1 was found decreased upon central chemogenetic activation of glutamatergic neurons, whereas warmth correlated with an increase of another SCG1 peptide. While no previous role in thermoregulation has been described for peptides derived from this precursor (as discussed in chapters 4 and 5), a major role of this protein is the synthesis of LDCVs. This could suggest that during warm stimulation, more LDCVs are released into the extracellular space, whilst during the activation of POA^{VGLUT2} neurons, and consequent hypothermia, less LDCVs would be secreted. In agreement to this, another granin, SCG3 was also found elevated in warm microperfusates. However, although these two granins, SCG1 and SCG3, were increased during warm, another protein of the same family, SCG2, was detected decreased, thus the hypothesis of more LDCV secretion is not totally supported by our data. In addition, neither SCG2 nor SCG3 were detected statistically different during the POA^{VGLUT2} chemogenetic activation.

Hence, based on these three datasets, only three out of eighteen neuroactive peptides were found significantly changed in common upon central stimulation of POA^{VGLUT2} neurons and peripheral thermal challenge. Thus, these results could suggest that different neuroendocrine circuits are engaged when preoptic glutamatergic neurons are specifically activated in contrast to when POA neurons are activated by peripheral thermal stimulation. In addition, it is possible that detection limitations prevented changes in peptide amounts to be identified in the samples.

6.1.2 Pattern of expression of neuroactive peptide receptors in POA

Our analysis of samples collected *in vivo* from the POA suggested the differential release of some neuroactive peptides, depending on the type of stimulus, summarized in table 6.1. If these peptides are indeed secreted at the preoptic region during thermal stimuli, a next question would be if they are able to exert any influence on neurons of this hypothalamic area. Thus, using the data available from a scRNA-seq of the POA performed by Moffitt and colleagues (2018), I explored if the receptor(s) of these peptides are expressed in preoptic neurons and in which type of neuron, if excitatory or inhibitory (summarized in table 6.2). According to the literature[87,145,167], ten of the eighteen neuroactive peptides have at least one receptor. Based on the scRNA-seq data, the mRNA of receptors of nine neuroactive peptides are expressed in the POA (labelled in blue in table 6.2), with the exception of KNG1, which gives rise to the peptide bradykinin. Therefore, this information suggests that peptides from at least these nine precursors of neuroactive peptides (in blue in table 6.2) could act in the POA through their respective GPCRs.

Table 6.2: Peptides derived from the precursors of neuroactive peptides found significant in the secretome datasets, their respective receptor(s) and pattern of expression of the receptor(s) according to scRNA-seq of POA (Moffitt et al, 2018).
N.D. = not described. The blue color highlights the peptide receptors putatively expressed at POA.

Precursor gene	**Products derived from precursor processing**	**Receptor(s) described in the literature?**	**Receptor expression in POA neurons according to Moffitt et al, 2018**
Adipo	Adiponectin	Adipor1	Excitatory, Inhibitory
		Adipor2	Excitatory, Inhibitory
Agt	Angiotensinogen, angiotensin-1, angiotensin 1-9, angiotensin-2, angiotensin 1-7, angiotensin 1-5, angiotensin 1-4, angiotensin-3, angiotensin-4	Agtr1a	Excitatory, Inhibitory
		Agtr1b	Not detected
		Agtr2	Excitatory, Inhibitory
Cbln2	Cerebellin-2	N.D.	N.D.
Cmga	Chromogranin-A, Beta-granin, Pancreastatin, WE-14, Catestatin, GE-25, Serpinin-RRG, Serpinin, p-Glu serpinin precursor	N.D.	N.D.
Dbi	Diazepam-binding protein	Gabra1 (?)	Excitatory, inhibitory
Hcrt	Orexin-A, Orexin-B	Hcrtr1	Excitatory, Inhibitory
		Hcrtr2	Excitatory, Inhibitory
Igf2	Insulin-like growth factor II, E peptide, Preptin	Igf2r	Excitatory, Inhibitory

Kgn1	Bradykinin, Kininogen-1	Bdkrb1	Not detected
		Bdkrb2	Not detected
Nucb1	Nesfatin-1-like peptide	N.D.	N.D.
Penk	Leu-enkephalin, Met-enkephalin, Synenkephalin, PENK(114-133), PENK(143-184), PENK(238-259), Met-enkephalin-Arg-Ser-Leu, Met-enkephalin-Arg-Phe	Oprd1	Inhbitory
		Oprk1	Excitatory, Inhbitory
		Oprm1	Excitatory, Inhbitory
Pnoc	Nociceptin, Nocistatin, Orphanin FQ2	Oprl1	Excitatory, Inhbitory
ProSAAS	ProSAAS, BigSAAS, KEP, Little SAAS, Big PEN-LEN, PEN, PEN-20, PEN-19, Big LEN, Little LEN	N.D.	N.D.
Scg1	Secretogranin-1, PE-11, CCB peptide	N.D.	N.D.
Scg2	Secretogranin-2, Secretoneurin, Manserin	N.D.	N.D.
Scg3	Secretogranin-3	N.D.	N.D.
Sst	Somatostatin-14, Somatostatin-28	Sstr1	Excitatory, Inhibitory
		Sstr2	Excitatory, Inhibitory
		Sstr3	Excitatory, Inhibitory
		Sstr4	Not detected
		Sstr5	Excitatory, Inhibitory
Trh	Thyrotropin-releasing hormone	Trhr	Excitatory, Inhibitory
		Trhr2	Not detected
Vgf	VGF, NERP-1, NERP-2, NAPP-129, TPGH, TLQP-62, TLQP-21, HHPD-41, AQEE-30, AQEE-11, LQEQ-19	N.D.	N.D.

6.1.3 Limitations of this study

In addition to the disadvantages of the different types of stimulation used in this study discussed above, I would like to make some considerations regarding other limitations of this thesis. As discussed in section 1.8, the *in vivo* investigation of neuroactive peptides is very challenging, due to their low extracellular concentration, fast degradation by peptidases, surface adsorption, and the intricacies of their production and secretion[90–92]. Despite the optimized protocol for the sampling and detection of neuroactive peptides in microperfusates, presented in chapter 3, the material that we were working with was still

limited. This was reflected in the data analysis, when there were many missing values for a given peptide or protein group. Our way to circumvent this issue, and only include peptides or protein groups that were more reliable, was to include those that were detected in at least three different samples from the baseline and three samples from the stimulus sampling. Thus, it is important to take this limitation in consideration when interpreting the results shown in this thesis. Therefore, further investigations regarding the thermoregulatory peptide candidates suggested by our analysis are required to infer a role of these molecules in thermoregulation.

Another technical limitation of this study was in regard to the sampling of the molecules. In my experiments, I implanted the OFM cannula and probe in the center of the POA. Thus, the probe covered dorsoventrally the whole length of the POA region of the right brain hemisphere. However, the exchangeable part of the probe extended beyond the POA limits and also covered part of other brain areas (shown in figure 3.1). Thus, I assumed that, with the *in vivo* sampling, I also collected peptides from the CSF, coming from the lateral and third ventricles, as well as from other brain regions, namely the BNST and the lateral septum, two regions part of the limbic system, proposed to participate in emotional regulation[168]. Specifically, the BNST is believed to control autonomic and neuroendocrine responses[169], whereas the lateral septum plays a role in several processes, including reward and anxiety[170]. Therefore, the results here presented have also to be interpreted in light of this methodological constraint.

This study was also limited in regard to the biological sex of mice used in the experiments. With the exception of the injection of orexin receptor antagonists, in which I used males and females, all the other experiments were only performed in male mice. This was done to reduce the complexity of the data analysis. However, this comes with the huge expense of biasing the results towards the male sex. This was also a limitation of several studies discussed here[49,57,70–72,89]. Therefore, it is unclear if the results of our neuroactive peptide screening can also be extended to females. Further clarification is needed before making

any generalization in regard to my results, and future studies should make the use of the two biological sexes a priority.

6.2 Future directions

6.2.1 Verification of results with targeted MS/MS

Our unbiased screening of neuroactive peptides in samples collected during thermal challenges suggested that some of these molecules could be differentially released during stimulation. Nevertheless, because of the randomness during data acquisition in unbiased proteomics, peptides are not always consistently detected[171]. Thus, it would be important to verify the unbiased LC-MS/MS results with other analytical methods. In chapter 5, I used ELISA to test if orexin-A and adiponectin were present in microperfusates. Using this method, I could not find orexin-A in all microperfusates, and in the samples I managed to detected it, amounts were close to the detection limit. In regard to adiponectin, despite it being detected in the samples, I did not observe a differential release of this protein comparing control and cold stimulation. Thus, this made me wonder if ELISA was sensitive enough to detect small changes in protein content in the microperfusates.

Therefore, provided that MS/MS-based methods are considered highly sensitive[106], we decided to use targeted MS approach to analyze the samples. In this case, selected peptides are examined based on their retention time in the LC and on their m/z in the MS[171]. For this, in collaboration with Dr. Max Sauter, a postdoc scientist from the laboratory of Prof. Dr. med. Walter Haefeli at the Heidelberg University Hospital, we investigated if some neuroactive peptides found in the previous analysis could be detected with targeted MS. For this, I collected additional *in vivo* samples using OFM in parallel to warm and cold ambient temperature, and Dr. Sauter performed the targeted MS analysis (described in details in the Methods section 2.2). Briefly, in this technique, a mix of peptides, synthesized upon request based on the candidate list, was run in the

targeted MS to define the monitored mass transitions and retention time of each peptide. Although the individual characteristics of each synthetic peptide were successfully defined, no peptide with the same characteristics were detected in the samples (data not shown).

Since this targeted MS differed from the secretome proteomics in regard to sample preparation and LC-MS/MS equipment, it could be that this approach was not the most adequate to verify the thermoregulatory peptide candidates. Thus, the current step is the measurement of samples using another targeted MS method, namely parallel reaction monitoring (PRM). In this current approach, the same sample processing and instrumentation used in our workflow, described in chapter 3, are being applied to quantify microperfusates collected during control and thermal stimulation conditions. PRM analysis is a targeted quantitative proteomics approach based on MS, that allows the quantification of selected peptide candidates, with the advantage of being highly specific in comparison to the other targeted MS approach used before.[171] For this experiment, I am currently working in collaboration with Dr. Dimitris Papageorgiou, a postdoc researcher from Dr. Krigsveld lab at DKFZ. Therefore, using PRM analysis, we aim to verify the presence of the neuroactive peptides detected in microperfusates collected during control and thermal challenges.

6.2.2 Open questions

In addition to the verification of the unbiased screening results, further functional investigation of the thermoregulatory peptide candidates is required. Our results suggested that that these peptides could be differentially released at the POA during thermal stimuli in male mice. Nevertheless, it is still unclear if these results can be extrapolated to female mice as well. In addition, it could be that the thermoregulatory peptide candidates are related to biological processes other than temperature regulation, such as water balance, as the POA has previously been implicated in the control of water consumption[21], or stress, given the quick changes in temperature to which mice were

exposed to during the thermal challenges. Therefore, additional experiments with the peptides found in our profiling are needed to better understand if they could play a role in thermoregulation.

Our results could be complemented with the evaluation of the effect of peptides on preoptic neurons as well as on Tcore. The investigation of the influence on POA neurons could be performed on preoptic slices with calcium imaging or electrophysiological approaches, such as patch clamp. It would also be interesting to know where the peptides' receptors are expressed in the POA and if there is an enrichment in one specific region. This could be further evaluated with immunohistochemistry. Additionally, the identity of the cellular circuitry that could be affected by the peptides' actions could be investigated with co-localization studies of the peptides or their receptors with glutamatergic and GABAergic markers, as well as with markers of thermoregulatory neurons.

On top of this, preventing peptides from acting on POA either at basal conditions or during thermal challenges would be very informative in regard to the impact of these peptides on Tcore. For this, *in vivo* pharmacological studies could be done using antagonists of the peptides' receptors with parallel Tcore monitoring. Similarly to what I performed for orexin receptors, these antagonists could also be administered during thermal challenges. Finally, a function on thermoregulation for the peptide candidates could also be examined by knocking out or knocking down the peptide or its receptor(s) in the POA and exposing these animals to different thermal stimuli. This would be preferentially done using a conditional gene manipulation, which allows targeting these molecules spatially and temporally[172]. The latter experiment would also help understanding when, during development, such peptides could start being important for controlling Tcore. Together, all these ideas could, more robustly, determine if a neuroactive peptide plays a role in thermoregulation.

6.2.3 Possible future outcomes based on this study

Investigating the role of neuroactive peptides in thermoregulation, as performed in basic studies as this thesis, has the potential of contributing to a better understanding of Tcore control in general. In addition to this, if a thermoregulatory function of the peptides suggested by this work is further validated by other approaches, as discussed above, these molecules or their analogues could, in the future, be also examined in clinical research, given the vital importance of Tcore. Along these lines, peptides that increase Tcore could be useful in situations in which higher Tcore could be beneficial to the patient. For instance, induced non-shivering BAT thermogenesis has been appreciated as a treatment for obesity[173]. On the other side, when decreasing Tcore would be advantageous, peptides that lead to hypothermia could be administered. An example of such situation is when an individual suffers cardiac arrest and, consequently, ischemia. In this context, therapeutic hypothermia has been suggested to help decreasing tissue damage and neurological side effects[174]. Therefore, in these two circumstances, a controlled modulation of thermoregulatory peptides' signalling could be proven useful.

6.3 Conclusions

Homeothermy and endothermy have been proposed to confer an evolutionary advantage that made possible the survival and propagation of mammals in a large variety of habitats[1,4]. Studying how this group of animals maintain their Tcore, thus, is essential to comprehend their physiology. Although several studies, as the ones discussed in this work, have provided remarkable contributions to our current understanding of thermoregulation, the molecular processes influencing Tcore requires further elucidation. Thus, with this doctoral thesis, I aimed to investigate the control of Tcore at the POA through a molecular angle. For this, together with my colleagues, we performed an unbiased screening of neuroactive peptides released at the POA of male mice during thermal challenges. Based on this results, our approach suggested a role in thermoregulation for these molecules derived from eighteen neuroactive peptide precursors. In addition, the further verification of these results focusing on orexin signaling may have provided further evidence for the engagement of pro-orexin derived

peptides in Tcore control. Given the vital relevance of thermoregulation, the possible outcomes of this study could contribute to a better comprehension of thermoregulatory molecular mechanisms in health and disease. Last but not least, in the worrying scenario of climate change, studying thermoregulation is not only essential to understand mammal physiology, but also to develop better strategies to cope with future challenges.

BIBLIOGRAPHY

1. Tan, C. L. & Knight, Z. A. Regulation of Body Temperature by the Nervous System. *Neuron* **98**, 31–48 (2018).

2. van den Pol, A. N. Neuropeptide Transmission in Brain Circuits. *Neuron* **76**, 98–115 (2012).

3. Morrison, S. F. & Nakamura, K. Central Mechanisms for Thermoregulation. *Annu. Rev. Physiol.* **81**, 285–308 (2019).

4. Romanovsky, A. A. The thermoregulation system and how it works. in *Handbook of Clinical Neurology* vol. 156 3–43 (Elsevier, 2018).

5. Blix, A. S. Adaptations to polar life in mammals and birds. *J. Exp. Biol.* **219**, 1093–1105 (2016).

6. Schwimmer, H. & Haim, A. Physiological adaptations of small mammals to desert ecosystems. *Integr. Zool.* **4**, 357–366 (2009).

7. Paricio-Montesinos, R. *et al.* The Sensory Coding of Warm Perception. *Neuron* S0896627320301860 (2020) doi:10.1016/j.neuron.2020.02.035.

8. DiCara, L. V. *Limbic and Autonomic Nervous Systems Research*. (Springer US, 1975). doi:10.1007/978-1-4613-4407-0.

9. Andersson, B., Grant, R. & Larsson, S. Central Control of Heat Loss Mechanisms in the Gost. *Acta Physiol. Scand.* **37**, 261–280 (1956).

10. Hamilton, C. L. & Brobeck, J. R. Food intake and temperature regulation in rats with rostral hypothalamic lesions. *Am. J. Physiol.-Leg. Content* **207**, 291–297 (1964).

11. Magoun, H. W., Harrison, F., Brobeck, J. R. & Ranson, S. W. ACTIVATION OF HEAT LOSS MECHANISMS BY LOCAL HEATING OF THE BRAIN. *J. Neurophysiol.* **1**, 101–114 (1938).

12. Ranson, S. W. HYPOTHALAMIC REGULATION OF TEMPERATURE IN THE MONKEY. *Arch. Neurol. Psychiatry* **38**, 445 (1937).

13. Ranson, S. W. Some functions of the hypothalamus. *Bull. N. Y. Acad. Med.* **13**, 1–17 (1937).

14. Szymusiak, R. & Satinoff, E. Acute thermoregulatory effects of unilateral electrolytic lesions of the medial and lateral preoptic area in rats. *Physiol. Behav.* **28**, 161–170 (1982).

15. Teague, R. S. & Ranson, S. W. THE ROLE OF THE ANTERIOR HYPOTHALAMUS IN TEMPERATURE REGULATION. *Am. J. Physiol.-Leg. Content* **117**, 562–570 (1936).

16. Boulant, J. A. Single Neuron Studies and Their Usefulness in Understanding Thermoregulation. 10 (1986).

17. Boulant, J. & Bignall, K. Hypothalamic neuronal responses to peripheral and deep-body temperatures. *Am. J. Physiol.-Leg. Content* **225**, 1371–1374 (1973).

18. Siemens, J. & Kamm, G. B. Cellular populations and thermosensing mechanisms of the hypothalamic thermoregulatory center. *Pflüg. Arch. - Eur. J. Physiol.* **470**, 809–822 (2018).

19. Machado, N. L. S. & Saper, C. B. Genetic identification of preoptic neurons that regulate body temperature in mice. *Temperature* 1–9 (2022) doi:10.1080/23328940.2021.1993734.

20. Abbott, S. B. G. & Saper, C. B. Median preoptic glutamatergic neurons promote thermoregulatory heat loss and water consumption in mice: Median preoptic neurons promote heat loss and water consumption. *J. Physiol.* **595**, 6569–6583 (2017).

21. Abbott, S. B. G., Machado, N. L. S., Geerling, J. C. & Saper, C. B. Reciprocal Control of Drinking Behavior by Median Preoptic Neurons in Mice. *J. Neurosci.* **36**, 8228–8237 (2016).

22. Park, S.-G. *et al.* Medial preoptic circuit induces hunting-like actions to target objects and prey. *Nat. Neurosci.* **21**, 364–372 (2018).

23. Zhang, G.-W. Medial preoptic area antagonistically mediates stress-induced anxiety and parental behavior. *Nat. Neurosci.* 30 (2021).

24. Norris, A. J., Shaker, J. R., Cone, A. L., Ndiokho, I. B. & Bruchas, M. R. Parabrachial opioidergic projections to preoptic hypothalamus mediate behavioral and physiological thermal defenses. *eLife* **10**, e60779 (2021).

25. Nakamura, K. & Morrison, S. F. A thermosensory pathway mediating heat-defense responses. *Proc. Natl. Acad. Sci.* **107**, 8848–8853 (2010).

26. Nakamura, K. & Morrison, S. F. A thermosensory pathway that controls body temperature. *Nat. Neurosci.* **11**, 62–71 (2008).

27. Miyata, S. New aspects in fenestrated capillary and tissue dynamics in the sensory circumventricular organs of adult brains. *Front. Neurosci.* **9**, (2015).

28. Allen mouse brain atlas. *Allen brain atlas* https://mouse.brain-map.org/search/index (2022).

29. Song, K. *et al.* The TRPM2 channel is a hypothalamic heat sensor that limits fever and can drive hypothermia. *Science* **353**, 1393–1398 (2016).

30. Takahashi, T. M. *et al.* A discrete neuronal circuit induces a hibernation-like state in rodents. *Nature* (2020) doi:10.1038/s41586-020-2163-6.

31. Krajewski-Hall, S. J., Santos, F. M. D., McMullen, N. T. & Rance, N. E. Glutamatergic Neurokinin 3 receptor neurons in the median preoptic nucleus modulate heat-defense pathways in female mice. 29 (2019).

32. Kroeger, D. *et al.* Galanin neurons in the ventrolateral preoptic area promote sleep and heat loss in mice. *Nat. Commun.* **9**, (2018).

33. Zhang, K. X. *et al.* Violet-light suppression of thermogenesis by opsin 5 hypothalamic neurons. *Nature* **585**, 420–425 (2020).

34. Piñol, R. A. *et al.* Preoptic BRS3 neurons increase body temperature and heart rate via multiple pathways. *Cell Metab.* **33**, 1389-1403.e6 (2021).

35. Tan, C. L. *et al.* Warm-Sensitive Neurons that Control Body Temperature. *Cell* **167**, 47-59.e15 (2016).

36. Upton, B. A., D'Souza, S. P. & Lang, R. A. QPLOT Neurons—Converging on a Thermoregulatory Preoptic Neuronal Population. *Front. Neurosci.* **15**, 665762 (2021).

37. Hrvatin, S. *et al.* Neurons that regulate mouse torpor. *Nature* (2020) doi:10.1038/s41586-020-2387-5.

38. Yu, S. *et al.* Glutamatergic Preoptic Area Neurons That Express Leptin Receptors Drive Temperature-Dependent Body Weight Homeostasis. *J. Neurosci.* **36**, 5034–5046 (2016).

39. Zhang, Z. *et al.* Estrogen-sensitive medial preoptic area neurons coordinate torpor in mice. *Nat. Commun.* **11**, 6378 (2020).

40. Tan, C.-H. & McNaughton, P. A. The TRPM2 ion channel is required for sensitivity to warmth. *Nature* **536**, 460–463 (2016).

41. Bautista, D. M. *et al.* The menthol receptor TRPM8 is the principal detector of environmental cold. *Nature* **448**, 204–208 (2007).

42. Ran, C., Hoon, M. A. & Chen, X. The coding of cutaneous temperature in the spinal cord. *Nat. Neurosci.* **19**, 1201–1209 (2016).

43. Bratincsák, A. & Palkovits, M. Activation of brain areas in rat following warm and cold ambient exposure. *Neuroscience* **127**, 385–397 (2004).

44. Uchida, Y., Onishi, K., Tokizawa, K. & Nagashima, K. Regional differences of cFos immunoreactive cells in the preoptic areas in hypothalamus associated with heat and cold responses in mice. *Neurosci. Lett.* **665**, 130–134 (2018).

45. Fricker, L. D. Neuropeptides and Other Bioactive Peptides: From Discovery to Function. *Colloq. Ser. Neuropept.* **1**, 1–122 (2012).

46. Chemelli, R. M. *et al.* Narcolepsy in orexin Knockout Mice: Molecular Genetics of Sleep Regulation. *Cell* **98**, 15 (1999).

47. Fuxe, K., Borroto-Escuela, D. O., Romero-Fernandez, W., Zhang, W. & Agnati, L. F. Volume transmission and its different forms in the central nervous system. *Chin. J. Integr. Med.* **19**, 323–329 (2013).

48. Taber, K. H. & Hurley, R. A. Volume Transmission in the Brain: Beyond the Synapse. *J. Neuropsychiatry Clin. Neurosci.* **26**, iv–4 (2014).

49. Brown, M., Ling, N. & River, J. Somatostatin-28, somatostatin-14 and somatostatin analogs: Effects on thermoregulation. *Brain Res.* **214**, 127–135 (1981).

50. Yoshimichi, G., Yoshimatsu, H., Masaki, T. & Sakata, T. Orexin-A Regulates Body Temperature in Coordination with Arousal Status. *Exp. Biol. Med.* **226**, 468–476 (2001).

51. Clark, W. G. & Fregly, M. J. Evidence for Roles of Brain Peptides in Thermoregulation. in *Comprehensive Physiology* (ed. Terjung, R.) cp040108 (John Wiley & Sons, Inc., 1996). doi:10.1002/cphy.cp040108.

52. Benmoussa, M., Chait, A., Loric, G. & De Beaurepaire, R. Low doses of neurotensin in the preoptic area produce hyperthermia. Comparison with other brain sites and with neurotensin-induced analgesia. *Brain Res. Bull.* **39**, 275–279 (1996).

53. Naylor, A. Thermoregulatory actions of centrally-administered vasopressin in the rat. *Neuropharmacology* **25**, 787–794 (1986).

54. Székely, M., Pétervári, E., Balaskó, M., Hernádi, I. & Uzsoki, B. Effects of orexins on energy balance and thermoregulation. *Regul. Pept.* **104**, 47–53 (2002).

55. Huidobro-Toro, J. P. & Way, E. L. RAPID DEVELOPMENT OF TOLERANCE TO THE HYPERTHERMIC EFFECT OF BETA-ENDORPHIN, AND CROSS-TOLERANCE BETWEEN THE ENKEPHALINS AND BETA-ENDORPHIN. 11 (1980).

56. Thornhill, J. A. & Saunders, W. S. Thermoregulatory (core, surface and metabolic) responses of unrestrained rats to repeated POAH injections of β-endorphin or adrenocorticotropin. *Peptides* **5**, 713–719 (1984).

57. Nemeroff, C. B., Iii, A. J. O., Manberg, P. J., ERVINt, G. N. & Prange, A. J. Alterations in nociception and body temperature after intracisternal administration of neurotensin, 3-endorphin, other endogenous peptides, and morphine. 4 (1979).

58. Sakurada, T. *et al.* Actions of intracerebroventricular administration of kyotorphin and an analog on thermoregulation in the mouse. *Peptides* **4**, 859–863 (1983).

59. Boschi, G. & Rips, R. Effects of thyrotropin releasing hormone injections into different loci of rat brain on core temperature. 6 (1981).

60. Pawlowski, L. & Kwiatek, H. The effect of highly selective inhibitors of the uptake of noradrenaline or 5-hydroxytryptamine on TRH-induced hyperthermia in mice. *Psychopharmacology (Berl.)* **81**, 48–53 (1983).

61. Skibicka, K. P., Alhadeff, A. L. & Grill, H. J. Hindbrain Cocaine- and Amphetamine-Regulated Transcript Induces Hypothermia Mediated by GLP-1 Receptors. *J. Neurosci.* **29**, 6973–6981 (2009).

62. Szreder, Z., Hori, T. & Kaizuka, Y. Thermoregulatory effect of intracerebral injections of neuropeptide Y in rats at different environmental temperatures. *Gen. Pharmacol. Vasc. Syst.* **25**, 85–91 (1994).

63. Esteban, J., Chover, A. J., Sánchez, P. A., Micó, J. A. & Gibert-Rahola, J. Central administration of neuropeptide y induces hypothermia in mice. Possible interaction with central noradrenergic systems. *Life Sci.* **45**, 2395–2400 (1989).

64. Cavicchini, E., Candeletti, S., Spampinato, S. & Ferri, S. Hypothermia Elicited by Some Prodynorphin-Derived Peptides: Opioid and Non-Opioid Action$. 6 (1989).

65. Shido, O. & Nagasaka, T. Effects of intraventricular angiotensin II on heat balance at various ambient temperatures in rats. *Jpn. J. Physiol.* **35**, 163–167 (1985).

66. Chen, X. *et al.* Possible mechanism of hypothermia induced by intracerebroventricular injection of orphanin FQ/nociceptin. *Brain Res.* **904**, 252–258 (2001).

67. Bissette, G., Nemeroff, C. B., Loosen, P. T., Prange, A. J. & Lipton, M. A. Hypothermia and intolerance to cold induced by intracisternal administration of the hypothalamic peptide neurotensin. *Nature* **262**, 607–609 (1976).

68. Guzman-Ruiz, M. A. *et al.* Role of the Suprachiasmatic and Arcuate Nuclei in Diurnal Temperature Regulation in the Rat. *J. Neurosci.* **35**, 15419–15429 (2015).

69. Ferri, S., Reina, R. A., Santagostino, A., Scoto, G. M. & Spadaro, C. Effects of met-enkephalin on body temperature of normal and morphine-tolerant rats. *Psychopharmacology (Berl.)* **58**, 277–281 (1978).

70. Klein, I. *et al.* AdipoR1 and 2 are expressed on warm sensitive neurons of the hypothalamic preoptic area and contribute to central hyperthermic effects of adiponectin. *Brain Res.* **1423**, 1–9 (2011).

71. Qiao, L. *et al.* Adiponectin reduces thermogenesis by inhibiting brown adipose tissue activation in mice. *Diabetologia* **57**, 1027–1036 (2014).

72. Wei, Q. *et al.* Adiponectin is required for maintaining normal body temperature in a cold environment. *BMC Physiol.* **17**, 8 (2017).

73. Zhao, Z.-D. *et al.* A hypothalamic circuit that controls body temperature. *Proc. Natl. Acad. Sci.* **114**, 2042–2047 (2017).

74. Peyron, C. *et al.* Neurons Containing Hypocretin (Orexin) Project to Multiple Neuronal Systems. *J. Neurosci.* **18**, 9996–10015 (1998).

75. Nambu, T. *et al.* Distribution of orexin neurons in the adult rat brain. 18 (1999).

76. Kolaj, M., Coderre, E. & Renaud, L. P. Orexin peptides enhance median preoptic nucleus neuronal excitability via postsynaptic membrane depolarization and enhancement of glutamatergic afferents. *Neuroscience* **155**, 1212–1220 (2008).

77. Yoshida, Y. *et al.* Fluctuation of extracellular hypocretin-1 (orexin A) levels in the rat in relation to the light-dark cycle and sleep-wake activities: Hypocretin release during the sleep-wake cycle. *Eur. J. Neurosci.* **14**, 1075–1081 (2001).

78. Mochizuki, T. Behavioral State Instability in Orexin Knock-Out Mice. *J. Neurosci.* **24**, 6291–6300 (2004).

79. Hara, J. *et al.* Genetic Ablation of Orexin Neurons in Mice Results in Narcolepsy, Hypophagia, and Obesity. *Neuron* **30**, 345–354 (2001).

80. Willie, J. T., Chemelli, R. M., Sinton, C. M. & Yanagisawa, M. To Eat or to Sleep? Orexin in the Regulation of Feeding and Wakefulness. *Annu. Rev. Neurosci.* **24**, 429–458 (2001).

81. Jones, D. N. C. *et al.* Effects of centrally administered orexin-B and orexin-A: a role for orexin-1 receptors in orexin-B-induced hyperactivity. *Psychopharmacology (Berl.)* **153**, 210–218 (2001).

82. Marcus, J. N. *et al.* Differential expression of orexin receptors 1 and 2 in the rat brain. *J. Comp. Neurol.* **435**, 6–25 (2001).

83. Berthoud, H.-R., Patterson, L. M., Sutton, G. M., Morrison, C. & Zheng, H. Orexin inputs to caudal raphé neurons involved in thermal, cardiovascular, and gastrointestinal regulation. *Histochem. Cell Biol.* **123**, 147–156 (2005).

84. Takahashi, Y. *et al.* Orexin neurons are indispensable for prostaglandin E $_2$ -induced fever and defence against environmental cooling in mice: Orexin neurons in PGE $_2$ and cooling-induced thermogenesis. *J. Physiol.* **591**, 5623–5643 (2013).

85. Wang, Y. *et al.* NeuroPep: a comprehensive resource of neuropeptides. *Database* **2015**, bav038–bav038 (2015).

86. Barbe, A. *et al.* Mechanisms of Adiponectin Action in Fertility: An Overview from Gametogenesis to Gestation in Humans and Animal Models in Normal and Pathological Conditions. *Int. J. Mol. Sci.* **20**, 1526 (2019).

87. Fang, H. & Judd, R. L. Adiponectin Regulation and Function. in *Comprehensive Physiology* (ed. Terjung, R.) 1031–1063 (Wiley, 2018). doi:10.1002/cphy.c170046.

88. Moffitt, J. R. *et al.* Molecular, spatial and functional single-cell profiling of the hypothalamic preoptic region. *Science* eaau5324 (2018) doi:10.1126/science.aau5324.

89. Hui, X. *et al.* Adiponectin Enhances Cold-Induced Browning of Subcutaneous Adipose Tissue via Promoting M2 Macrophage Proliferation. *Cell Metab.* **22**, 279–290 (2015).

90. DeLaney, K. *et al.* New techniques, applications and perspectives in neuropeptide research. *J. Exp. Biol.* **221**, jeb151167 (2018).

91. Van Eeckhaut, A., Maes, K., Aourz, N., Smolders, I. & Michotte, Y. The absolute quantification of endogenous levels of brain neuropeptides *in vivo* using LC–MS/MS. *Bioanalysis* **3**, 1271–1285 (2011).

92. Zhou, Y., Wong, J.-M. T., Mabrouk, O. S. & Kennedy, R. T. Reducing Adsorption To Improve Recovery and in Vivo Detection of Neuropeptides by Microdialysis with LC-MS. *Anal. Chem.* **87**, 9802–9809 (2015).

93. Chefer, V. I., Thompson, A. C., Zapata, A. & Shippenberg, T. S. Overview of Brain Microdialysis. *Curr. Protoc. Neurosci.* **47**, 7.1.1-7.1.28 (2009).

94. Schaupp, L. *et al.* Recirculation—a novel approach to quantify interstitial analytes in living tissue by combining a sensor with open-flow microperfusion. *Anal. Bioanal. Chem.* **406**, 549–554 (2014).

95. Stamford, J. A. In Vivo Voltammetry. in *Methods in Neurosciences* vol. 4 127–142 (Elsevier, 1991).

96. Inutsuka, A., Ino, D. & Onaka, T. Detection of neuropeptides in vivo and open questions for current and upcoming fluorescent sensors for neuropeptides. *Peptides* **136**, 170456 (2021).

97. Patriarchi, T. *et al.* Ultrafast neuronal imaging of dopamine dynamics with designed genetically encoded sensors. *Science* **360**, eaat4422 (2018).

98. Ravotto, L., Duffet, L., Zhou, X., Weber, B. & Patriarchi, T. A Bright and Colorful Future for G-Protein Coupled Receptor Sensors. *Front. Cell. Neurosci.* **14**, 67 (2020).

99. Ghosh, A. *et al.* Assessment of Blood-Brain Barrier Function and the Neuroinflammatory Response in the Rat Brain by Using Cerebral Open Flow Microperfusion (cOFM). *PLoS ONE* **9**, e98143 (2014).

100. Steen, H. & Mann, M. The abc's (and xyz's) of peptide sequencing. *Nat. Rev. Mol. Cell Biol.* **5**, 699–711 (2004).

101. Joanneum Research. Open flow microperfusion scheme. https://www.joanneum.at/en/health/productssolutions/pharmacokinetics-pharmacodynamics-bioequivalence/pkpd-in-the-brain.

102. Jadhav, S. B., Khaowroongrueng, V. & Derendorf, H. Microdialysis of Large Molecules. *J. Pharm. Sci.* **105**, 3233–3242 (2016).

103. Ide, S. *et al.* Opposing Roles of Corticotropin-Releasing Factor and Neuropeptide Y within the Dorsolateral Bed Nucleus of the Stria Terminalis in the Negative Affective Component of Pain in Rats. *J. Neurosci.* **33**, 5881–5894 (2013).

104. Yoshimoto, K. *et al.* Enhanced alcohol-drinking behavior associated with active ghrelinergic and serotoninergic neurons in the lateral hypothalamus and amygdala. *Pharmacol. Biochem. Behav.* **153**, 1–11 (2017).

105. Kleinert, M. *et al.* Time-resolved hypothalamic open flow micro-perfusion reveals normal leptin transport across the blood–brain barrier in leptin resistant mice. *Mol. Metab.* **13**, 77–82 (2018).

106. Lanckmans, K., Sarre, S., Smolders, I. & Michotte, Y. Quantitative liquid chromatography/mass spectrometry for the analysis of microdialysates. *Talanta* **74**, 458–469 (2008).

107. Glass, J. D., Guinn, J., Kaur, G. & Francl, J. M. On the intrinsic regulation of neuropeptide Y release in the mammalian suprachiasmatic nucleus circadian clock. *Eur. J. Neurosci.* **31**, 1117–1126 (2010).

108. Andren, P. E. & Caprioli, R. M. Determination of extracellular release of neurotensin in discrete rat brain regions utilizing in vivo microdialysisrelectrospray mass spectrometry. 7 (1999).

109. Fenzl, T., Flachskamm, C., Rossbauer, M., Deussing, J. M. & Kimura, M. Circadian rhythms of basal orexin levels in the hypothalamus are not influenced by an impaired corticotropin-releasing hormone receptor type 1 system. *Behav. Brain Res.* **203**, 143–145 (2009).

110. Aslam, B., Basit, M., Nisar, M. A., Khurshid, M. & Rasool, M. H. Proteomics: Technologies and Their Applications. *J. Chromatogr. Sci.* **55**, 182–196 (2017).

111. Bernay, B. *et al.* Discovering New Bioactive Neuropeptides in the Striatum Secretome Using in Vivo Microdialysis and Versatile Proteomics□S. 13 (2009).

112. Roth, B. L. DREADDs for Neuroscientists. *Neuron* **89**, 683–694 (2016).

113. Grienberger, C. & Konnerth, A. Imaging Calcium in Neurons. *Neuron* **73**, 862–885 (2012).

114. Tian, L., Akerboom, J., Schreiter, E. R. & Looger, L. L. Neural activity imaging with genetically encoded calcium indicators. in *Progress in Brain Research* vol. 196 79–94 (Elsevier, 2012).

115. McCombs, J. E. & Palmer, A. E. Measuring calcium dynamics in living cells with genetically encodable calcium indicators. *Methods* **46**, 152–159 (2008).

116. BioRender. *BioRender* https://biorender.com/.

117. Franklin, K. B. J. & Paxinos, G. *The mouse brain in stereotaxic coordinates*. (Elsevier, AP, 2008).

118. Birngruber, T. *et al.* Cerebral open flow microperfusion: A new *in vivo* technique for continuous measurement of substance transport across the intact blood-brain barrier. *Clin. Exp. Pharmacol. Physiol.* **40**, 864–871 (2013).

119. Bertani, S. *et al.* Circadian Profile of Peripheral Hormone Levels in Sprague- Dawley Rats and in Common Marmosets (Callithrix jacchus). *In Vivo* 10 (2010).

120. Harikai, N., Sugawara, T., Tomogane, K., Mizuno, K. & Tashiro, S. Acute heat stress induces jumping escape behavior in mice. *Physiol. Behav.* **83**, 373–376 (2004).

121. Yamaguchi, Y. *et al.* Mice Genetically Deficient in Vasopressin V1a and V1b Receptors Are Resistant to Jet Lag. *Science* **342**, 85–90 (2013).

122. Erami, E., Azhdari-Zarmehri, H., Ghasemi-Dashkhasan, E., Esmaeili, M.-H. & Semnanian, S. Intra-paragigantocellularis lateralis injection of orexin-A has an antinociceptive effect on hot plate and formalin tests in rat. *Brain Res.* **1478**, 16–23 (2012).

123. Ritz, C., Baty, F., Streibig, J. C. & Gerhard, D. Dose-Response Analysis Using R. *PLOS ONE* **10**, e0146021 (2015).

124. Schindelin, J. *et al.* Fiji: an open-source platform for biological-image analysis. *Nat. Methods* **9**, 676–682 (2012).

125. Hughes, C. S. *et al.* Ultrasensitive proteome analysis using paramagnetic bead technology. *Mol. Syst. Biol.* **10**, 757–757 (2014).

126. Parker, B. L. *et al.* Multiplexed Temporal Quantification of the Exercise-regulated Plasma Peptidome. *Mol. Cell. Proteomics* **16**, 2055–2068 (2017).

127. Caers, J. *et al.* Peptidomics of Neuropeptidergic Tissues of the Tsetse Fly Glossina morsitans morsitans. *J. Am. Soc. Mass Spectrom.* **26**, 2024–2038 (2015).

128. Cox, J. & Mann, M. MaxQuant enables high peptide identification rates, individualized p.p.b.-range mass accuracies and proteome-wide protein quantification. *Nat. Biotechnol.* **26**, 1367–1372 (2008).

129. Tyanova, S., Temu, T. & Cox, J. The MaxQuant computational platform for mass spectrometry-based shotgun proteomics. *Nat. Protoc.* **11**, 2301–2319 (2016).

130. Uniprot database. *Uniprot* https://www.uniprot.org/ (2022).

131. R Core Team. R: A language and environment for statistical computing. *R: A language and environment for statistical computing* https://www.R-project.org/ (2021).

132. Huber, W. *et al.* Orchestrating high-throughput genomic analysis with Bioconductor. *Nat. Methods* **12**, 115–121 (2015).

133. Ritchie, M. E. *et al.* limma powers differential expression analyses for RNA-sequencing and microarray studies. *Nucleic Acids Res.* **43**, e47–e47 (2015).

134. Giovannucci, A. *et al.* CaImAn an open source tool for scalable calcium imaging data analysis. 45.

135. Pnevmatikakis, E. A. *et al.* Simultaneous Denoising, Deconvolution, and Demixing of Calcium Imaging Data. *Neuron* **89**, 285–299 (2016).

136. Liland, K. H., Almøy, T. & Mevik, B.-H. Optimal Choice of Baseline Correction for Multivariate Calibration of Spectra. *Appl. Spectrosc.* **64**, 1007–1016 (2010).

137. McHenry, J. A. *et al.* Hormonal gain control of a medial preoptic area social reward circuit. *Nat. Neurosci.* **20**, 449–458 (2017).

138. Zapata, A., Chefer, V. I. & Shippenberg, T. S. Microdialysis in Rodents. *Curr. Protoc. Neurosci.* **47**, 7.2.1-7.2.29 (2009).

139. Cox, J. *et al.* Accurate Proteome-wide Label-free Quantification by Delayed Normalization and Maximal Peptide Ratio Extraction, Termed MaxLFQ. *Mol. Cell. Proteomics* (2014).

140. Liang, Z., Schmerberg, C. M. & Li, L. Mass spectrometric measurement of neuropeptide secretion in the crab, Cancer borealis, by in vivo microdialysis. *The Analyst* **140**, 3803–3813 (2015).

141. Manousopoulou, A. *et al.* Hypothalamus proteomics from mouse models with obesity and anorexia reveals therapeutic targets of appetite regulation. *Nutr. Diabetes* **6**, e204–e204 (2016).

142. Bartolomucci, A. *et al.* The Extended Granin Family: Structure, Function, and Biomedical Implications. *Endocr. Rev.* **32**, 755–797 (2011).

143. Chakraborty, T. R. *et al.* Quantification of VGF- and pro-SAAS-derived peptides in endocrine tissues and the brain, and their regulation by diet and cold stress. *Brain Res.* **1089**, 21–32 (2006).

144. Francesconi, R. & Mager, M. Thermoregulatory effects of centrally administered bombesin, bradykinin, and methionine-enkephalin. *Brain Res. Bull.* **7**, 63–68 (1981).

145. Bravo-San Pedro, J. M. *et al.* Acyl-CoA-Binding Protein Is a Lipogenic Factor that Triggers Food Intake and Obesity. *Cell Metab.* **30**, 754-767.e9 (2019).

146. Barnett, P. Somatostatin and Somatostatin Receptor Physiology. *Endocrine* **20**, 255–264 (2003).

147. Stengel, A. *et al.* SELECTIVE CENTRAL ACTIVATION OF SOMATOSTATIN RECEPTOR 2 INCREASES FOOD INTAKE, GROOMING BEHAVIOR AND RECTAL TEMPERATURE IN RATS. 9.

148. Lin, M. T., Uang, W. N., Ho, L. T., Chuang, J. & Fan, L. J. Somatostatin: a hypothalamic transmitter for thermoregulation in rats. *Pfl*[illegible]*gers Arch. Eur. J. Physiol.* **413**, 528–532 (1989).

149. Reinscheid, R. K., Nothacker, H.-P. & Civelli, O. The orphanin FQ/nociceptin gene: structure, tissue distribution of expression and functional implications obtained from knockout mice. *Peptides* **21**, 901–906 (2000).

150. Uezu, K. *et al.* Lack of nociceptin receptor alters body temperature during resting period in mice: *NeuroReport* **15**, 751–755 (2004).

151. Brancia, C. *et al.* VGF Protein and Its C-Terminal Derived Peptides in Amyotrophic Lateral Sclerosis: Human and Animal Model Studies. *PLOS ONE* **11**, e0164689 (2016).

152. Watson, E. *et al.* Analysis of knockout mice suggests a role for VGF in the control of fat storage and energy expenditure. *BMC Physiol.* **9**, 19 (2009).

153. Kim, T., Gondré-Lewis, M. C., Arnaoutova, I. & Loh, Y. P. Dense-Core Secretory Granule Biogenesis. *Physiology* **21**, 124–133 (2006).

154. Wiedermann, C. J. Secretoneurin: a functional neuropeptide in health and disease. *Peptides* **21**, 1289–1298 (2000).

155. Saria, A. *et al.* Secretoneurin releases dopamine from rat striatal slices: A biological effect of a peptide derived from secretogranin II (chromogranin C). *Neuroscience* **54**, 1–4 (1993).

156. Ramesh, N., Mohan, H. & Unniappan, S. Nucleobindin-1 encodes a nesfatin-1-like peptide that stimulates insulin secretion. *Gen. Comp. Endocrinol.* **216**, 182–189 (2015).

157. Gawli, K., Ramesh, N. & Unniappan, S. Nesfatin-1-like peptide is a novel metabolic factor that suppresses feeding, and regulates whole-body energy homeostasis in male Wistar rats. *PLOS ONE* **12**, e0178329 (2017).

158. Livingstone, C. & Borai, A. Insulin-like growth factor-II its role in metabolic and endocrine disease.pdf. *Clin. Endocrinol. (Oxf.)* (2014).

159. Lechan, R. M. & Fekete, C. The TRH neuron: a hypothalamic integrator of energy metabolism. in *Progress in Brain Research* vol. 153 209–235 (Elsevier, 2006).

160. Rondeel, J., de Greef, W., Hop, W., Rowland, D. & Visser, T. Effect of cold exposure on the hypothalamic release of thyrotropin-releasing hormone and catecholamines. (1991).

161. Yuzaki, M. Cbln1 and its family proteins in synapse formation and maintenance. *Curr. Opin. Neurobiol.* **21**, 215–220 (2011).

162. Watanabe, T. Angiotensin II: its effects on fever and hypothermia in systemic inflammation. *Front. Biosci.* **9**, 438 (2004).

163. Wilson, K. M. & Fregly, M. J. Angiotensin II-induced hypothermia in rats. *J. Appl. Physiol.* **58**, 534–543 (1985).

164. Kakizaki, M. *et al.* Differential Roles of Each Orexin Receptor Signaling in Obesity. *iScience* **20**, 1–13 (2019).

165. Scammell, T. E. & Winrow, C. J. Orexin Receptors: Pharmacology and Therapeutic Opportunities. *Annu. Rev. Pharmacol. Toxicol.* **51**, 243–266 (2011).

166. Kubota, N. *et al.* Adiponectin Stimulates AMP-Activated Protein Kinase in the Hypothalamus and Increases Food Intake. *Cell Metab.* **6**, 55–68 (2007).

167. G protein-coupled receptors. *IUPHAR/BPS Guide to PHARMACOLOGY* https://www.guidetopharmacology.org/GRAC/GPCRListForward?class=A (2022).

168. Schröder, H., Moser, N. & Huggenberger, S. *Neuroanatomy of the Mouse: An Introduction*. (Springer International Publishing, 2020). doi:10.1007/978-3-030-19898-5.

169. Crestani, C. *et al.* Mechanisms in the Bed Nucleus of the Stria Terminalis Involved in Control of Autonomic and Neuroendocrine Functions: A Review. *Curr. Neuropharmacol.* **11**, 141–159 (2013).

170. Rizzi-Wise, C. A. & Wang, D. V. Putting Together Pieces of the Lateral Septum: Multifaceted Functions and Its Neural Pathways. *eneuro* **8**, ENEURO.0315-21.2021 (2021).

171. Rauniyar, N. Parallel Reaction Monitoring: A Targeted Experiment Performed Using High Resolution and High Mass Accuracy Mass Spectrometry. *Int. J. Mol. Sci.* **16**, 28566–28581 (2015).

172. Lewandoski, M. Conditional control of gene expression in the mouse. *Nat. Rev. Genet.* **2**, 743–755 (2001).

173. Celi, F. S., Le, T. N. & Ni, B. Physiology and relevance of human adaptive thermogenesis response. *Trends Endocrinol. Metab.* **26**, 238–247 (2015).

174. Azmoon, S. *et al.* Neurologic and Cardiac Benefits of Therapeutic Hypothermia: *Cardiol. Rev.* **19**, 108–114 (2011).